Mechanisms of CXCL10 Antimicrobial Activity against *Bacillus anthracis*

Katie R. Margulieux

Bachelor of Science, University of Idaho – Moscow, ID, 2010

A Dissertation Presented to the Graduate Faculty of the University of Virginia in Candidacy for the Degree of Doctor of Philosophy

Department of Microbiology, Immunology, and Cancer Biology

University of Virginia
August, 2016

Abstract

Bacillus anthracis is a bacterial pathogen that is the causative agent of anthrax with a high risk for bioweapon development. The chemokine CXCL10 has been described as an important component of the innate and adaptive immune system for its chemoattractant properties influencing various leukocytes. *B. anthracis* spores and vegetative cells have been shown to be directly killed by the chemokine CXCL10 through previously unknown mechanisms. We first studied the role of the identified bacterial target FtsX, as well as the role of various portions of CXCL10 in killing *B. anthracis* vegetative cells. We show that CXCL10 acts as a bifunctional molecule that can utilize at least two separate mechanisms for eliciting antimicrobial activity: 1) An FtsE/X-dependent mechanism through interaction of a portion of CXCL10 (presumably, the CXCL10 N-terminal region) other than the C-terminal α-helix with FtsE/X and 2) An FtsE/X-independent mechanism observed at high concentrations of intact CXCL10 and in the absence of FtsX- this latter mechanism requires the presence of the CXCL10 C-terminal α-helix and results in membrane depolarization. Further work was performed to investigate the FtsE/X-dependent antimicrobial mechanism, and we hypothesized that CXCL10 kills through disruption of peptidoglycan processing through the bacterial FtsE/X complex. We characterized the peptidoglycan phenotype of *B. anthracis* parent strain and the *B. anthracis* bacterial mutants Δ*ftsX* and *ftsE(K123A/D481N)* to use as a baseline comparator to CXCL10 treated cells. Studies conducted with CXCL10 and a C-terminal truncated CXCL10 showed that exposure of the *B. anthracis* parent strain to both molecules resulted in disruption of peptidoglycan processing. The *B. anthracis* bacterial mutants Δ*ftsX* and *ftsE(K123A/D481N)* strains did not exhibit disruption of peptidoglycan processing in the

presence of CXCL10 or the C-terminal truncated CXCL10. These data indicate that CXCL10 exerts an antimicrobial effect against *B. anthracis* vegetative cells through the FtsE/X complex by disrupting peptidoglycan remodeling, resulting in bacterial lysis. Finally, studies were conducted to identify key bacterial components involved in CXCL10 activity against *B. anthracis* spores. A transposon mutant library of *B. anthracis* Sterne strain spores identified the gene encoding BAS0651, a putative DL-endopeptidase involved in peptidoglycan hydrolysis and cell wall remodeling during cellular elongation. Further analyses supported that CXCL10 causes a delay in *B. anthracis* spore germination and also leads to an increase in spore permeability, a possible mechanism for the resulting loss of spore viability. *In vivo* mouse studies were conducted that showed the absence of *BAS0651 in B. anthracis* parent strain resulted in an increase in spore germination and vegetative cell proliferation during initial pulmonary infection in C57BL/6 mice. It appears CXCL10 targets *B. anthracis* spores through BAS0651, which may result in the dysregulation of peptidoglycan remodeling during spore germination. The findings in this dissertation reveal novel mechanisms of CXCL10 antimicrobial activity against *B. anthracis* spores and vegetative cells. Understanding how CXCL10 kills *B. anthracis* will potentially result in the development of a new class of antimicrobials based on CXCL10, as well as the identification of important new antimicrobial bacterial targets.

Table of Contents

List of Figures

Chapter 1: Introduction

Chapter 2:

List of Abbreviations

AVA: Anthrax vaccine adsorbed

CAMP: cationic antimicrobial peptide

GAG: glycosaminoglycan

EDA: Ethynyl-D-alanine

ELR: Glutamic Acid-Leucine-Arginine or Glu-Leu-Arg

ERK: extracellular signal-regulated kinases

FSAP: Federal Select Agent Program

GlcNAc: N-acetylglucosamine

ID: infectious dose

IFN: interferon

IPTG: isopropyl β-D-1-thiogalactopyranoside

JNK: c-Jun-N-terminal kinase

MAPKK: mitogen-activated protein kinase kinase

MurNAc: N –acetylmuramic acid

TDL: TAMRA-D-lysine

TNF-α: tumor necrosis factor-α

Acknowledgments

To my friends, family, and friends who have become family, your support has meant the world.

To my labmates, thank you for the camaraderie that has made the lab a great place to work.

To my committee, thank you for invaluable direction and advice.

To my mentor, Molly Hughes, thank you for showing me how data always drives the science and sharing your passion for discovery.

CHAPTER 1:

INTRODUCTION

1.1 *Bacillus anthracis*

Bacillus anthracis is a Gram-positive, rod shaped bacterium that is the causative agent of the disease anthrax (1, 2). Scientifically, the pathogen has a rich past, as the work of Robert Koch in 1876 was the first to show that a microbe was the cause of a specific disease thus, launching the field of pathogenic bacteriology (3). Anthrax is primarily a zoonotic infection that affects livestock animals, such as cattle and sheep (4). Herbivores typically acquire *B. anthracis* infection by ingesting or inhaling spores from the soil (1, 5). The spore is the infectious form of the organism and can withstand a range of harsh environments. Spores germinate into metabolically active vegetative cells through a cascade of environment- or host-derived factors following uptake into a susceptible host; subsequent multiplication and toxin synthesis results in disease and death (6–9). Upon host death, the vegetative form of the organism can detect a loss of nutrients and suitable environment, for example a drop in temperature, which triggers sporulation (8). *B. anthracis* remains in the inert spore state until uptake by another host, where the cycle repeats itself (1, 10, 11). Spore particles are present in soil worldwide and have been shown to remain viable for extended periods of time, even decades (8, 12). Spores of *B. anthracis* can germinate and replicate within the soil amoeba, *Acanthamoeba castellanii*, thus potentially contributing to the continual presence of viable spores in the environment (13). Humans are not considered a natural host for *B. anthracis*, but spore exposure through various routes can result in a serious infection if not diagnosed and treated rapidly (2, 14).

There are four types of human anthrax based on the route by which the spore enters the host: cutaneous, gastrointestinal, injectional, and inhalational (Figure 1.1) (2, 14).

FIGURE 1.1

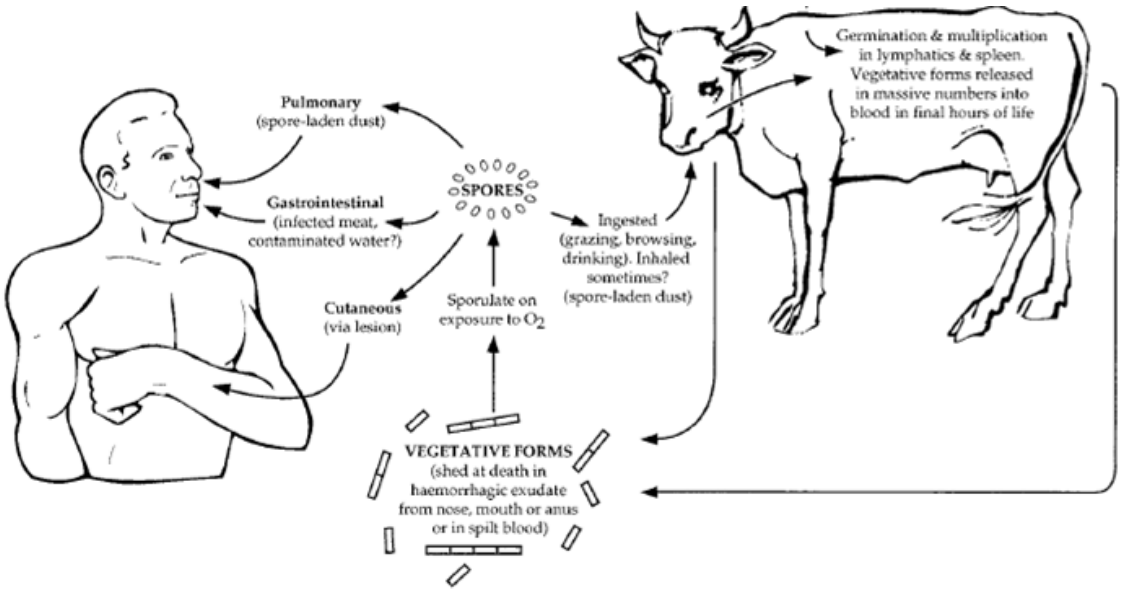

Figure 1.1: Routes of *B. anthracis* infection. Human *B. anthracis* spore exposure through multiple routes results in the disease anthrax. Cutaneous anthrax, the most common naturally acquired anthrax infection, occurs by spore introduction into the body through a cut or abrasion on the skin, as well as by insect vector transmission (not shown). Gastrointestinal anthrax is acquired through consumption of contaminated food products. Injectional anthrax is the result of spore-contaminated drug injection into intramuscular regions (not shown). Inhalational anthrax develops from pulmonary introduction of spores and results in the highest mortality rate. Modified from Anthrax in Humans and Animals. 4th edition. Geneva: World Health Organization, 2008 (4).

Cutaneous anthrax is the most common form, comprising about 95% of all reported infections. It is characterized by a painless black eschar at the site of infection. Naturally acquired infection is an occupational disease, which occurs in workers (including veterinarians) exposed to infected herd animals or contaminated animal products worldwide (4). Insect vectors, such as house flies (*Musca domestica*) and mosquitos (*Aedes aegypti* and *A. taeniorhynchus*), have been shown to transmit anthrax to result in cutaneous infections (15, 16). Cutaneous infections generally result in a mortality rate of 5-20% if untreated but less than 1% if treated with an appropriate antibiotic (2, 14). Gastrointestinal infections are the second most prevalent form of anthrax. Infection occurs following ingestion of spore-contaminated meat. Gastrointestinal anthrax presents with ubiquitous gastrointestinal symptoms, which may result in an underreported rate of infection due to attribution of the symptoms to more common enteric pathogens. The mortality rate is estimated to be 25-60% if untreated, with antibiotic treatment lowering the rate to ≤40% (17). Injectional anthrax is a recently recognized form that was first identified in 2000 (18). It occurs in intravenous drug users that directly inject spore-contaminated drugs into intramuscular regions (18). Introduction of the spores into typical injection sites causes skin and soft tissue infection with a high mortality rate (34%), even with antibiotic treatment (19). Inhalational anthrax is the most severe form of anthrax and is acquired through spore entry in the lungs followed by subsequent germination into vegetative bacteria that eventually disseminate into the bloodstream and throughout the body (20–22). Natural occurring inhalational anthrax infections occur rarely and mainly among workers who process dried animal hides or wool (i.e., Woolsorter's disease) (4). Mortality rates range from 45-94%, with a rapid diagnosis greatly increasing the odds of survival (2, 23).

Early signs and symptoms of inhalational anthrax infection can mimic other pulmonary bacterial or viral infections, which can complicate the diagnosis and treatment (20).

A wide variety of antibiotics such as beta-lactam antibiotics (e.g., penicillin, cephalosporins) and fluoroquinolones have been used to successfully treat anthrax infections. With the potential for either naturally-acquired or nefariously-introduced β-lactamase resistance mechanisms, the current post-exposure prophylaxis treatment guidelines recommend an extended course of ciprofloxacin or doxycycline (2). While vegetative cells are more readily killed by antibiotics, the spores can persist in an inert state that is unaffected by any currently available antibiotics. Primate studies of inhalational anthrax revealed the presence of spores in the lungs for up to 100 days after exposure, underscoring the risk for an extended incubation period in the host (24). In 1979, an accidental release of anthrax spores in the town of Sverdlovsk, Russia resulted in an outbreak of inhalational anthrax cases. The modal incubation period was 9-10 days, but an extended incubation period of 43 days before illness occurred was observed in a few cases (25). For these reasons, prophylactic treatment is prescribed for 60 days to allow enough time for spores to germinate into vegetative cells so they can be killed by the antibiotic (2).

An anthrax vaccine, Anthrax Vaccine Adsorbed (AVA), is commercially available and is recommended for military personnel and laboratory workers who have contact with fully virulent strains (26). It is administered in a series of five doses over 18 months, with a yearly booster after completion. There is evidence that three intramuscular doses are

sufficient for protection for up to 3.5 years (27). Studies to evaluate the most effective vaccination schedule are ongoing (27). There has been some debate about the safety of the vaccine with reports of chronic adverse effects such as fever, malaise, and joint pain (28). Although AVA is currently not recommended for the general public, if an exposure is suspected or an infection is detected early enough, current post-exposure prophylaxis treatment guidelines (29) recommend that at least the first three doses in the AVA series should be administered to help the immune system identify and clear the vegetative cells and spores (14, 28).

B. anthracis is listed by the Federal Select Agent Program (FSAP) as a Tier One Select Agent, indicative of high risk for bioweapon development and subsequent attack (5). Notably, multiple countries experimented with anthrax in bioweapon development programs during the Cold War period (30). The Amerithrax attacks of 2001 emphasized the threat potential of *B. anthracis* with spores being mailed through the United States Postal Service to target politicians and other recipients (23, 31). *B. anthracis* has many unique characteristics that make it an effective bioweapon. The inert spore form is very hardy with the ability to withstand extreme environmental conditions with a 50% infectious dose (ID_{50}) for humans calculated to be about $1.1x10^5$ spores (20, 32–34). Following dissemination, treatment of the exposed population would be difficult, especially if identification of *B. anthracis* as the causative agent was delayed, since the disease progresses quickly and death can occur within days (2, 35). The development of new therapeutic strategies is needed to treat both spores and vegetative cells in the event of a *B. anthracis* outbreak or attack.

1.2 *B. anthracis* Life Cycle and Virulence Factors

B. anthracis undergoes a cycle between the dormant spore form and growing/dividing vegetative cells, and this cycle is largely determined by environmental factors and the availability of nutrients (12). The process of sporulation is regulated by multiple signal transduction networks activated by a change in environmental factors, such as the presence of O_2, lack of available nutrients, high vegetative cell concentration, and a downward temperature shift (1, 8). In the process of sporulation, *B. anthracis* and related *Bacillus* spp. begin asymmetrical cell division, followed by processes that package the chromosomal DNA into the core and build the protective spore layers. After spore formation is complete, lysis of the vegetative cell releases the spore into the environment for eventual uptake by another host (36). Spores are comprised of multiple layers that protect the spore core, which contains the tightly packaged chromosomal DNA (Figure 1.2). The core also contains small acid-soluble proteins, high levels of calcium dipicolinic acid, and ions that protect the chromosomal DNA from degradation in the presence of heat or UV radiation. Surrounding the spore core is a layer of peptidoglycan (spore cortex) that also helps protect the core from outside elements. The middle layer (spore coat) and outermost layer (exosporium) act as further protective barriers from lytic molecules and other microbes (8). The spore cortex, coat, and exosporium also play a vital role in environmental signaling by detecting germinants via receptors located within the membranes that indicate the appropriate time to germinate (6, 8).

FIGURE 1.2

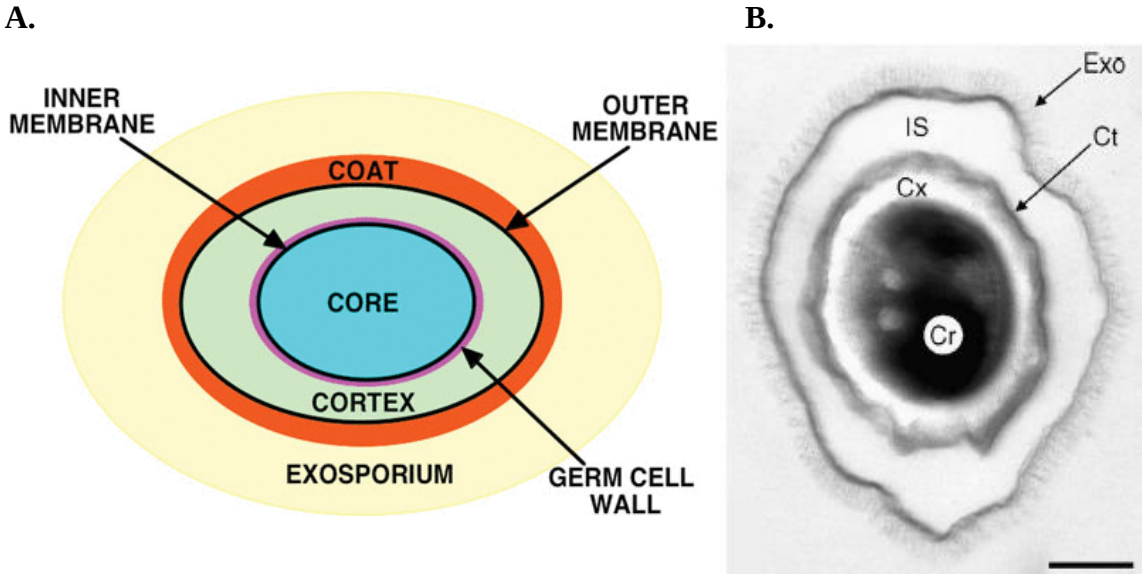

Figure 1.2: *B. anthracis* spore. The layers of a spore serve to protect the core, which contains tightly packaged chromosomal DNA, from damage as well as to detect germination signals from the environment. (A) Schematic of *B. anthracis* spore composition and layers, not drawn to scale. Modified from Setlow, 2014 (32). (B) Transmission electron micrograph of a *B. anthracis* Sterne strain spore. (Cr): core, (Cx): cortex, (Ct): coat, (Is): interspace, also considered part of the exosporium, and (Exo): exosporium. Modified from Driks, 2009 (8). Scale bar is 700 nm.

Spores undergo germination upon detection of a favorable environment, and the germination process results in the outgrowth of a metabolically active and dividing vegetative cell (Figure 1.3) (6). The binding of small molecules (for example, single amino acids, purine nucleotides, or various sugars) by proteins embedded in the outer spore layers initiates the process of germination, which traditionally has been considered to occur in two stages (6). The first stage involves the release of hydrogen ions and calcium dipicolinic acid, which allows partial hydration of the core to occur through water molecules taking the place of the ions. The second stage is considered to be the activation of cortex hydrolysis to break down the peptidoglycan layer, allowing further hydration of the spore core. Finally, spore outgrowth and complete spore coat shedding give rise to a growing/dividing vegetative cell (6, 7, 37). Morphologically, the vegetative cells form square-ended chains of Gram-positive rods that have the appearance of box cars in a train (38). The cell envelope of the vegetative cell consists of a cell membrane, thick peptidoglycan layer, S-layer, and a poly-D-glutamic acid (PDGA) capsule (Figure 1.4) (39). The S-layer is a surface component of *B. anthracis* comprised of two proteins [surface array protein (SAP) and extractable antigen 1 (EA1)] arranged in a lattice-like structure (1). These S-layer proteins function as adhesins as well as a protective layer that mediates environmental interaction (39).

B. anthracis vegetative cells produce a number of virulence factors that contribute to its pathogenesis. The plasmid pXO1 (182 kb) contains the genes for lethal factor, edema factor, and protective antigen (40). Proteolytic processing of the 83 kD protective antigen

……

FIGURE 1.3

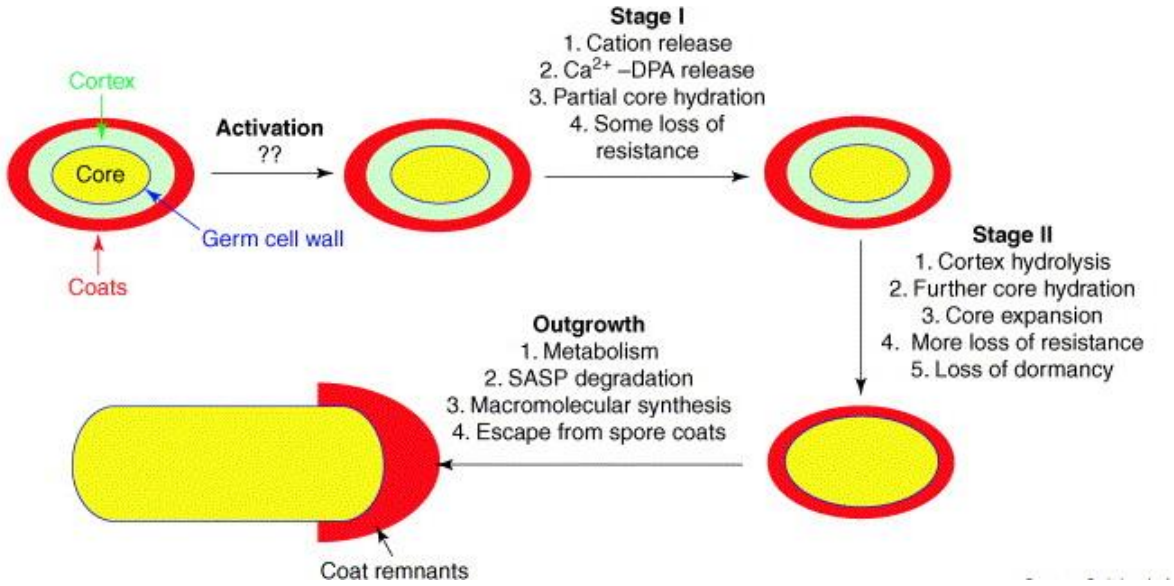

Figure 1.3: Schematic overview of *B. anthracis* spore germination. After activation, the spore undergoes multiple stages during germination that result in the full outgrowth of metabolically active vegetative cell. Modified from Setlow, 2003 (6).

……

……

FIGURE 1.4

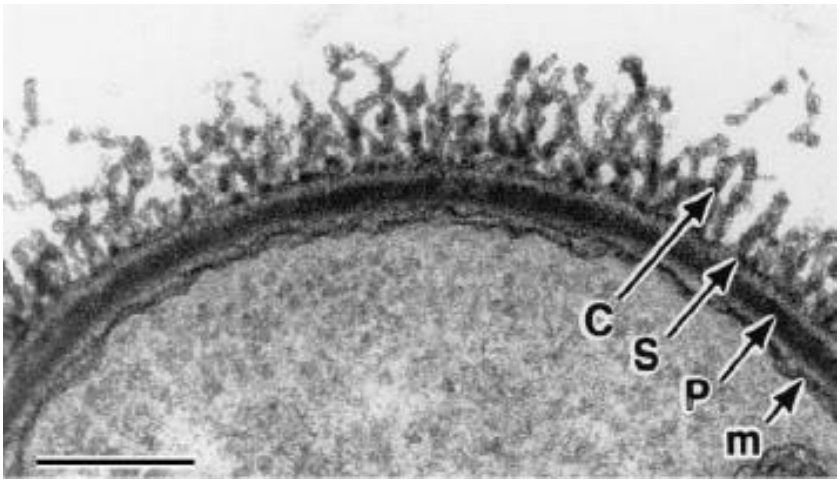

Figure 1.4: *B. anthracis* vegetative cells. *B. anthracis* is a Gram-positive, rod-shaped bacterium. The surface of a fully virulent, encapsulated *B. anthracis* strain consists of a cell membrane, thick peptidoglycan layer, S-layer, and a poly-D-glutamic acid capsule. (M): cytoplasmic membrane, (P): peptidoglycan layer, (S): S-layer, (C): poly-D-glutamic acid capsule. Modified from Fouet, 2009 (39). Scale bar is 250 nm.

……

monomer by host cells removes 20 kD from the N-terminus of the protective antigen to form a 63 kD active subunit that is able to form a heptamer or octamer and bind to the mammalian cell receptors, anthrax toxin receptor 1 (ANTRXR-1) [formerly named anthrax toxin receptor (ATR)] or ANTRXR-2 [formerly named capillary morphogenesis protein 2 (CMG)] (41–43). The protective antigen can bind lethal factor to form lethal toxin or with edema factor to form edema toxin (44). The protective antigen assists delivery of lethal factor or edema factor into target cells (14, 40) through endocytosis of the entire complex into the cell (Figure 1.5). Once engulfed by the cell, the endosome acidifies, and the lowered pH triggers the protective antigen complex to form a pore that facilitates the release of lethal factor and/or edema factor into the cytoplasm (42, 45, 46). Lethal factor is a 90 kD metalloprotease enzyme that disrupts key cellular signaling through the cleavage of the mitogen-activated protein kinase (MAPK) kinase (MAPKK) (42, 47). The cleavage of MAPKK results in disruption of three signaling pathways: extracellular signal-regulated kinases (ERK), c-Jun-N-terminal kinase (JNK), and p28 MAPK (47). Edema factor is an 89 kD protein that is an adenylate cyclase that converts ATP to cAMP, resulting in the dysregulation of signaling pathways (42, 44, 47). Both toxins ultimately result in the disruption of signaling pathways and mammalian cell function, leading to cell dysfunction and death (14, 42, 44, 47). In addition to interrupting cellular signaling pathways, lethal factor and edema factor also interfere with the response of the host immune system by blocking bacterial clearance through phagocytes (42, 47–49). In fully virulent *B. anthracis* strains, such as Ames strain, a second virulence plasmid pXO2 (92 kb) encodes genes for a thick PDGA capsule (40). The capsule inhibits vegetative cell phagocytosis by immune cells, thus contributing to increased survival, replication, and dissemination of the

……

FIGURE 1.5

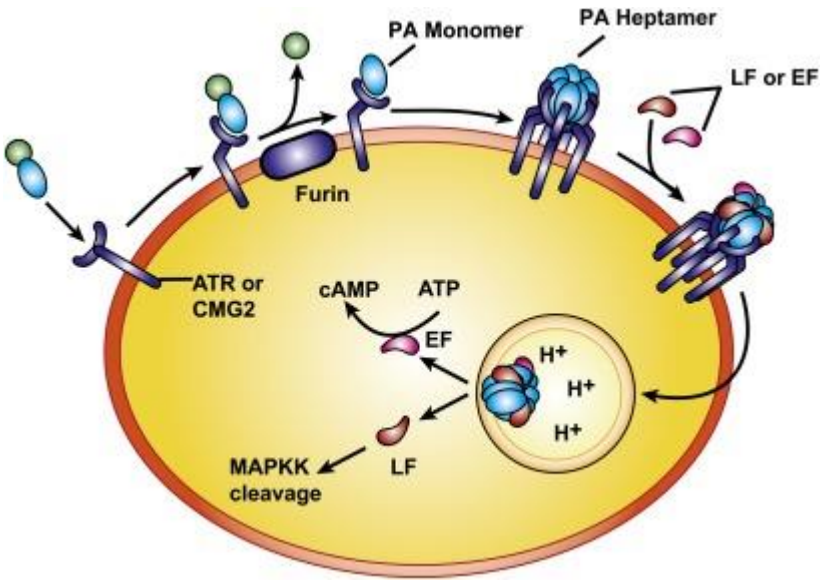

Figure 1.5: *B. anthracis* toxin assembly. Protective antigen monomers are processed by host cell tryptic enzymes (furins) into a 63 kD unit and then assemble to form a heptamer or octamer (not shown in schematic) that binds to mammalian cell receptors. Lethal factor and/or edema factor bind to the protective antigen heptamer or octamer, and the complex is endocytosed. Endosomal acidification triggers a conformational change of the protective antigen complex, resulting in a pore through which lethal factor or edema factor is released into the cell cytoplasm. Lethal factor disrupts signaling pathways through MAPKK cleavage. Edema factor is an adenylate cyclase enzyme that increases intracellular cAMP levels. Lethal factor and edema factor each disrupt cell signaling pathways to cause cellular dysfunction and systemic toxemia. Modified from Sweeney, 2011 (14).

……

vegetative cells in the host (50–52). Together, these virulence factors allow *B. anthracis* vegetative cells to survive in the host and reach bacterial concentrations of up to $1x10^8$ organisms per ml of blood (53). With the host immune system unable to function properly, toxemia and bacteremia rapidly lead to host death.

1.3 Chemokines

Chemokines are small 8-10 kD proteins that are an integral part of the immune system with approximately 50 known chemokine ligands and 20 receptor proteins identified to date (54–56). Chemokines were first identified and studied based on their potent chemoattractant abilities to recruit leukocytes to sites of injury or infection as a response to inflammatory or infectious processes (56, 57). Chemokines are characterized as homeostatic and/or inflammatory based on whether they are constitutively expressed or induced by an inflammatory molecule, such as interferon-γ (IFN-γ) or interferon-α/β (IFN-α/β) (58). Homeostatic chemokines are constitutively produced by a wide variety of cell types and are thought to be involved in the maintenance of resident immune cells, immune surveillance, and non-lymphoid tissue positioning and homing (59). In contrast, inflammatory chemokines are upregulated when needed and recruit activated immune cells into target sites through chemotaxis (55). The intricate interactions between the chemokines and their respective receptors result in finely orchestrated control over cellular immune functions as well as the activation and recruitment of adaptive immune cells (59).

Multiple roles for both homeostatic and inflammatory chemokines have been described beyond immune system homeostasis and adaptive immune response. Chemokines play an

integral role in initiating development and continuing differentiation in the process of lymphocyte maturation (56, 60). They also have been shown to be important for central nervous system development and maintenance (61). Underscoring the diversity of their roles in the host, chemokines have been found to play a role in either inhibition or augmentation of angiogenesis during inflammatory conditions (62, 63). Chemokines also help direct and regulate wound repair by promoting an environment conducive to regenerating tissue (64–66). Additionally, a number of chemokines have been found to demonstrate direct antimicrobial activity against a wide variety of microbial pathogens, a characteristic that will be discussed in more detail in the following sections (67–69).

There are four families of chemokines, C, CC, CXC, and CX3C, which are classified based on the number and position of conserved cysteine residues (54, 55). In general, chemokines share a similar overall structure with an unstructured N-terminal end, three β-sheets that serve as a backbone, and a C-terminal α-helix (Figure 1.6). One or two disulfide bonds determine the tertiary structure of the molecule (58, 70, 71). CC and CXC chemokines all share this common structure, and in a monomeric form, C chemokines adopt a traditional chemokine structure as well. However, in a dimeric form, C chemokines are unique in forming a head-to-tail molecule that performs a separate function (72, 73). The CX3C chemokine also has a unique feature, as it contains an additional transmembrane domain at the C-terminus (distal to the characteristic C-terminal α-helix) that allows anchoring in cell walls (71). Cleavage of CX3C can occur under certain conditions that produces a soluble derivative of CX3C (71, 74). Chemokine dimers and other complexes have been observed

FIGURE 1.6

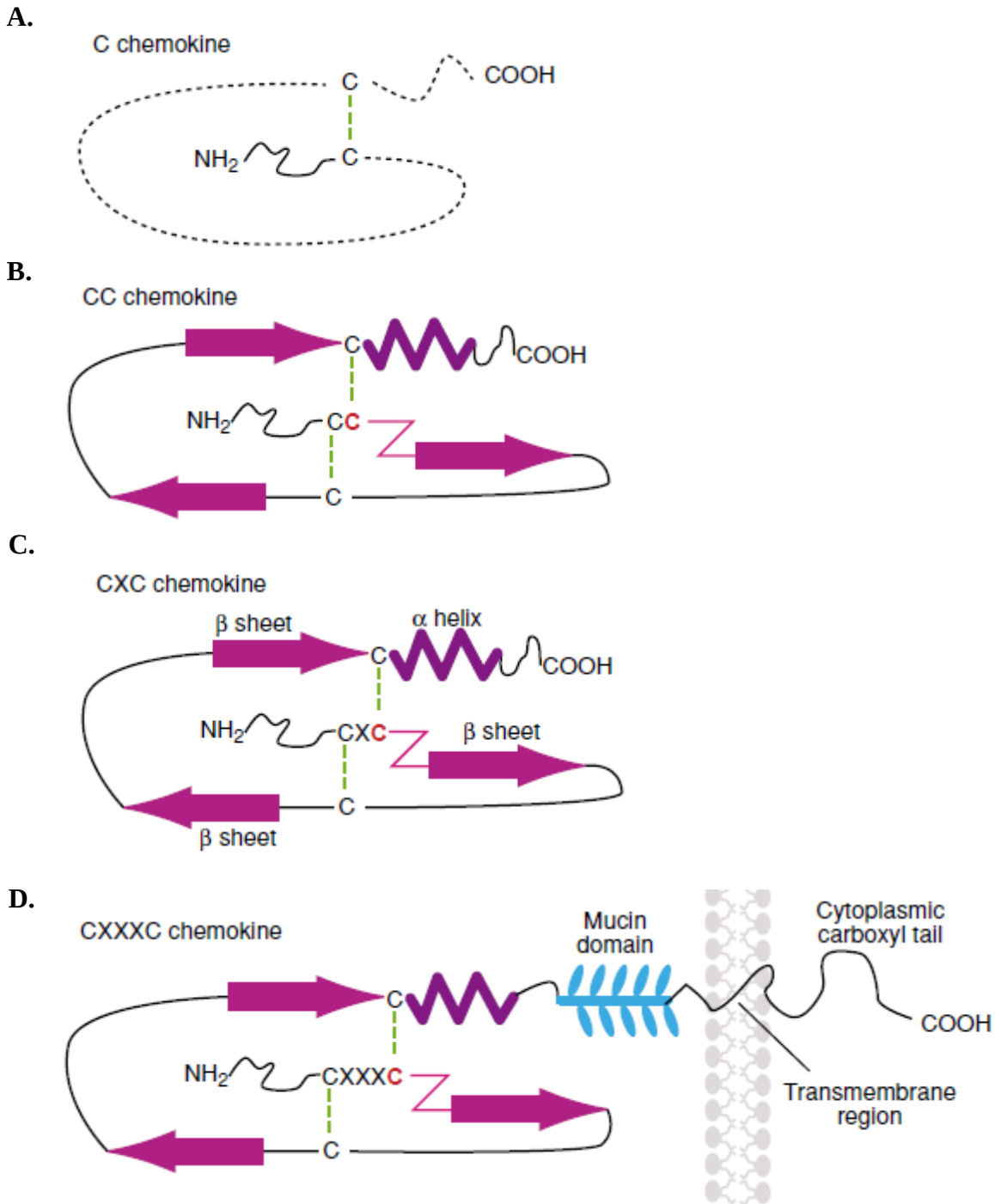
A.
C chemokine
C
COOH
NH2
C
B.
CC chemokine
C
COOH
NH2
CC
C
C.
CXC chemokine
β sheet
α helix
C
COOH
NH2
CXC
β sheet
C
β sheet
D.
CXXXC chemokine
Mucin domain
Cytoplasmic carboxyl tail
C
COOH
NH2
CXXXC
Transmembrane region
C

Figure 1.6: Chemokine families. Chemokines are divided into families based on conserved cysteine residues and demonstrate conserved secondary structures of a traditional unstructured N-terminus, three β-sheet backbones, and an α-helical C-terminus. (A) C chemokines transition between a more traditional monomeric chemokine structure and a dimeric structure that does not resemble the rest of the superfamily (Kuloglu 2002, Guzzo 2015). (B-C) CC chemokines and CXC chemokines retain traditional overall structure. CXC chemokines contain a non-conserved amino acid between the conserved cysteine residues. (D) CX3C has an additional mucin domain after the α-helix that transitions into a transmembrane domain. It can also undergo cleavage at the mucin site to become a soluble protein in certain conditions. Modified from Frederick and Clayman, 2001 (71).

……

at high concentrations as well as with other molecules present in the solution, but it is thought that most biological processes of chemokines are effected as monomers (70).

Chemokines have been shown to interact with both specific chemokine receptors and nonspecific cell surface glycosaminoglycans (GAGs) (58, 75). Inflammatory chemokine receptors are relatively promiscuous and are able to interact with and be activated by multiple ligands that are typically in the same family (55, 76, 77). Homeostatic chemokines only activate one chemokine receptor (55). The receptors are classified as G-coupled protein receptors, with interaction of a chemokine ligand with a receptor triggering an intracellular signaling pathway that ultimately directs cellular function (78). Signaling bias has been reported with chemokine receptors; the exact downstream cascade or signaling effect is modified based on the ligand detected, the receptor variant, or the cell type where the receptor is located (79). Nonspecific interactions with GAGs are thought to be important for the chemotactic activity of chemokines. Interactions of the chemokines with GAGs create the gradient effect needed to direct immune cells to the area of inflammation and/or infection (58, 75). The interactions of chemokines and their receptors create a network and signaling environment that creates an effective immune system response under both homeostatic and inflammatory conditions.

1.4 IFN-γ-inducible ELR(-) CXC Chemokines and CXCR3

CXCL9, CXCL10, and CXCL11 comprise a group of IFN-γ-inducible, Glu-Leu-Arg negative (ELR-) chemokines that share about 40% amino acid sequence identity (55, 80). The lack of an ELR(-) motif indicates activation of a type one immune response, mostly

targeting Th1 T-cells, natural killer cells, and monocytes (81). IFN-γ-inducible ELR(-) CXC chemokines are classified as inflammatory chemokines and are produced by a wide variety of cells, including human fibroblasts, endothelial cells, keratinocytes, mesangial cells, astrocytes, and neutrophils during periods of inflammation or infection (76, 82, 83). IFN-γ induces production of all three IFN-γ-inducible ELR(-) CXC chemokines, but CXCL10 and CXCL11 can also be induced by IFNα/β and tumor necrosis factor-α (TNF-α) (80). Notably, CXCL9, CXCL10, and CXCL11 can induce the production of IFN-γ, a quality that results in a highly effective positive feedback loop that quickly upregulates the three chemokines and allows them to reach high concentrations *in vivo* (80). CXCL9, CXCL10, and CXCL11 form classic chemokine secondary structures noted above, but when compared to other chemokines, they contain a higher degree of positively-charged amino acids in the C-terminal α-helix (Figure 1.7A) (67). The three β-sheets and C-terminal α-helix interact through various charges and two disulfide bonds to form a compact molecule (Figure 1.7B) (84, 85).

Although CXCL9, CXCL10, and CXCL11 bind to the same mammalian receptor, CXCR3, these three chemokines have been shown to elicit distinct downstream effects that contribute to the biological signaling differences between them (76, 86). CXCL11 has also been shown to bind to the receptor CXCR7 (62). CXCR3 is a G-protein coupled receptor and is activated through a two-step interaction pattern with the IFN-γ-inducible ELR(-) CXC chemokines (86, 87). The unstructured N-terminus of the IFN-γ-inducible ELR(-) CXC chemokines interacts with the extracellular N-terminal region of CXCR3. Other

FIGURE 1.7

A.

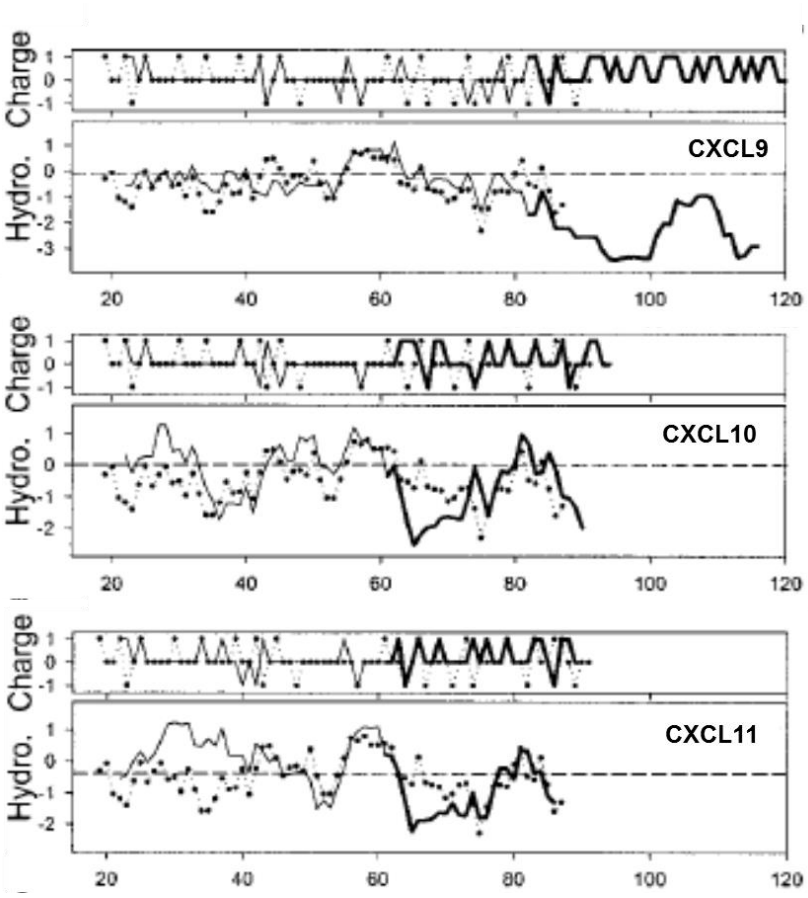
Charge
Hydro.
CXCL9
CXCL10
CXCL11
20
40
60
80
100
120

B.

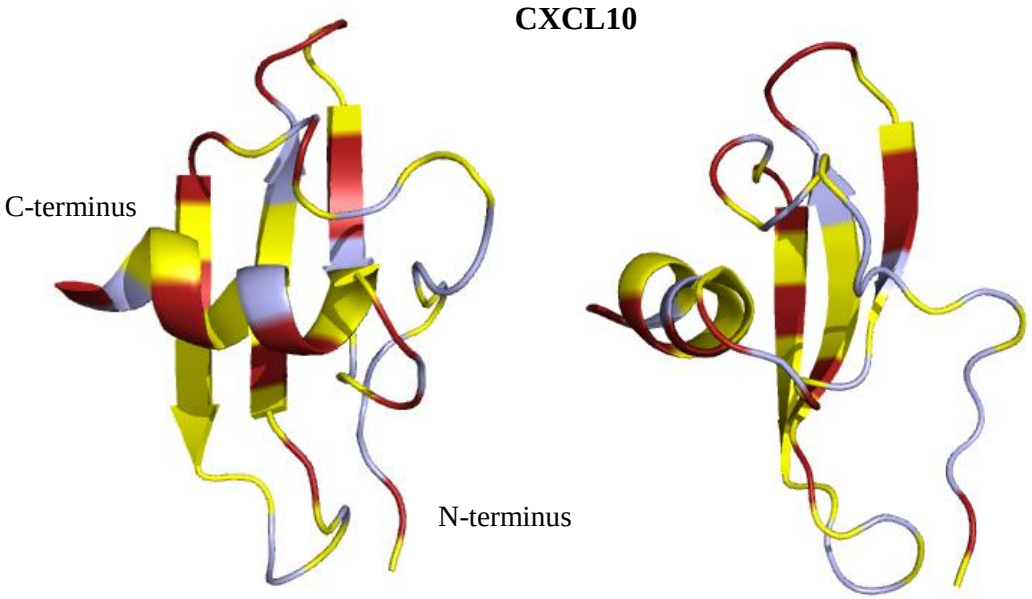
CXCL10
C-terminus
N-terminus

Figure 1.7: Charge and hydrophobicity profiles of CXCL9, CXCL10, and CXCL11 and predicted tertiary structure of CXCL10. (A) The charge and hydrophobicity of CXCL9, CXCL10, and CXCL11 were determined using the Expasy program ProtScale. The charge profiles of the CXC chemokines reveal the C-terminal α-helices contain highly charged amino acids, a characteristic not shared with other chemokine families but similar to α-helical cationic antimicrobial peptides (CAMPs) . Modified from Cole, *et al.*, 2001 (67). (B) Front and side views of the tertiary structure of CXCL10 show the predicted compact nature of the folded protein. Amino acid characteristics have been noted in the following various colors. (Blue): Neutral, (Yellow): Hydrophobic, (Red): Positively charged. Structure modified from the protein database reference number 1080 and analyzed using PyMOL software by K. Margulieux.

……

portions of CXCL9, CXCL10, or CXCL11, then interact via distinctive interactions for each of the three chemokines with the extracellular loops of CXCR3 to activate internal cell signaling pathways (83, 86). Specific amino acid residues in CXCR3 have been identified that result in the activation of different pathways based on which of the IFN-γ-inducible ELR(-) CXC chemokines binds to the CXCR3 receptor (86). CXCR3 can be found on a range of immune cells and is processed into two variants, CXCR3A and CXCR3B (80). Many studies have focused on characterizing the impact CXCR3 activation has on CD4+ Type-1 helper (Th1) cells and CD8+ cytotoxic lymphocytes signaling and chemotaxis. However, CXCR3 is also highly expressed on the innate immune lymphocytes, natural killer cells, dendritic cells, and some B-cells. Interaction of CXCL9, CXCL10, or CXCL11 with CXCR3 found on those immune cells activates the cells to undergo chemotaxis, cell migration, angiostasis, and adhesion (62, 83). The IFN-γ-inducible ELR (-) CXC chemokines, CXCL9, CXCL10, and CXCL11, comprise an important sub-family of chemokines that are vital in maintaining and activating a variety of immune cells through CXCR3.

1.5 Chemokine Antimicrobial Activity

Perhaps pointing to a shared evolutionary past, many chemokines have been found to also exhibit antimicrobial properties (55, 88). Interestingly, cationic antimicrobial peptides (CAMPs) or defensin-like small molecules that are classically defined as antimicrobials, have been shown to demonstrate immunomodulatory activities (55, 88–90). These observations raise interesting possibilities about the role(s) that chemokines and CAMPs or defensin-like small molecules may play in adaptive immune cell maintenance and

activation, as well as serving as a first line of defense within the innate immune system. Chemokines spanning the XC, CC, and CXC families have been demonstrated to kill both Gram-positive and Gram-negative bacterial species such as *Escherichia coli*, *Bacillus* spp., and *Staphylococcus aureus* (67–69, 88, 89, 91). Further demonstrating the range of chemokine microbial targets, anti-fungal effects by interferon-inducible ELR-CXC chemokines have been demonstrated against *Cryptococcus neoformans*, anti-viral effects by CC chemokines have been detected against herpes simplex virus, and anti-parasitic effects by CCL28 have been described against *Leishmania mexicana* (92–95). Studying how chemokines target pathogenic microbes may lead to the development of novel antimicrobial strategies, which is increasingly important given the increase in multi-drug resistant microbes across the globe.

In general, CAMPs and defensin-like small molecules contain secondary structures that influence interaction with and killing of bacterial pathogens, such as amphipathic α-helices or an overall positive charge (88, 96, 97). As mentioned in the above sections, chemokines have a conserved structure of an unstructured N-terminus, three β-sheet backbones, and a C-terminal α-helix. Notably, chemokine-derived peptides from both the N-terminal region of CXCL7 and C-terminal regions from CCL28 have been shown to retain antimicrobial activity (90, 98). Various peptides derived from the N-terminal region of CXCL7 retain comparative antimicrobial activity against *E. coli* and *S. aureus* compared to intact CXCL7, and a C-terminal peptide from CCL28 retains antimicrobial activity against *Candida albicans* (90, 98). However, chemokine peptide derived activity is not conserved in all cases, indicating each chemokine may have unique active properties (69, 91, 99–102). The

overall positive charge of chemokines may point to non-specific membrane interaction and disruption (69). The antimicrobial activity of many chemokines, for example CCL28 and CCL20, is disrupted when tested in high salt conditions, similar to other charged CAMPs and defensin-like small molecules (68, 98, 103). However, salt concentration does not affect antimicrobial activity of CXCL9, CXCL10, or CXCL11 against *B. anthracis* or *Streptococcus pyogenes* (69, 91, 104, 105). Thus, there is a great deal yet to learn about how the structure and charge of various chemokines impact the antimicrobial effects they exert against microbial pathogens.

The IFN-γ-inducible ELR(-) CXC chemokines, CXCL9, CXCL10, and CXCL11, have been demonstrated to kill a wide variety of Gram-positive and Gram-negative bacterial species including *E. coli*, *Listeria monocytogenes*, *S. aureus*, *Citrobacter rodentium*, *Neisseria gonorrhea*, *S. pyogenes*, and *B. anthracis* (67, 69, 101, 104–108). Studies have shown an increase in production of CXCL9, CXCL10, and/or CXCL11 from various cells types in response to bacterial infections at a concentration thought necessary for their antimicrobial activity (67, 104, 105, 107, 109). Chemokine antimicrobial activity is an important component of the innate immune system, and determining the mechanisms by which they kill bacteria may lead to novel antibacterial therapeutics.

1.6 Antimicrobial effect of IFN-γ-inducible ELR(-) CXC chemokines against *B. anthracis*

The IFN-γ-inducible ELR(-) CXC chemokines, CXCL9, CXCL10, and CXCL11, have been demonstrated by our laboratory to exert antimicrobial activity against *B. anthracis*

spores and vegetative cells (105, 110, 111). CXCL9, CXCL10, or CXCL11 treatment results in inhibition of spore germination as well as decrease in spore viability and an antimicrobial killing effect against vegetative cells (Figure 1.8). There is a hierarchical effect of activity such that recombinant human CXCL10 > CXCL9 > CXCL11 in terms of killing potency against both forms of *B. anthracis* (105). Interestingly, it has been observed that there is a different hierarchy of potency with the murine IFN-γ-inducible ELR(-) CXC chemokines, such that murine CXCL9 > CXCL10 > CXCL11 (110). Recombinant human CXCL10 was chosen for use in the majority of subsequent studies in the laboratory since it exhibited the most potent antimicrobial effect of the three recombinant human IFN-γ-inducible ELR(-) CXC chemokines against *B. anthracis* spores and vegetative cells. Treatment of *B. anthracis* spores with CXCL10, or to a lesser degree CXCL9 or CXCL11, resulted in a notable lack of germination in germination-permissive medium as well as a decrease in viability of the spores (105). Immunolocalization of CXCL10 by electron microscopy revealed that CXCL10 localized not only to the exosporium but also to inner layers of the spores, specifically, the spore coat and spore cortex (105). The ability of CXCL10 to penetrate outer spore layers indicates a potential mechanism for anti-spore activity, perhaps through altering of spore germination, viability, or maintenance (105). Treatment of *B. anthracis* vegetative cells with CXCL9 or CXCL10 resulted in significant killing of the bacteria with CXCL10 causing a 4-5 log decrease in colony forming units (CFUs) and CXCL9 causing a 2-3 log decrease in CFUs (105). Immunolocalization electron microscopy studies revealed that CXCL10 primarily localized to the bacterial cell membrane; under light microscopy and electron microscopy, treatment of the vegetative

FIGURE 1.8

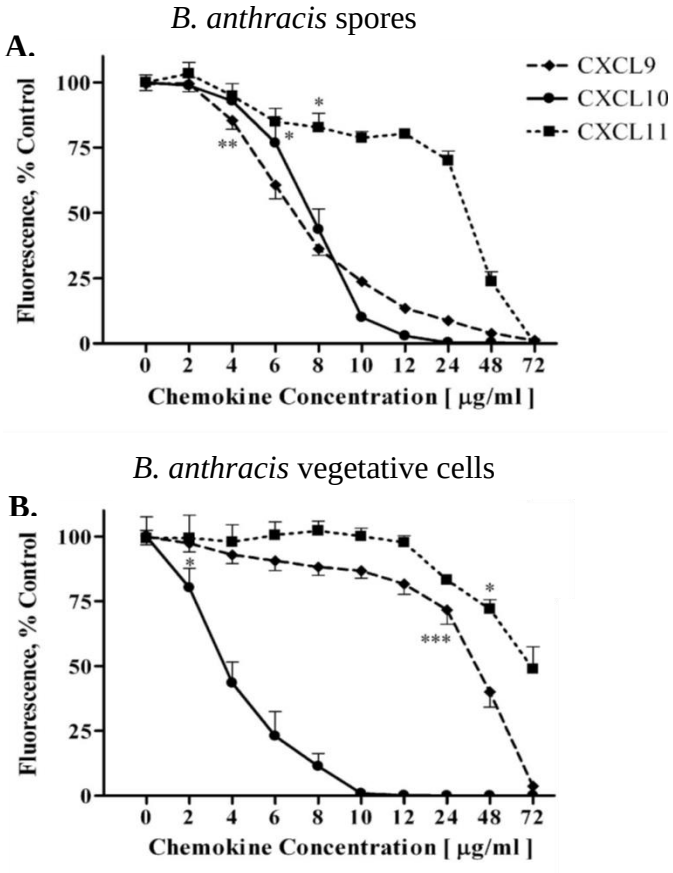

Figure 1.8: Antimicrobial effect of IFN-γ-inducible ELR(-) CXC chemokines against *B. anthracis.* CXCL9, CXCL10, and CXCL10 exhibit an antimicrobial effect against *B. anthracis* spores and vegetative cells. (A) All three chemokines exhibit an antimicrobial effect against spores with differences in potency observed. (B) CXCL10 shows a concentration-dependent effect against vegetative cells with no viability detected at concentrations ≥12 µg/ml. CXCL9 and CXCL11 exert less potent activity with killing only detected at higher concentrations. Modified from Crawford *et al.*, 2009 (105).

cells resulted in eventual destruction of the vegetative bacteria, presumably via dissolution of the cell wall and cell membrane with bacterial cell lysis (105, 111) (Figure 1.9).

Subsequent studies showed the *in vitro* killing of *B. anthracis* by the IFN-γ-inducible ELR(-) CXC chemokines was biologically relevant by using *in vivo* murine studies with antibody neutralization of these CXC chemokines or their CXCR3 receptor. An inhalational anthrax murine model using C57BL/6 mice was used to study the impact of CXCL9, CXCL10, and CXCL11 during spore lung infection. C57BL/6 mice are resistant to inhalational *B. anthracis* Sterne strain spore infection, in contrast to other mouse strains, such as A/J mice that are highly susceptible to Sterne strain lung infection. Initial mouse studies conducted by the Hughes laboratory revealed that C57BL/6 mice produce significantly higher concentrations of CXCL9, CXCL10, and/or CXCL11 in the lungs during an inhalational anthrax infection as compared to A/J mice under the same conditions (105). Therefore, antibody neutralization of CXCL9, CXCL10, and/or CXCL11 was performed to test the biological relevance of these chemokines during infection in C57BL/6 mice (110). Importantly, antibody neutralization of CXCL9 or CXCL9/CXCL10 or CXCL9/CXCL10/CXCL11 resulted in significant mortality of the mice (110). Since CXCL9, CXCL10, and CXCL11 are also involved in immune cell recruitment, the receptor CXCR3 was neutralized to test if disruption of this specific receptor responsible for signaling chemotaxis in response to the chemokines was responsible for the higher mortality observed. However, CXCR3 neutralization had no impact on mortality, such that the mouse survival results were the same as with control mice that received serum only with no antibody neutralization (110). This result supported there is an antimicrobial

FIGURE 1.9

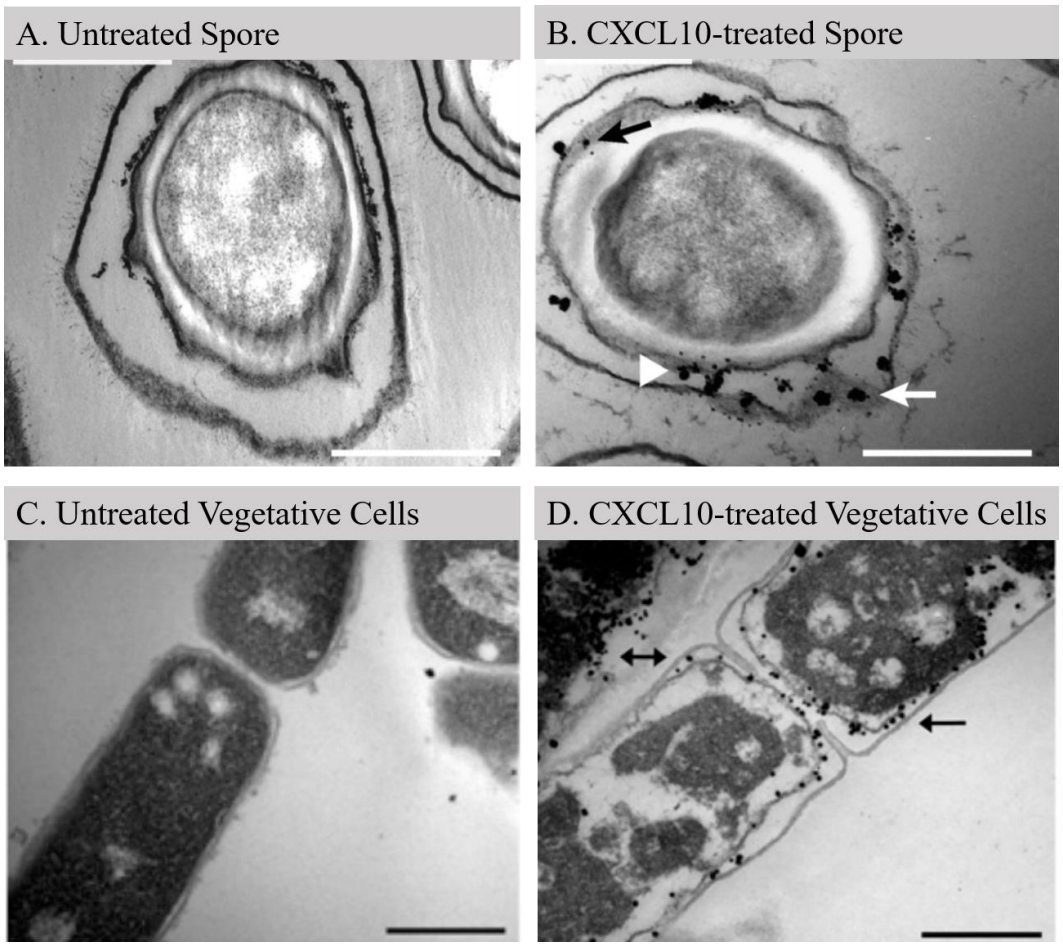
A. Untreated Spore
B. CXCL10-treated Spore
C. Untreated Vegetative Cells
D. CXCL10-treated Vegetative Cells

Figure 1.9: CXCL10 localization in *B. anthracis* spores and vegetative cells. (A) Untreated spore. (B) CXCL10 treated spore. Arrows indicate CXCL10 localization to the spore coat/cortex interface as well as the exosporium, as detected by anti-CXCL10 immunogold antibody localization by transmission electron microscopy at 30,000x magnification. Scale bar is 0.5 μm. Modified from Crawford *et al.,* 2009 (105). (C) Untreated vegetative cell. (D) CXCL10 treated vegetative cell. Arrows indicate CXCL10 localization to the bacterial cell membrane, again, detected by anti-CXCL10 immunogold antibody localization with 30,000x magnification. Scale bar is 0.5 μm. Modified from Crawford *et al.,* 2011 (111).

……

killing effect through direct chemokine interaction with *B. anthracis* rather than via an indirect recruitment of immune cells to the site of infection (110) (Figure 1.10).

A *B. anthracis* transposon library screen was conducted to identify bacterial components important in mediating the antimicrobial activity of CXCL10 (111). This innovative forward genetics screen resulted in the identification of three *B. anthracis* vegetative cell genes, *ftsX*, *BAS0651*, and *lytE* as being important for mediating the antimicrobial activity of CXCL10 (111). Transposon disruption of *ftsX* in *B. anthracis* Sterne strain resulted in the highest degree of resistance to CXCL10 compared to the parent strain (111). Transposon disruption of *BAS0651* in vegetative cells conferred an intermediate degree of resistance to CXCL10 (111). Transposon disruption of *lytE* resulted in a low level of resistance to CXCL10 (111) (Figure 1.11). The gene *ftsX* is a membrane component of an ABC transporter-like complex that is thought to be involved with peptidoglycan processing during cellular elongation (112, 113). *BAS0651* and *lytE* are both *B. anthracis* hypothetical proteins that contain hydrolytic domains, suggesting a potential role in processing peptidoglycan bonds within the bacterial cell wall during growth and/or spore formation. While these observations established the foundation for identifying and understanding CXCL10 antimicrobial activity against *B. anthracis*, the exact mechanism of action for CXCL10-mediated bacterial killing has remained unclear and was the focus of the work leading to the subsequent chapters of this dissertation.

FIGURE 1.10

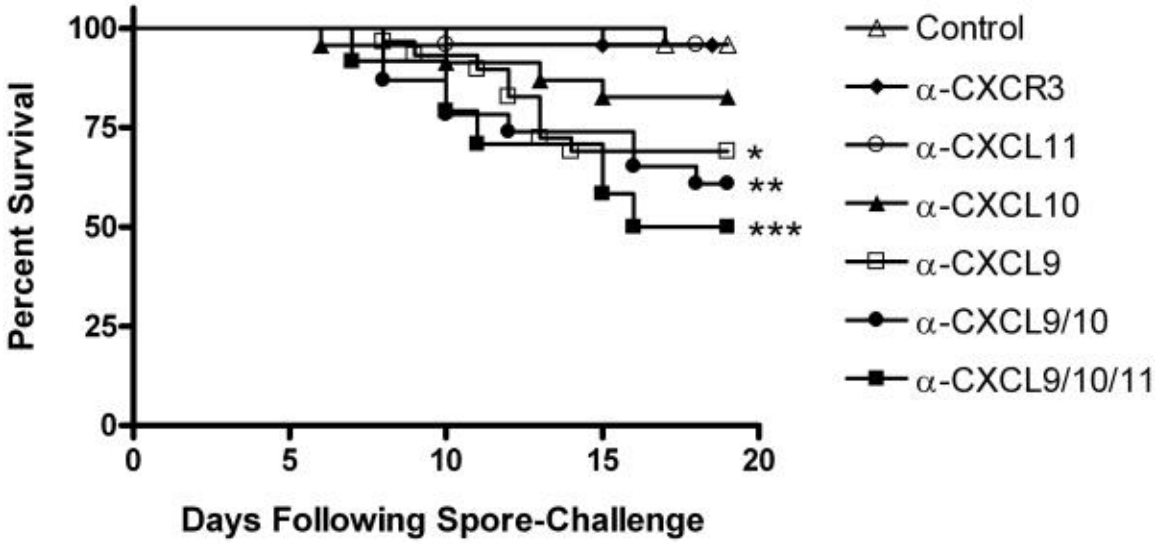

Figure 1.10: IFN-γ-inducible ELR(-) CXC chemokine or CXCR3 neutralization *in vivo.* Antibody neutralization of CXCL9, CXCL10, and/or CXCL11 resulted in a higher mortality rate in a C57BL/6 mouse strain that is inherently resistant to pulmonary spore infection. Neutralization of the chemokine receptor CXCR3 did not impact survival, indicating a biological role for direct antimicrobial activity of the chemokines against the bacteria at the site of infection. Modified from Crawford, *et al.*, 2010 (110).

FIGURE 1.11

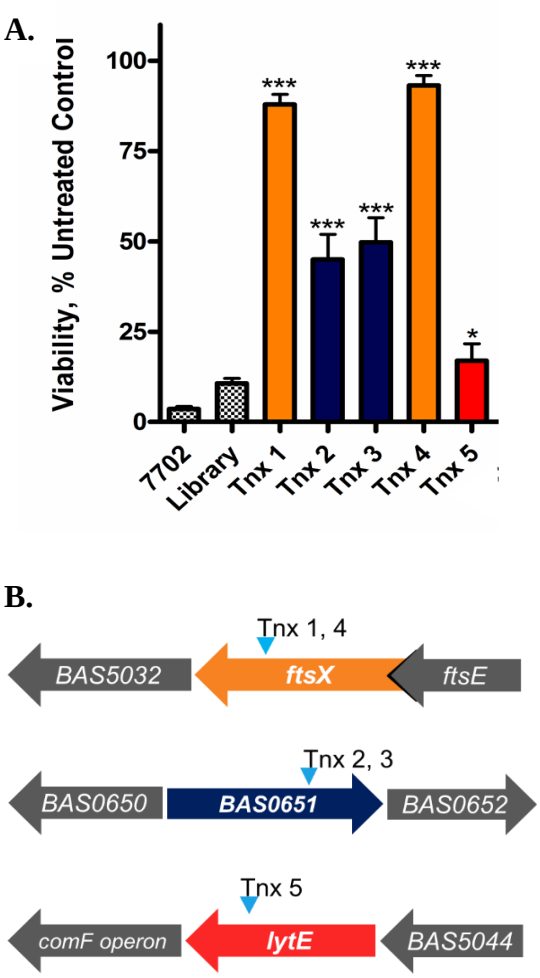

Figure 1.11: Transposon library screen to identify *B. anthracis* genes involved in CXCL10-mediated antimicrobial effect. (A-B) Three genes were identified by a transposon library screen that, when disrupted, conferred resistance to CXCL10. Disruption of *ftsX* resulted in the highest level of resistance, *BAS0651* disruption resulted in an intermediate level of resistance, and *lytE* disruption resulted in a low level of resistance. Modified from Crawford *et al.*, 2011 (111).

1.7 Dissertation Research Aims and Significance

B. anthracis is a widespread pathogen that has the added risk of being developed into a potential bioweapon. Combined with concerns regarding emergence of multi-drug antibiotic resistance in bacteria throughout the world, the development of new therapeutic strategies is urgently needed. Development of novel therapies that will kill both the spore form and vegetative form of an organism such as *B. anthracis* would be both innovative and the basis for new antimicrobials that target multiple forms of an organism. The goal of the research presented in this dissertation is to determine the antimicrobial mechanism(s) of action that CXCL10 utilizes to kill *B. anthracis* vegetative cells and spores. The aims are 1) Determine the role of bacterial FtsX in CXCL10 antimicrobial activity (Chapter 2 and 3) and 2) Identify portions of CXCL10 important for a bactericidal effect against *B. anthracis* (Chapter 2) and 3) Identify spore target(s) of CXCL10 using a *B. anthracis* spore transposon library screen and determine the role that identified bacterial components have during spore inhibition and/or killing (Chapter 3).

CHAPTER 2:

CXCL10 Acts as a Bifunctional Antimicrobial Molecule against *Bacillus anthracis*

Adapted from: Margulieux KR, Fox JW, Nakamoto RK, Hughes MA (2016). CXCL10 Acts as a Bifunctional Antimicrobial Molecule against *Bacillus anthracis*. *mBio*. 7(3): pii: e00334-16.

2.1 Abstract

Bacillus anthracis is killed by the interferon-inducible ELR(-) CXC chemokine, CXCL10. Previous studies showed disruption of the gene encoding FtsX, a conserved membrane component of the ABC transporter-like complex FtsE/X, resulted in resistance to CXCL10. FtsX exhibits some sequence similarity to the CXCL10 mammalian receptor, CXCR3, suggesting that the CXCL10 N-terminal region that interacts with CXCR3 may also interact with FtsX. A C-terminal truncated CXCL10 was tested to determine if the FtsX-dependent antimicrobial activity was associated with the CXCR3-interacting N-terminus. The truncated CXCL10 exhibited antimicrobial activity against the *B. anthracis* parent strain but not Δ*ftsX*, which supports a key role for the CXCL10 N-terminus. Mutations in FtsE, the conserved ATP-binding protein of the FtsE/X complex, resulted in resistance to both CXCL10 and truncated CXCL10, indicating that both FtsX and FtsE are important. Higher concentrations of CXCL10 overcame resistance of the Δ*ftsX* mutant to CXCL10, suggesting an FtsX-independent killing mechanism, likely involving its C-terminal α-helix, which resembles a cationic antimicrobial peptide. Membrane depolarization studies revealed that CXCL10 disrupted membranes of *B. anthracis* parent strain and Δ*ftsX*, but only the parent strain underwent depolarization with truncated CXCL10. These findings suggest that CXCL10 is a bifunctional molecule that kills *B. anthracis* by two mechanisms. The FtsE/X-dependent killing is mediated through an N-terminal portion of CXCL10 and is not reliant upon the C-terminal α-helix. The FtsE/X-independent mechanism involves membrane depolarization by CXCL10, likely due to its α-helix. These findings present a new paradigm for understanding mechanisms by which CXCL10 and related chemokines kill bacteria.

2.2 Introduction

Infections caused by Gram-positive and Gram-negative bacteria are a major cause of morbidity and mortality worldwide (114). A wide variety of strategies have evolved to prevent or treat these infections. With the global increase in multi-drug resistant bacterial pathogens, current antibiotic therapies are becoming less reliable, highlighting the need for the development of new treatment strategies. Amongst a wide variety of molecules being studied as novel antimicrobials, chemokines represent a distinct class of proteins. Chemokines are small proteins, 8-10 kilodaltons, known best for their highly potent chemoattractant properties that serve an immunomodulatory role within both the innate and adaptive immune systems (54–57, 115). Chemokines were initially studied for their ability to attract adaptive immune cells into sites of injury or inflammation. However, they also play a key role in a variety of physiological processes such as angiogenesis and hematopoiesis (58, 60, 62, 78, 86, 116). Interestingly, over the past twenty years, there has been increasing recognition of a direct antimicrobial effect of multiple chemokines (67–69, 89, 90, 105, 107). While antimicrobial activity against Gram-negative and Gram-positive bacteria, viruses, and fungi has been reported for a variety of chemokines, the mechanism(s) through which that effect is achieved remains widely uncharacterized.

CXCL10 is an interferon-inducible, Glu-Leu-Arg-negative (ELR(-)) CXC chemokine, a group that also includes CXCL9 and CXCL11 (80). It exerts direct antimicrobial activity against a wide variety of Gram-negative and Gram-positive bacteria such as *Escherichia coli, Staphylococcus aureus, Listeria monocytogenes, and Bacillus anthracis* (67, 68, 90, 105). Additionally, CXCL10 exerts an antimicrobial effect against both laboratory strains

and clinical isolates of *E. coli*, including a multi-drug resistant strain obtained from a clinical sample (108). Like other chemokines, the structure of CXCL10 consists of a relatively unstructured N-terminus, three antiparallel β-sheets, and a C-terminal amphipathic α-helix (71, 82, 85). The interferon-inducible ELR(-) CXC chemokines interact with CXCR3, a receptor that is found on host immune cells such as T-cells, B-cells, and natural killer cells (83, 117). These chemokines bind to the receptor via a series of interactions that are dependent upon the interaction of the chemokine N-terminus with the extracellular domain of CXCR3 (aa 1-35) (86, 87). Further interaction of the chemokine N-terminus and β-sheets with other regions of CXCR3 then occurs in order to activate the signaling cascade necessary to initiate chemotaxis of host immune cells (83, 86, 87).

B. anthracis is a Gram-positive, spore-forming bacterium that causes the disease anthrax following exposure of susceptible mammals to spores and their subsequent germination into vegetative bacilli (1, 2, 14, 118). Our laboratory has previously shown that CXCL10 exhibits *in vitro* antimicrobial activity against both *B. anthracis* spores and vegetative cells (105, 110). *In vivo* neutralization of CXCL10 resulted in significantly higher mortality in a mouse lung infection model with C57BL/6 mice, which are inherently resistant to intranasal infection by *B. anthracis* Sterne strain (110). Blocking of CXCR3 resulted in no difference in survival compared to control (vehicle treated) mice (110). These *in vivo* data support a direct antimicrobial role for CXCL10 that is unrelated to its interaction with CXCR3 and suggest CXCL10 is produced locally at a high enough concentration to actively kill the bacteria at sites of infection. Given the charge and structural similarity of

the CXCL10 C-terminal α-helix to cationic antimicrobial peptides, it was initially hypothesized that the α-helix was responsible for its antimicrobial activity, likely via membrane disruption based on characterized mechanisms utilized by cationic antimicrobial peptides, like LL37 (69, 119, 120).

Our laboratory previously screened a *B. anthracis* Sterne strain transposon mutant library to identify bacterial gene products associated with the antimicrobial activity of recombinant human CXCL10 (105, 110, 111). Of particular interest was the finding that disruption of the *ftsX* gene, which encodes FtsX, resulted in resistance of *B. anthracis* vegetative cells to CXCL10 (111). FtsX is a conserved membrane component of the FtsE/X complex that appears to be a prokaryotic ATP-binding cassette (ABC) transporter (111, 121–123). The FtsE/X complex in other bacterial species such as *Bacillus subtilis*, *E. coli*, and *Mycobacterium tuberculosis* has been shown to play a key role in cell wall peptidoglycan processing through the activation of peptidoglycan hydrolytic enzymes by FtsX (112, 113, 122–124). FtsE possesses conserved Walker motifs that are responsible for ATP binding and hydrolysis (112, 125, 126). Work conducted by others using *B. subtilis* and *M. tuberculosis* suggests that ATP hydrolysis by FtsE induces a conformational change in FtsX resulting in the activation of peptidoglycan hydrolases for cell wall processing, a critical function for maintaining bacterial cell integrity (112, 113). Major classes of antimicrobials (e.g., beta-lactam antibiotics) kill bacteria by inhibiting specific steps in peptidoglycan synthesis, which also affects bacterial cell integrity (127).

In silico protein analysis of *B. anthracis* FtsX revealed that a twenty-seven amino acid region (aa 54-80) in the large external loop had 45% similarity to the N-terminal amino acid sequence of CXCR3 (aa 9-35), the mammalian receptor for CXCL10 (111). Importantly, this N-terminal amino acid sequence is involved in binding the N-terminal region of CXCL10 (59, 86, 128). The similarity between CXCR3 and FtsX suggested that the N-terminal region of CXCL10 may also interact with the CXCR3-similar region of FtsX. Thus, the antimicrobial activity of CXCL10 may be primarily the result of a receptor-mediated effect that leads to cell lysis and not necessarily to depolarization resulting from the insertion of the C-terminal α-helix into the cytoplasmic membrane. In the present study, we investigated two potential ways by which CXCL10 may kill bacteria. Our data suggest that the antimicrobial activity of CXCL10 is mediated by its interaction with FtsE/X, which utilizes a separate mechanism than that of the C-terminal α-helix. In the absence of functional FtsE/X, higher concentrations of CXCL10 exhibit a bactericidal effect that appears to be dependent on the presence of its C-terminal α-helix and general membrane depolarization. However, the end result of each pathway (i.e., cell lysis) is the same, with killing of *B. anthracis* being the most effective when both mechanisms are present and active.

2.3 Results

CXCR3-similar region of FtsX is involved in CXCL10 interaction with *B. anthracis*

FtsE/X is widely conserved among Gram-positive and Gram-negative bacterial species with a similarity ranging between 46-75% as determined by Blastp analysis and amino acid sequence alignment (Text 2.1) (129, 130). In general, bacterial FtsX protein structures

……

Text 2.1

Sequence alignment of FtsX from representative bacterial species

Ba: *B. anthracis* parent (Gram-positive)

Bs: *B. subtilis* (Gram-positive) 60% identity; 75% positive

Mt: *M. tuberculosis* (Acid-fast) 22% identity; 46% positive

Sp: *S. pneumoniae* (Gram-positive) 41% identity; 60% positive

Ec: *E. coli* (Gram-negative) 28% identity; 49% positive

Kp: *K. pneumoniae* (Gram-negative) 26% identity; 47% positive

% Identity and % Positive are notated when compared to *B. anthracis* FtsX after Blastp analysis.

Red underline designates CXCR3-similar regions of *B. anthracis* parent strain FtsX.

Black highlighting designates conserved residues, gray highlighting designates characteristically similar residues.

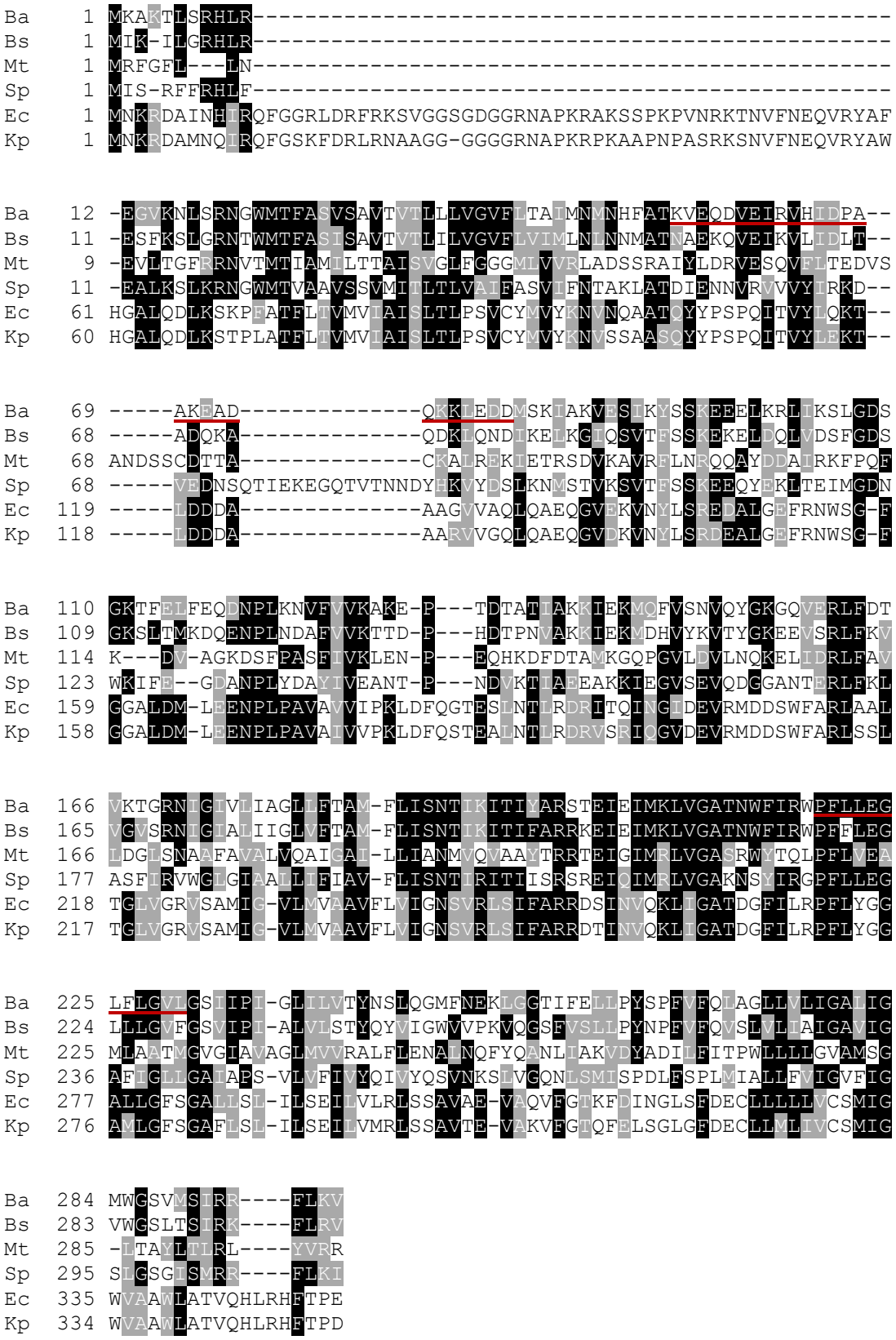
Ba 1 MKAKTLSRHLR
Bs 1 MIK-ILGRHLR
Mt 1 MRFGFL---LN
Sp 1 MIS-RFFRHLF
Ec 1 MNKRDAINHIRQFGGRLDRFRKSVGGSGDGGRNAPKRAKSSPKPVNRKTNVFNEQVRYAF
Kp 1 MNKRDAMNQIRQFGSKFDRLRNAAGG-GGGGRNAPKRPKAAPNPASRKSNVFNEQVRYAW
Ba 12 -EGVKNLSRNGWMTFASVSAVTVTLLLVGVFLTAIMNMNHFATKVEQDVEIRVHIDPA--
Bs 11 -ESFKSLGRNTWMTFASISAVTVTLILVGVFLVIMLNLNNMATNAEKQVEIKVLIDLT--
Mt 9 -EVLTGFRRNVTMTIAMILTTAISVGLFGGGMIVVRLADSSRAIYLDRVESQVFLTEDVS
Sp 11 -EALKSLKRNGWMTVAAVSSVMITLTLVAIFASVIFNTAKLATDIENNVRVVVYIRKD--
Ec 61 HGALQDLKSKPFATFLTVMVLAISLTLPSVCYMVYKNVNQAATQYYPSPQITVYLQKT--
Kp 60 HGALQDLKSTPLATFLTVMVLAISLTLPSVCYMVYKNVSSAASQYYPSPQITVYLEKT--
Ba 69 -----AKEAD--------------QKKLEDDMSKIAKVESIKYSSKEEELKRLIKSLGDS
Bs 68 -----ADQKA--------------QDKLQNDIKELKGIQSVTFSSKEKELDQLVDSFGDS
Mt 68 ANDSSCDTTA--------------CKALREKIETRSDVKAVRFLNRQQAYDDAIRKFPQF
Sp 68 -----VEDNSQTIEKEGQTVTNNDYHKVYDSLKNMSTVKSVTFSSKEEQYEKLTEIMGDN
Ec 119 -----LDDDA--------------AAGVVAQLQAEQGVEKVNYLSREDALGEFRNWSG-F
Kp 118 -----LDDDA--------------AARVVGQLQAEQGVDKVNYLSRDEALGEFRNWSG-F
Ba 110 GKTFELFEQDNPLKNVFVVKAKE-P---TDTATLAKKIEKMQFVSNVQYGKGQVERLFDT
Bs 109 GKSLTMKDQENPLNDAFVVKTTD-P---HDTPNVAKKIEKMDHVYKVTYGKEEVSRLFKV
Mt 114 K---DV-AGKDSFPASFIVKLEN-P---EQHKDFDTAMKGQPGVLDVLNQKELIDRLFAV
Sp 123 WKIFE--GDANPLYDAYIVEANT-P---NDVKTIAEEAKKIEGVSEVQDGGANTERLFKL
Ec 159 GGALDM-LEENPLPAVAVVIPKLDFQGTESLNTLRDRITQINGIDEVRMDDSWFARLAAL
Kp 158 GGALDM-LEENPLPAVAIVVPKLDFQSTEALNTLRDRVSRIQGVDEVRMDDSWFARLSSL
Ba 166 VKTGRNIGIVLIAGLLFTAM-FLISNTIKITIYARSTEIEIMKLVGATNWFIRWPFLLEG
Bs 165 VGVSRNIGIALIIGLVFTAM-FLISNTIKITIFARRKEIEIMKLVGATNWFIRWPFFLEG
Mt 166 LDGLSNAAFAVALVQAIGAI-LLIANMVQVAAYTRRTEIGIMRLVGASRWYTQLPFLVEA
Sp 177 ASFIRVWGLGIAALLIFIAV-FLISNTIRITIISRSREIQIMRLVGAKNSYIRGPFLLEG
Ec 218 TGLVGRVSAMIG-VLMVAAVFLVIGNSVRLSIFARRDSINVQKLIGATDGFILRPFLYGG
Kp 217 TGLVGRVSAMIG-VLMVAAVFLVIGNSVRLSIFARRDTINVQKLIGATDGFILRPFLYGG
Ba 225 LFLGVLGSIIPI-GLILVTYNSLQGMFNEKLGGTIFELLPYSPFVFQLAGLLVLIGALIG
Bs 224 LLLGVFGSVIPI-ALVLSTYQYVIGWVVPKVQGSFVSLLPYNPFVFQVSLVLIAIGAVIG
Mt 225 MLAATVGVGIAVAGLMVVRALFLENALNQFYQANLIAKVDYADILFITPWLLLLGVAMSG
Sp 236 AFIGLIGAIAPS-VLVFIVYQIVYQSVNKSLVGQNLSMISPDLFSPLMIALLFVIGVFIG
Ec 277 ALLGFSGALLSL-ILSEILVLRLSSAVAE-VAQVFGTKFDINGLSFDECLLLLLVCSMIG
Kp 276 AMLGFSGAFLSL-ILSEILVMRLSSAVTE-VAKVFGTQFELSGLGFDECLLMLIVCSMIG
Ba 284 MWGSVMSIRR----FLKV
Bs 283 VWGSLTSIRK----FLRV
Mt 285 -LTAYLTLRL----YVRR
Sp 295 SLGSGISMRR----FLKI
Ec 335 WVAAWLATVQHLRHFTPE
Kp 334 WVAAWLATVQHLRHFTPD

Text 2.1: Supplemental Bacterial FtsX Amino Acid Sequence Alignments. An amino acid sequence alignment using *B. anthracis* Sterne strain FtsX as the reference protein was conducted with select Gram-positive, acid-fast, and Gram-negative bacterial species. FtsE/X is widely conserved among bacterial species with a similarity ranging between 46-75% as determined by Blastp analysis and amino acid sequence alignment. The following species and FtsX identification codes were used to perform individual Blastp analyses: *B. anthracis* Sterne (AAT57322.1), *B. subtilis* 168 (NP_391405.1), *M. tuberculosis* H37Rv (CAA49620.1), *S. pneumoniae* (AJD71681.1), *E. coli* F11 (EDV68789.1), and *K. pneumoniae* (KLA37751.1). Full sequence alignment of all six strains was conducted using the multiple sequence alignment software T-Coffee (http://tcoffee.crg.cat/apps/tcoffee/do:regular) and formatted using the program Boxshade (http://www.ch.embnet.org/software/BOX_form.html) (129, 130).

……

consist of four transmembrane domains and two extracellular loops although functional differences have been observed between the FtsX of Gram-positive and Gram-negative bacterial species (111, 125). In Gram-positive bacteria, FtsX, along with FtsE, exists as an FtsE/X complex that is involved in peptidoglycan processing during cellular elongation and spore formation. In Gram-negative bacteria, FtsX and its FtsE/X complex have been shown to direct peptidoglycan processing at the bacterial septum during cell division (112, 113, 122–124, 131). Our initial investigation into *B. anthracis* FtsX identified two regions of similarity between FtsX and the known mammalian CXCL10 receptor, CXCR3 (Text 2.1). While those specific regions are not conserved between Gram-positive and -negative species, there are other regions of similarity between CXCR3 and FtsX, notably located in the exposed outer loops (132). In this study, the focus of investigation involved the region of *B. anthracis* FtsX (aa 54-80) with sequence similarity to the region of human CXCR3 (aa 9-35) that is primarily responsible for chemokine binding, since that similarity between FtsX and CXCR3 suggested a region for possible interaction with CXCL10.

A peptide competition assay was performed to determine if the CXCR3-similar region of FtsX was involved in facilitating antimicrobial activity of CXCL10. A 27 amino acid peptide representing the CXCR3-similar region of FtsX was synthesized, as well as a scrambled peptide to control for sequence specificity (Figure 2.1A). The antimicrobial activity of CXCL10 alone or the peptide:CXCL10 mixture against *B. anthracis* Sterne strain, hereby designated as parent strain, was examined after two hours of incubation (111). There was a statistically significant increase in the survival of bacteria exposed to

FIGURE 2.1

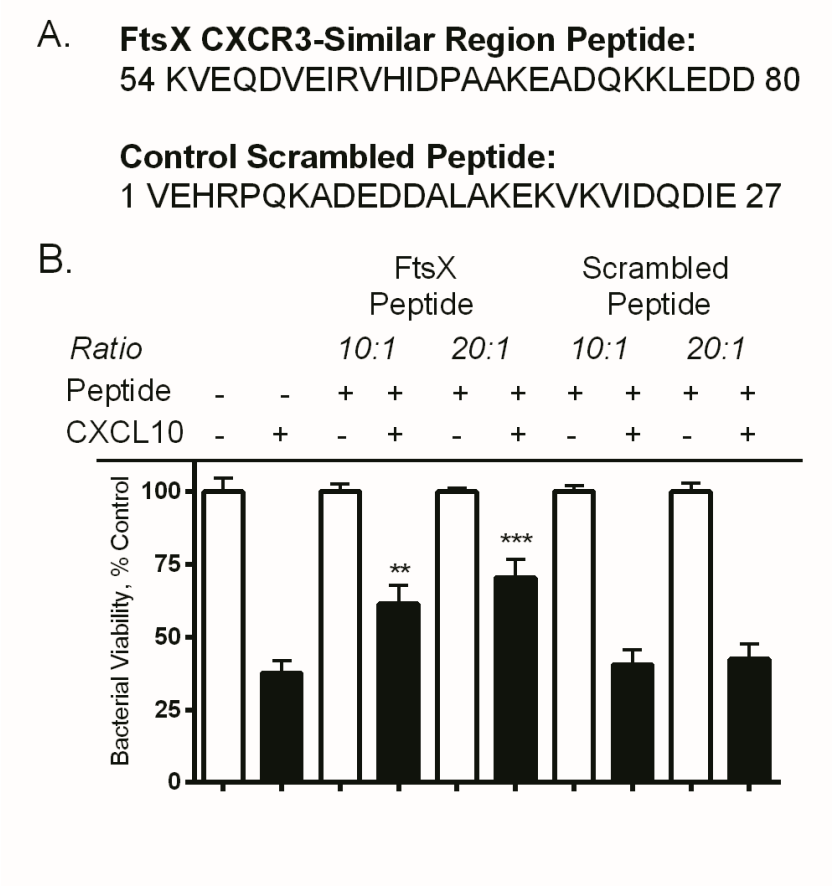
A.
FtsX CXCR3-Similar Region Peptide:
54 KVEQDVEIRVHIDPAAKEADQKKLEDD 80
Control Scrambled Peptide:
1 VEHRPQKADEDDALAKEKVKVIDQDIE 27
B.
FtsX Peptide
Scrambled Peptide
Ratio
10:1
20:1
10:1
20:1
Peptide - - + + + + + + + +
CXCL10 - + - + - + - + - +
Bacterial Viability, % Control
100
75
50
25
0
**
***

Figure 2.1: CXCR3-similar region of FtsX is important in mediating CXCL10 antimicrobial activity against *B. anthracis* parent strain. (A) A synthetic peptide consisting of the 27 amino acids (aa 54-80) of FtsX with similarity to the CXCR3 binding region (aa 9-35) of CXCL10 (111) and scrambled control. (B) A peptide competition assay with FtsX peptide in a 10:1 or 20:1 molar ratio with 0.46 μM CXCL10 resulted in a statistically significant decrease in the killing of *B. anthracis* parent strain when compared to killing by CXCL10 alone. Incubation with the control peptide had no effect on killing. Bacterial viability was measured using Alamar blue reduction, and fluorescence units were expressed as a percentage of the strain-specific untreated control. Data points represent mean values ± SEM; n=3 separate experiments using triplicate wells. $^{**}p \leq 0.001$, $^{***}p \leq 0.0001$

……

the FtsX peptide:CXCL10 mixture at molar ratios of both 10:1 and 20:1 (Figure 2.1B). No significant increase in survival was observed with the scrambled peptide:CXCL10 competition assay (Figure 2.1B). These results suggested that the CXCR3-similar region of FtsX was important in mediating the antimicrobial effect of CXCL10, and that the interaction required a specific sequence and was not just due to peptide charge interactions.

C-terminal truncated CXCL10 (CTTC) synthesis and physical characteristics

The importance of the CXCR3-similar region of FtsX indicated a possible site for the interaction of CXCL10 with *B. anthracis*. It was previously determined through the work of others that the relatively unstructured N-terminal region of CXCL10 initially interacts with CXCR3, resulting in immune cell activation (86, 87). We hypothesized that the N-terminal region of CXCL10 may also interact with bacterial FtsX, resulting in an antimicrobial effect. The amphipathic α-helix of various chemokines has been considered to be the portion of the protein responsible for antimicrobial activity because of its positive charge and secondary structural resemblance to cationic antimicrobial peptides and defensins (69, 119, 120). However, since our findings unexpectedly implicated the N-terminal portion of CXCL10 in eliciting an antimicrobial effect, we conducted the following series of experiments.

To determine if it was the N-terminal region or the C-terminal α-helix of CXCL10 that was responsible for antimicrobial activity against *B. anthracis*, a truncated CXCL10 protein was synthesized that lacked the C-terminal 23 amino acids (Figure 2.2A). The sequence

FIGURE 2.2

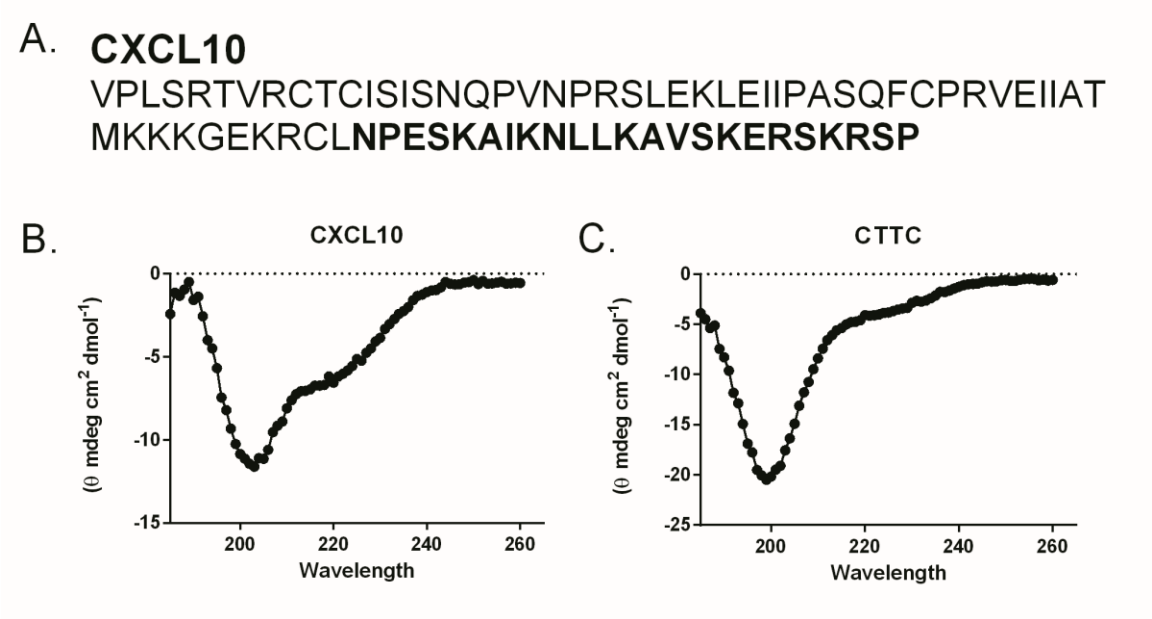

Figure 2.2: Complete amino acid sequence and secondary structure comparison of CXCL10 and C-terminal truncated CXCL10 (CTTC). (A) Amino acid sequences for intact CXCL10 and synthetic protein CTTC (aa 1-54) lacking the C-terminal α-helix. Amino acids removed from intact CXCL10 are indicated in bold. (B-C) Circular dichroism showed a distinct alpha helical pattern in the intact CXCL10 spectrum, as indicated by peaks at wavelengths of 190 and 210 nm; these peaks were absent in the CTTC spectrum. The calculated β-sheet content from both the CXCL10 and CTTC spectra was consistent with the estimated percentage of β-sheets from the published CXCL10 crystal structure (45).

of the C-terminal truncated CXCL10 (CTTC) was confirmed by mass spectrometry (data not shown). Circular dichroism (CD) spectra confirmed that CTTC lacked the α-helical content as evidenced by an absence of characteristic spectral peaks at 190 and 210 nm compared to intact CXCL10 (Figure 2.2B and 2.2C). Importantly, analysis of the CTTC spectrum revealed that the content of β-strands (39%) was similar to that of the properly folded chemokine based on the published crystal structure, thus, confirming that the secondary structures of CTTC were intact (PBD: 1080) (85, 128, 133).

C-terminal truncated CXCL10 retained antimicrobial activity against *B. anthracis* parent strain

Various concentrations of CXCL10 and CTTC were compared for antimicrobial activity against *B. anthracis* parent strain. Concentrations were based on μM instead of the previously published μg ml^{-1} due to mass difference between CXCL10 and CTTC (111). A concentration-dependent killing of *B. anthracis* parent strain was observed with no viable bacteria detected at concentrations ≥ 1.2 μM CXCL10. CTTC also exhibited concentration-dependent killing, but was less potent than intact CXCL10 (Figure 2.3A). A statistically significant difference in antimicrobial activity was observed between CXCL10 and CTTC at all concentrations. Thus, in the absence of the amphipathic α-helix, CTTC retained some antimicrobial activity, suggesting that the N-terminus and other portions of CXCL10 could kill *B. anthracis* by a mechanism that was independent of the presence of the C-terminal α-helix.

FIGURE 2.3

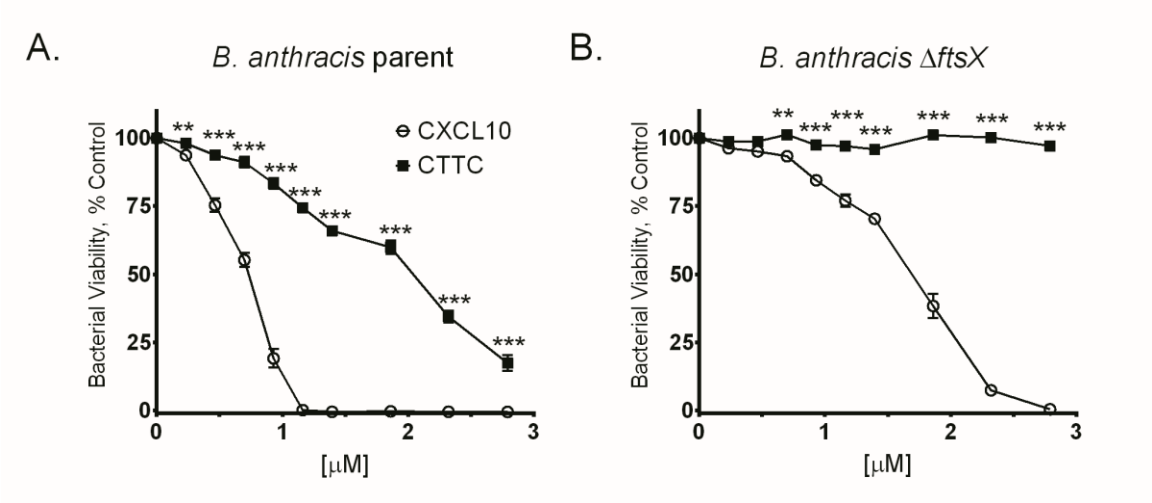

Figure 2.3: Antimicrobial activity of C-terminal truncated CXCL10 (CTTC) was retained, albeit less potently, against *B. anthracis* parent strain but not against *B. anthracis* Δ*ftsX*. (A) The CTTC killed *B. anthracis* parent strain but was less potent than intact CXCL10 at concentrations ranging from 0-2.8 μM. (B) CTTC at 0-2.8 μM exhibited no antimicrobial effect against *B. anthracis* Δ*ftsX* with a statistical difference observed between intact CXCL10 versus CTTC. Bacterial viability was measured using Alamar blue reduction, and fluorescence units were expressed as a percentage of the strain-specific untreated control. Data points represent mean values ± SEM; n=3 separate experiments using triplicate wells in each experiment. $^{**}p \leq 0.001$, $^{***}p < 0.0001$

B. anthracis Δ*ftsX* is not susceptible to CTTC

Based on previous studies in our laboratory (111), *B. anthracis* Δ*ftsX* was relatively resistant to CXCL10 when compared with the parent strain. However, this resistance could be overcome with higher concentrations of CXCL10 (Figure 2.3B). In a previously published study, we showed that complementation of *B. anthracis* Δ*ftsX* with the plasmid pUVA113 encoding an isopropyl β-D-1-thiogalactopyranoside (IPTG) -inducible wild-type *ftsX* gene restored susceptibility to CXCL10 compared to Δ*ftsX* complemented with the empty control vector pUTE973 (111). Therefore, to investigate whether the CXCL10 C-terminal α-helix played a role in this killing, the antimicrobial activity of CTTC was assessed against *B. anthracis* Δ*ftsX*. In the absence of both FtsX and the CXCL10 α-helix, no antimicrobial activity was observed (Figure 2.3B). A statistically significant difference was observed between the activity of CXCL10 and that of CTTC against Δ*ftsX* at all concentrations ≥ 0.70 μM. The *ftsX* complemented strain, *B. anthracis* Δ*ftsX* pUVA113, was susceptible to CTTC, whereas Δ*ftsX* complemented with an empty vector plasmid pUTE973, remained resistant (Figure 2.4). These results suggested at least two possible mechanisms by which CXCL10 kills *B. anthracis*: 1) one mechanism is mediated through the interaction between the N-terminal region of CXCL10 and the bacterial FtsX and does not require the C-terminal α-helix (Figure 2.3A); and 2) a second mechanism, observed at higher concentrations of intact CXCL10 and in the absence of bacterial FtsX, requires the presence of the C-terminal α-helix (Figure 2.3B).

B. anthracis FtsE Walker motif mutant strain

To test whether an active FtsE/X complex is necessary for CXCL10-mediated

FIGURE 2.4

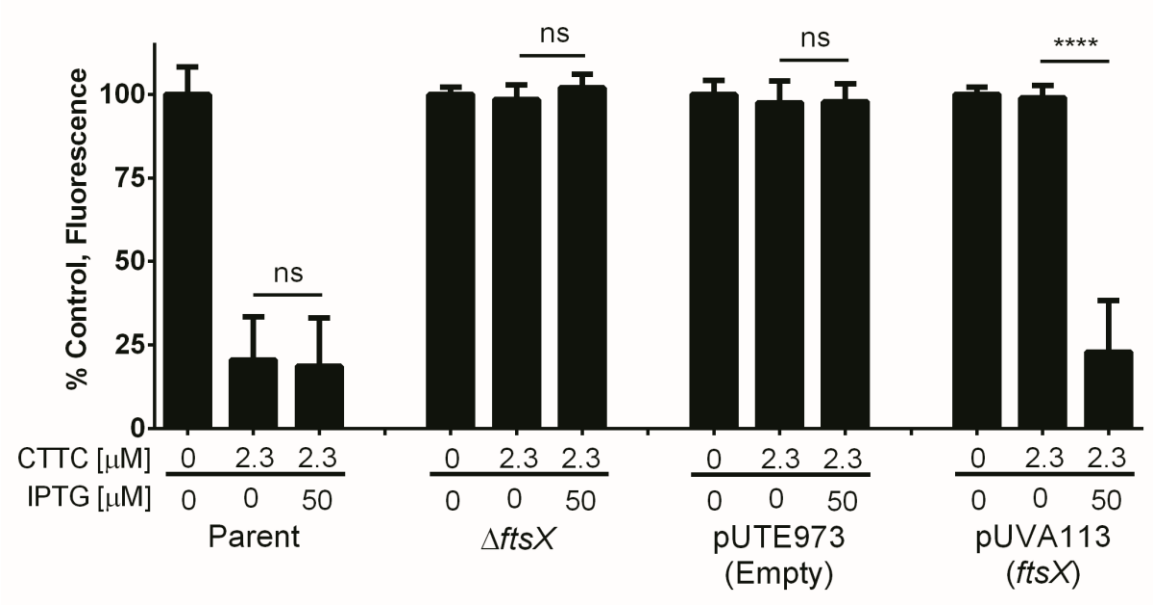

Figure 2.4: *B. anthracis* Δ*ftsX* regained susceptibility to CTTC after genetic complementation with *ftsX*. *B. anthracis* parent strain exhibited susceptibility to 2.3 μM CTTC with or without 50 μM IPTG present, while *B. anthracis* Δ*ftsX* was fully resistant to 2.3 μM CTTC. Testing of *B. anthracis* Δ*ftsX* expressing the empty control vector, pUTE973, resulted in retention of resistance to CTTC. Testing of *B. anthracis* Δ*ftsX* expressing the *ftsX* complementation plasmid, pUVA113, resulted in restoration of susceptibility to CTTC in the IPTG-induced sample, but not the noninduced control.

antimicrobial activity, an FtsE mutant was generated with point mutations in the Walker A and Walker B motifs (134). FtsE/X is encoded within a single operon, and point mutations within the *ftsE* gene Walker motifs disrupt the function of FtsE without interfering with the expression of FtsX (112). Walker motifs are highly conserved between bacterial species and are involved in ATP binding and hydrolysis. Point mutations within Walker motifs are well documented to result in the loss of the protein energy providing function (112, 125, 126, 131, 135, 136). Point mutations in *ftsE* resulted in two amino acid substitutions, K123A and D481N. The resulting mutant strain was designated as *B. anthracis ftsE(K123A/D481N)*. A genetically complemented *B. anthracis ftsE(K123A/D481N)* strain was generated. The wild-type *B. anthracis* parent strain *ftsE* gene was inserted into the plasmid pUTE973 (137) to generate the plasmid pUVA424 in which *ftsE* was under the control of an IPTG-inducible promoter. Because *B. anthracis ftsE(K123A/D481N)* was generated by chromosomal mutations, *B. anthracis ftsE(K123A/D481N)* pUVA424 carried both a mutated and wild-type copy of *ftsE*.

Phenotypically, the *B. anthracis* parent strain grew as long, smooth chains of bacilli which were not affected by the presence and/or expression of pUTE973 or pUVA424 (Figure 2.5A-F). In comparison, *B. anthracis ftsE(K123A/D481N)* bacilli resembled *B. anthracis* Δ*ftsX* (111) with a "kinked" appearance (Figure 2.5G). Addition of IPTG alone in the absence of any plasmids had no effect on the mutant phenotype of *B. anthracis ftsE(K123A/D481N)* (Figure 2.5J). The similarity in morphology between the *ftsE(K123A/D481N)* and Δ*ftsX* strains was as expected for mutations within the same functional complex. This morphological phenotype was also observed in similar mutants

FIGURE 2.5

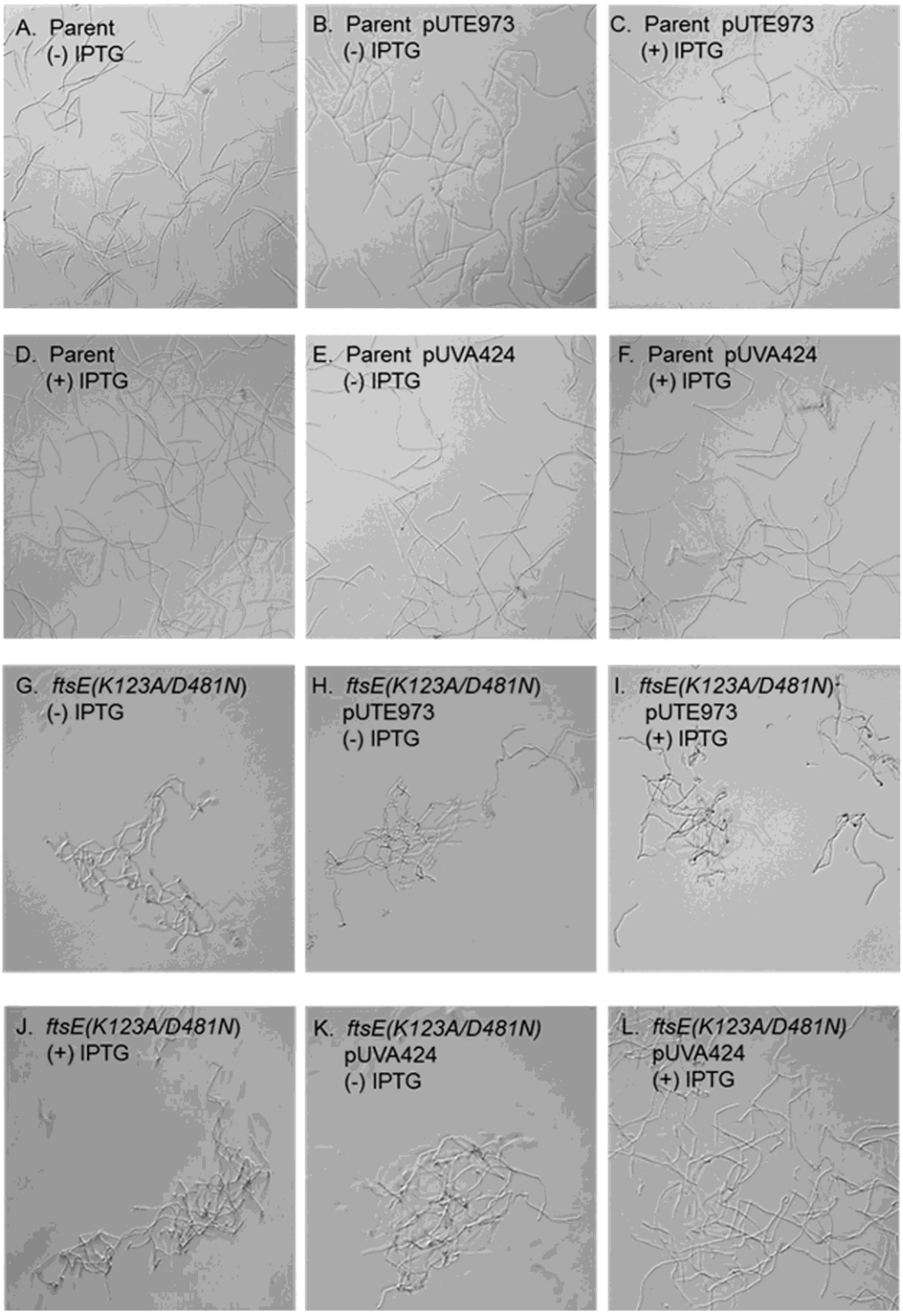
A. Parent
(-) IPTG
B. Parent pUTE973
(-) IPTG
C. Parent pUTE973
(+) IPTG
D. Parent
(+) IPTG
E. Parent pUVA424
(-) IPTG
F. Parent pUVA424
(+) IPTG
G. ftsE(K123A/D481N)
(-) IPTG
H. ftsE(K123A/D481N)
pUTE973
(-) IPTG
I. ftsE(K123A/D481N)
pUTE973
(+) IPTG
J. ftsE(K123A/D481N)
(+) IPTG
K. ftsE(K123A/D481N)
pUVA424
(-) IPTG
L. ftsE(K123A/D481N)
pUVA424
(+) IPTG

Figure 2.5: *B. anthracis ftsE(K123A/D481N)* exhibited a "kinked" phenotype when observed under light microscopy. (A) *B. anthracis* parent strain exhibited long, smooth chains of bacilli. (B-C) *B. anthracis* transformed with the empty control vector pUTE973 retained the parent phenotype without and with induction using 50 μM IPTG. (D) Addition of 50 μM IPTG alone in the absence of all plasmids had no effect on parent strain morphology. (E-F) The presence and induction of the *ftsE* complementation vector pUVA424 within the parent strain also elicited no morphological change. (G) *B. anthracis ftsE(K123A/D481N)* exhibited a "kinked" phenotype, similar to that previously observed for *B. anthracis* Δ*ftsX* (111). (H-I) *B. anthracis ftsE(K123A/D481N)* transformed with the empty control vector pUTE973 retained the "kinked" characteristics of the mutant strain with or without induction using 50 μM IPTG. (J) Addition of IPTG alone in the absence of any plasmids had no effect on the mutant phenotype of *B. anthracis ftsE(K123A/D481N).* (K) *B. anthracis ftsE(K123A/D481N)* transformed with the *ftsE* complementation vector pUVA424 exhibited a "kinked" appearance in the absence of IPTG. (L) *B. anthracis ftsE(K123A/D481N)* transformed with pUVA424 exhibited a phenotype similar to the *B. anthracis* parent strain only when *ftsE* gene expression was induced with 50 μM IPTG. Representative fields from three independent experiments are shown at 200x magnification.

……

constructed in *B. subtilis* (112). *B. anthracis ftsE(K123A/D481N)* carrying the empty vector control (pUTE973) or *ftsE* complementation plasmid (pUVA424) with no IPTG induction had the morphologic phenotype of the *ftsE(K123A/D481N)* strain (Figure 2.5H, 2.5 I, 2.5 K). Induction of *ftsE* gene expression with IPTG generated a morphologic phenotype similar to the *B. anthracis* parent strain (Figure 2.5L). A 24-hour growth curve revealed that the *ftsE(K123A/D481N)* mutant strain had a slightly longer lag phase prior to initiating log phase growth compared to the parent strain (Figure 2.6A). The kinked morphology of *ftsE(K123A/D481N)* and that previously reported for Δ*ftsX* (111), suggested that FtsE and FtsX play a key role in cell wall synthesis and/or cell division, as has been observed in other bacterial species (113, 138, 139).

B. anthracis ftsE(K123A/D481N) is resistant to CXCL10 and CTTC

To test the potential role of FtsE, as part of an active FtsE/X complex, in CXCL10-mediated antimicrobial activity, *B. anthracis ftsE(K123A/D481N)* was exposed to CXCL10 or CTTC at various concentrations. *B. anthracis ftsE(K123A/D481N)* exhibited an increase in resistance to CXCL10-mediated killing compared to parent strain (Figure 2.6B). This resistance of *ftsE(K123A/D481N)* was overcome at higher concentrations of CXCL10 (Figure 2.6B), similar to what was observed with Δ*ftsX* (Figure 2.3B). *B. anthracis ftsE(K123A/D481N)* strain was resistant to CTTC at all concentrations tested (Figure 2.6B), similar to Δ*ftsX*. IPTG-induced expression of the *ftsE*-containing vector (pUVA424) in the *ftsE(K123A/D481N)* strain restored susceptibility to CXCL10 at 0.9 μM (Figure 2.6C) and to CTTC at 2.3 μM (Figure 2.6D). In contrast, IPTG induction of the empty vector control (pUTE973) in the *ftsE(K123A/D481N)* strain did not restore

FIGURE 2.6

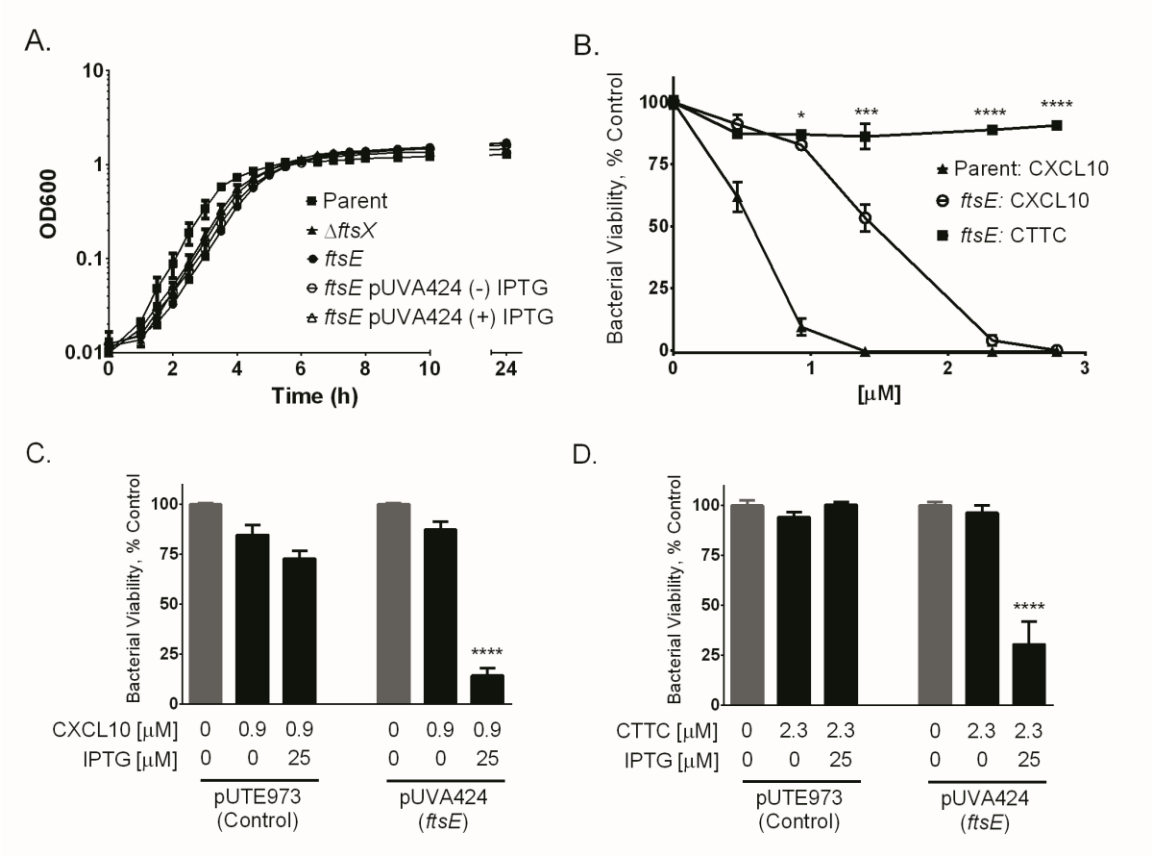
A.
OD600
Time (h)
Parent
ΔftsX
ftsE
ftsE pUVA424 (-) IPTG
ftsE pUVA424 (+) IPTG
B.
Bacterial Viability, % Control
[μM]
Parent: CXCL10
ftsE: CXCL10
ftsE: CTTC
C.
Bacterial Viability, % Control
CXCL10 [μM]
IPTG [μM]
pUTE973 (Control)
pUVA424 (ftsE)
D.
Bacterial Viability, % Control
CTTC [μM]
IPTG [μM]
pUTE973 (Control)
pUVA424 (ftsE)

Figure 2.6: *B. anthracis ftsE(K123A/D481N)* was resistant to CXCL10 and CTTC compared to parent strain. (A) *B. anthracis ftsE(K123A/D481N)* (designated as "*ftsE*" in this figure) had a slightly longer lag phase prior to initiating log phase growth compared to the *B. anthracis* parent strain, a growth characteristic similar to what has been observed with *B. anthracis* Δ*ftsX* (111). (B) *B. anthracis ftsE(K123A/D481N)* was relatively resistant to CXCL10 and resistant to CTTC at all concentrations tested, 0-2.8 μM. Results were similar to those for *B. anthracis* Δ*ftsX*. A statistically significant difference was observed between CXCL10 and CTTC at concentrations ≥ 0.9 μM. (C) *B. anthracis ftsE(K123A/D481N)* transformed with the IPTG-inducible plasmid pUTE973 (empty vector control) exhibited resistance to 0.9 μM CXCL10 in the absence or presence of 25 μM IPTG. *B. anthracis ftsE(K123A/D481N)* transformed with the IPTG-inducible plasmid pUVA424 (*ftsE* complementation vector) resulted in restoration of susceptibility to 0.9 μM CXCL10 only upon treatment with 25 μM IPTG to induce gene expression. (D) *B. anthracis ftsE(K123A/D481N)* transformed with plasmid pUTE973 exhibited resistance to 2.3 μM CTTC in the absence or presence of 25 μM IPTG. *B. anthracis ftsE(K123A/D481N)* transformed with pUVA424 exhibited susceptibility to 2.3 μM CTTC only upon addition of 25 μM control. Data points represent mean values ± SEM; n=3 separate experiments using IPTG to induce gene expression. Bacterial viability was measured using Alamar blue reduction, and fluorescence units were expressed as a percentage of the strain-specific untreated triplicate wells in each experiment. *$p \leq 0.01$, ***$p \leq 0.0001$, ****$p < 0.0001$

……

susceptibility to CXCL10 or CTTC (Figure 2.6C and 2.6D). These data suggest that a functional FtsE/X complex is important for the antimicrobial effect of CXCL10. Importantly, the *ftsX* gene was intact (i.e., wild type) in the *ftsE(K123A/D481N)* strain in these experiments. Therefore, the data indicate that interaction of CXCL10 or CTTC with *B. anthracis* FtsX was not, in and of itself, sufficient for killing. Instead, an active FtsE/X complex was necessary for FtsX-mediated killing. Table 1 summarizes the fifty percent effective concentration (EC_{50}) values calculated for CXCL10 and CTTC against the *B. anthracis* parent, Δ*ftsX*, and *ftsE(K123A/D481N)* strains.

B. anthracis parent strain membrane depolarization in response to CXCL10 or CTTC exposure

The CXCL10 C-terminal α-helix does not appear to be required for the FtsX-mediated antimicrobial activity of CXCL10 in *B. anthracis*. However, it likely plays a role in the non-FtsX-dependent mechanism of killing. Therefore, membrane depolarization studies were conducted to further investigate the role of the amphipathic α-helix of CXCL10. Initially, a peptide representing the CXCL10 α-helix (amino acids 54-77) was synthesized to test whether it had antimicrobial activity and depolarized the membrane. CD studies revealed that this peptide formed an α-helix in the presence of trifluoroethylene, a membrane mimetic, at a concentration that was toxic to *B. anthracis* (data not shown). However, the C-terminal peptide did not form an α-helix in a buffer suitable for antimicrobial testing (data not shown). Therefore, a comparison of intact CXCL10 versus CTTC on membrane depolarization was used to assess the effect of the α-helix (or lack thereof).

TABLE 2.1

Calculated EC_{50} values of CXCL20 and CTTC for the *B. anthracis* parent, Δ*ftsX*, and *ftsE*(*K123A/D481N)* strains [a]

	EC_{50} (μM) for:		
Strain	CXCL10	CTTC	Fold Change
Parent	0.68 ± 0.03	1.83 ± 0.07	2.7
Δ*ftsX* mutant	1.59 ± 0.05	NA [b]	NA
ftsE(K123A/D481N) mutant	1.39 ± 0.07	NA	NA

[a] The fold difference between the EC_{50} values of CXCL10 and CTTC for the *B. anthracis* parent strain is shown. The mutant strains showed no susceptibility to CTTC; thus, there is no EC_{50} or fold change compared to CXCL10.

[b] NA, not applicable because no killing was observed.

B. anthracis parent strain was pre-loaded with the fluorescent dye 3,3'-dipropylthiadicarbocyanine (diSC3-5). The fluorescence of diSC3-5 is quenched upon cellular uptake by the negative membrane potential; membrane depolarization releases diSC3-5, which produces a fluorescent signal upon release. The fluorescent signal elicited by a test molecule is compared to that resulting from complete depolarization by the addition of the bee venom peptide, melittin at 20 μM (140). The percentage of depolarization could then be calculated for each antimicrobial test molecule (141). Concurrently, colony forming units ml^{-1} (CFU ml^{-1}) were determined to assess bacterial survival in this assay.

LL-37, a cationic antimicrobial peptide that causes membrane disruption in bacteria, was used as a positive control at 25 μM (119). LL-37 produced a comparable degree of membrane depolarization in both the parent and Δ*ftsX* strains (Figure 2.7A and 2.7B). CCL5, which has a similar molecular mass and charge as CXCL10 but exhibits no antimicrobial activity against *B. anthracis* (105), was used as a negative control. Exposure of *B. anthracis* parent and Δ*ftsX* to the same concentration of CCL5 as CXCL10 did not cause membrane depolarization (Figure 2.7A and 2.7B).

The membrane of *B. anthracis* parent strain underwent depolarization in the presence of CXCL10. The extent of depolarization increased with increasing concentrations of CXCL10 (Figure 2.7A). Depolarization occurred to a lesser, but statistically significant degree, in the presence of CTTC (Figure 2.7A). The degree of depolarization also

FIGURE 2.7

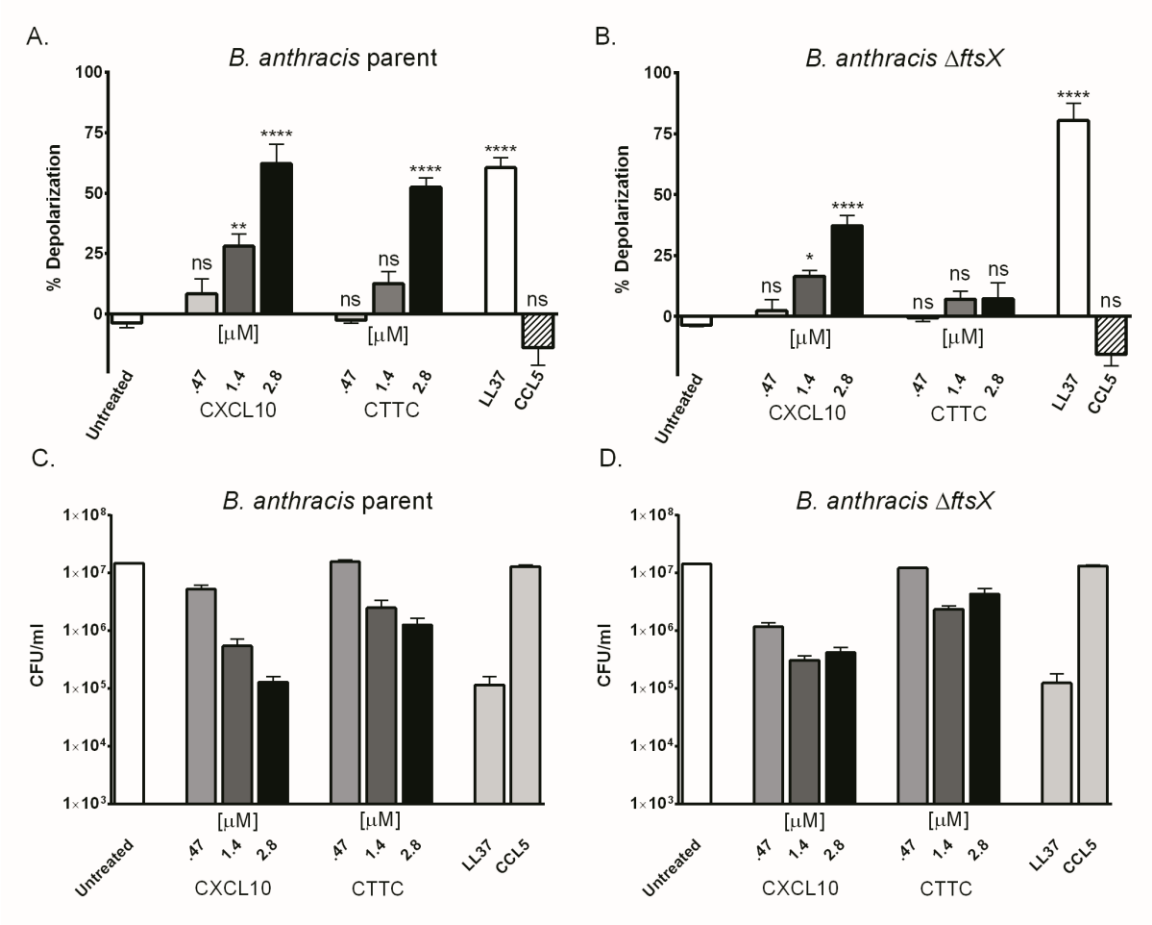
A.
B. anthracis parent
% Depolarization
100
75
50
25
0
ns
**
****
ns
****
****
ns
[μM]
[μM]
Untreated
.47
1.4
2.8
CXCL10
CTTC
LL37
CCL5
B.
B. anthracis ΔftsX
% Depolarization
ns
*
****
ns
ns
****
ns
C.
B. anthracis parent
CFU/ml
1×10⁸
1×10⁷
1×10⁶
1×10⁵
1×10⁴
1×10³
D.
B. anthracis ΔftsX

Figure 2.7: Membrane depolarization occurred after exposure of *B. anthracis* to CXCL10. (A) *B. anthracis* parent strain membrane depolarization occurred after exposure to CXCL10 or CTTC. (B) *B. anthracis* Δ*ftsX* membrane depolarization occurred upon exposure to CXCL10, but not CTTC. The positive control (LL-37, 25 μM) induced membrane depolarization. Exposure to the negative control (CCL5, 2.8 μM) did not cause membrane depolarization (n=4-5 separate experiments). (C) Antimicrobial killing of the bacteria by CXCL10 or CTTC was correlated with the membrane depolarization assay results performed under the same conditions (n=4-5 separate experiments). CFU/ml determinations were plotted on a log scale. (D) Treatment of *B. anthracis* Δ*ftsX* with CXCL10 or CTTC at the indicated concentrations resulted in less killing compared to the parent strain shown in Panel A (n=4-5 separate experiments). For both strains, incubation with the positive control (LL-37) resulted in decreased survival compared to the untreated control. The negative control (CCL5) was not bactericidal (n=4-5 separate experiments). Statistical analysis was performed using a two-way ANOVA test. ns = not significant, *$p \leq 0.01$; **$p \leq 0.001$, ***$p \leq 0.0001$, ****$p < 0.0001$

……

increased with increasing concentrations of CTTC (Figure 2.7A). Statistical analysis was conducted by comparing untreated and treated groups through a two-way ANOVA. The effect of CTTC on the parent strain may indicate that some other portion of CXCL10 can produce depolarization, not just the α-helix or that cell lysis mediated through the FtsX-mediated pathway also leads to depolarization. The corresponding viability from CFU determination was plotted on a log scale and showed that the cells died upon exposure to either CXCL10 or to CTTC (Figure 2.7C). Due to an inoculum effect resulting from the higher bacterial concentration used in this particular assay relative to the concentration of CXCL10 or CTTC, the degree of bacterial killing was less than that observed in the standard antimicrobial assay shown in Figure 3.

Membrane depolarization of *B. anthracis* Δ*ftsX* only occurs in the presence of the CXCL10 α-helix

CXCL10 caused significant membrane depolarization of *B. anthracis* Δ*ftsX* compared to the untreated control (Figure 2.7B). However, no significant membrane depolarization was observed when *B. anthracis* Δ*ftsX* was treated with CTTC (Figure 2.7B). These data suggested that the membrane depolarization induced by CTTC in the parent strain was dependent upon the presence of FtsX. Thus, an FtsE/X-dependent pathway likely leads to a lack of cell integrity with concomitant membrane disruption. A decrease in bacterial viability was correlated with membrane depolarization upon incubation with CXCL10; a less pronounced decrease in viability was observed with CTTC (Figure 2.7D). These results indicated that the C-terminal α-helix of CXCL10 was capable of causing membrane depolarization and that its activity was independent of FtsX.

2.4 Discussion

The antimicrobial activity of the interferon-inducible ELR(-) CXC chemokine CXCL10 has been demonstrated against a broad range of Gram-positive (including *B. anthracis*, *L. monocytogenes*, and *S. aureus*) and Gram-negative (*E. coli* and *Pseudomonas aeruginosa*) pathogens, but the exact mechanism(s) of action have remained unclear (67–69, 90, 107). In the current study, we showed that CXCL10 can kill *B. anthracis* through multiple mechanisms. One mechanism involves the bacterial FtsE/X complex and is mediated through interaction with the N-terminal region or regions of CXCL10. It is independent of the amphipathic C-terminal α-helix. Another mechanism is FtsE/X-independent and is mediated by the depolarization of the cytoplasmic membrane by the CXCL10 C-terminal α-helix. Such findings are novel and unexpected in the chemokine field and open up a number of mechanistic possibilities for how chemokines are targeting microbes beyond non-specific membrane disruption, while also supporting defensin-like antibacterial targeting as a second mechanism.

Previous electron microscopy studies have shown that CXCL10 localizes to the bacterial membrane in vegetative cells, and to the internal coat/cortex interface in spores (105). That an extracellular region of FtsX, a membrane protein, had limited similarity to CXCR3 suggested a possible interaction with CXCL10 through receptor mimicry. This observation led to the hypothesis that the N-terminus of CXCL10 was important for interaction with the target microorganism through that region of FtsX, especially since it is the portion of the chemokine that facilitates interaction with CXCR3. A peptide competition assay

showed the CXCR3-similar region of FtsX was indeed important in interacting with CXCL10 and mediating antimicrobial activity. We then tested a C-terminal truncated CXCL10, CTTC, molecule to determine if the N-terminal region of CXCL10 promoted antimicrobial activity, or if the C-terminal α-helix of CXCL10 was necessary for killing. CTTC was less active against the *B. anthracis* parent strain and did not kill the Δ*ftsX* strain. The EC_{50} values indicated that CTTC is 2.7 fold less effective than CXCL10 at killing the parent strain and lacks the ability to kill the Δ*ftsX* strain altogether (Table 1). These results indicated that an FtsX-dependent mechanism of killing was independent of the CXCL10 C-terminal α-helix, highlighting a novel interaction between the CXCR3-receptor binding region(s) of CXCL10 with the bacterial FtsX (Figure 2.8A) as chemokine antimicrobial activity has previously been hypothesized to be mediated through the C-terminal α-helix (69, 119, 120). The finding that other portions of CXCL10 may mediate killing represents a paradigm shift and opens avenues for the study and development of new therapies based on chemokine architecture.

FtsE/X is a unique bacterial complex that warrants further study as an antimicrobial target since its pivotal role in peptidoglycan processing through hydrolase activation is widely conserved between bacterial species (112, 113, 123, 124, 126, 142). Interestingly, there are differences between Gram-positive and Gram-negative bacteria in the roles of FtsE/X (112, 113, 122–124, 131). In Gram-positive bacteria, namely *Bacillus* spp., there appear to be redundancies in the enzymatic activities involved in peptidoglycan processing during cellular elongation, such that a disruption in one pathway could result in cell wall instability and bacterial cell lysis (127, 143, 144). Notably, the *B. anthracis ftsE(K123A/D481N)*

FIGURE 2.8

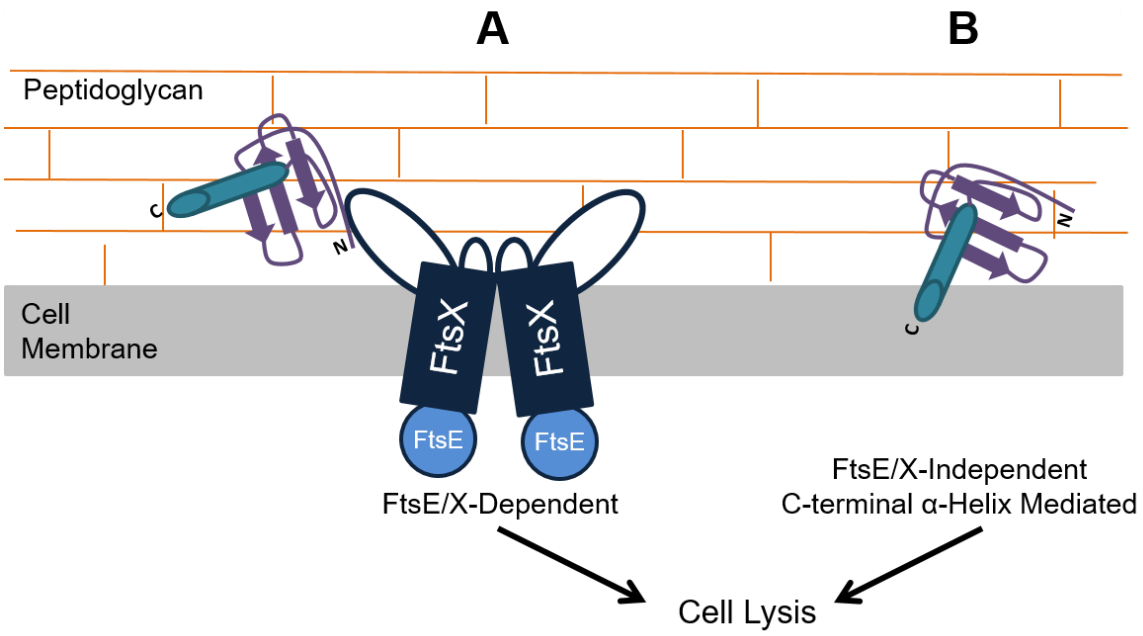

Figure 2.8: Hypothetical model for the bifunctional antimicrobial activity of CXCL10 against *B. anthracis*. (A) ***FtsE/X-mediated antimicrobial activity of CXCL10*:** CXCL10 elicits an antimicrobial effect against *B. anthracis* via an FtsE/X-dependent pathway through the N-terminal portion and/or other regions of CXCL10, independent of the C-terminal α-helix. Cell death results through lysis. (B) ***FtsE/X-independent antimicrobial activity of CXCL10:*** CXCL10 interacts with *B. anthracis* in an FtsX-independent manner to cause bacterial killing, likely through interaction or insertion of the C-terminal α-helix into the bacterial membrane, resulting in cell lysis. While the mechanistic pathways are different, both pathways appear to lead to the same end result of cell lysis.

mutant in our study exhibited a morphology similar to that previously reported for Δ*ftsX* in which bacilli appeared "kinked" with frequent curves and sharp angles among the growing chains, consistent with an alteration in cell wall processing (113, 138, 139). The interaction of CXCL10 with FtsE/X may provoke or disrupt peptidoglycan processing from which the bacteria cannot recover, resulting in bacterial cell death. Our results determined that CXCL10 FtsX-dependent antimicrobial activity requires both FtsX and a functional FtsE ATP-binding protein, thus implicating an energy requirement for the CXCL10-mediated mechanism. As such, this report is the first description of an active FtsE/X complex contributing to the bactericidal effect of an antimicrobial molecule. The above membrane disruption studies showed that depolarization also occurred through the FtsX-mediated mechanism. Given the role of FtsE/X in peptidoglycan processing, it is possible that CXCL10 provokes peptidoglycan turnover, which leads to cell lysis through peptidoglycan degradation and the loss of the cell's ability to withstand environmental conditions. Studies are currently underway in our laboratory to investigate the nature of this interaction and how bacterial cell death may occur in response to CXCL10, potentially from provoking or disrupting the peptidoglycan processing pathway. Understanding the function of the unique and widely conserved FtsE/X complex may lead to the utilization of this novel bacterial target for new antimicrobial therapies.

The FtsE/X-independent mechanism of killing by CXCL10 is likely mediated through the non-specific interaction of its C-terminal α-helix with the bacterial membrane, similar to what has been described for cationic antimicrobial peptides, such as LL-37 or defensins (69, 119, 120) (Figure 2.8B). *B. anthracis* Δ*ftsX* only undergoes membrane depolarization

in the presence of intact CXCL10, suggesting that the amphipathic, structural characteristics of the C-terminal region are responsible for membrane disruption and lysis. It appears that the CXCL10 C-terminal α-helix is not necessary for killing the parent strain. However, in the absence of FtsX and at higher concentrations of CXCL10, death can occur through membrane disruption. When both mechanisms are present/active, CXCL10-mediated bacterial killing appears to be the most effective. Further study of the structural characteristics of CXCL10 and its related chemokines should lead to a better understanding of their biological activities as well as a broader application of therapeutic potential for chemokine α-helices against a wide range of bacterial species.

Our findings present an exciting advance in the understanding of how chemokines function as antimicrobial molecules as well as in the study of host-pathogen interactions within the innate immune system. The primary significance is the new information involving the bifunctional activity of CXCL10 with mechanisms involving a previously unrecognized portion of CXCL10 that exhibits antimicrobial activity through interaction with the novel bacterial target FtsE/X and also the CXCL10 C-terminal α-helix-mediated antimicrobial killing of *B. anthracis*. Our research suggests that as chemokines are further studied as antimicrobial molecules, there will be heightened recognition of more specific mechanisms by which they kill microorganisms beyond non-specific membrane targeting and disruption. Studies into the antimicrobial effects of chemokines are likely to reveal additional mechanisms of killing and lead to the development of novel small molecules as innovative therapies to treat a wide range of bacterial pathogens, including already established and emerging antibiotic resistant organisms.

2.5 Materials and Methods

Bacterial strains and culture conditions. *B. anthracis* Sterne strain ATCC 7702 ($pXO1^+$, $pXO2^-$, American Type Culture Collection, Manassas, VA) was used in these experiments and designated as parent strain. *B. anthracis* Δ*ftsX*, *B. anthracis* Δ*ftsX* pUTE973, *B. anthracis* Δ*ftsX* pUVA113, and *B. anthracis ftsE(K123A/D481N)* were derived from the Sterne strain (111). Vegetative cells were prepared by inoculating *B. anthracis* parent strain spore stocks or *B. anthracis* Δ*ftsX* and *B. anthracis ftsE(K123A/D481N)* vegetative cell frozen stocks into 10 ml of brain heart infusion (BHI) broth (Difco, Franklin Lakes, New Jersey) and incubating overnight at 37°C with shaking (250 rpm). Mid-log phase cultures were prepared the next day by diluting the overnight culture 1:20 in fresh BHI broth followed by incubation at 37°C with shaking for ~2 h until an optical density at 600 nm between 0.6 and 0.65 was achieved, at which time the cultures were used for experiments. All laboratory work involving *B. anthracis* Sterne or Sterne-derived strains was approved through the University of Virginia Institutional Biosafety Committee. Biosafety level 2 practices were used for all work involving *B. anthracis* Sterne or Sterne-derived strains.

Amino acid sequence alignment. The National Library of Medicine sequence alignment program, Basic Local Alignment Search Tool (http://blast.ncbi.nlm.nih.gov/Blast.cgi), was used to align Gram-positive and Gram-negative FtsX protein sequences to *B. anthracis* Sterne (parent) strain FtsX (Text 2.1). The following species and FtsX identification codes were used to perform individual Blastp analyses: *B. anthracis* Sterne (AAT57322.1), *B.*

subtilis 168 (NP_391405.1), *M. tuberculosis* H37Rv (CAA49620.1), *S. pneumoniae* (AJD71681.1), *E. coli* F11 (EDV68789.1), and *K. pneumoniae* (KLA37751.1). Full sequence alignment of all six strains was conducted using the multiple sequence alignment software T-Coffee (Text 2.1) (http://tcoffee.crg.cat/apps/tcoffee/do:regular) and formatted using the program Boxshade (http://www.ch.embnet.org/software/BOX_form.html) (129, 130).

Generation of *B. anthracis ftsE(K123A/D481N)* strain and the plasmid vector, pUVA424, for gene complementation studies in *B. anthracis ftsE(K123A/D481N)* (111, 134)**.** *B. anthracis ftsE* was cloned into the plasmid vector pGEM in α-select silver efficiency *E. coli* (Bioline, Taunton, MA) in preparation for PCR mediated point mutations the Walker A and Walker B motifs. The Walker A mutation (K123A) was performed using the forward primer: AGTGGAGCCGGGGCATCTACATTTATT and reverse primer: CGGTCCAACTACGTATACAAACTCACC. The Walker B mutation (D481N) was performed sequentially using the forward primer: GTCGTAATTGCCAATGAGCCAACA and reverse primer: TTTCGGCTTGTTTACAATTGCTCTC. The Walker motif mutated *ftsE* construct was then cloned into plasmid pRP1028 and placed in *E. coli* 138 in preparation for chromosomal integration through homologous recombination. *E. coli* 138 containing the pRP1028 *ftsE* plasmid was conjugated with *B. anthracis* parent strain to integrate the mutated *ftsE* into the *B. anthracis* chromosome. Plasmid pBKJ236 was introduced through electroporation to facilitate chromosomal recombination to obtain colonies with a single copy of the mutated *ftsE*. Individual colonies were isolated and screened for loss of

erythromycin resistance. The *ftsE gene* was amplified by PCR and sequenced to verify the mutations in the Walker A and B motifs. The plasmid pBJK233 was lost spontaneously by multiple passages in media lacking tetracycline. This bacterial strain with the two point mutations (K123A and D481N) in the *ftsE* Walker A and Walker B motifs was designated *ftsE(K123A/D481N)*.

Gene complementation of *ftsE* in the *B. anthracis ftsE(K123A/D481N)* was performed as described in detail (111). Briefly, the native *B. anthracis* parent strain *ftsE* gene was amplified using a forward primer carrying a ribosome binding site and SphI restriction site (CCGGATACTCGAGTGAGGAGGAGGCTACCTTCAACAAGAGTGG) and a reverse primer carrying PspXI restriction site (GCCTAGGCATGCTTCACACCTTCTCGCAAATG). The *ftsE* PCR product was double digested with SphI-HF and PspXI, purified, and ligated into the empty plasmid vector pUTE973 that had been digested with SphI-HF and Salk-HF (137). The resulting vector was transformed into α-select silver efficiency *E. coli* and verified by sequencing. The verified plasmid was isolated and electroporated into GM119 *E. coli* to remove all methylation. The resulting *ftsE(K123A/D481N)* complementation plasmid (pUVA424), or the empty vector control plasmid (pUTE973), was then electroporated into the *B. anthracis ftsE(K123A/D481N)* bacterial strain. All isolates were tested and verified by PCR and sequencing.

CXCL10 and C-terminal truncated CXCL10 (CTTC). Recombinant human CXCL10 was purchased from Peprotech (Rocky Hill, New Jersey). CXCL10 was dissolved in sterile

H_2O containing 0.3% (w/v) human serum albumin (HSA) (Grifols, Los Angeles, CA) at a concentration of 1 mg ml^{-1} and stored at -80°C in 10 µl aliquots to limit freeze-thaw cycles to no more than one. The CTTC peptide was commercially synthesized and capped by amidation on the C-terminus by United Biosystems (Herndon, VA) (Text S2.2B). Lyophilized CTTC was dissolved in sterile H_2O at a concentration of 5 mg ml^{-1} and stored in 20 µl aliquots as described above. The CTTC peptide, -VPLSRTVRCTCISISNQPVNPRSLEKLEIIPASQFCPRVEIIATMKKKGEKRCL-NH2, was commercially synthesized and capped by amidation on the C-terminus by United Biosystems (Herndon, VA). Sequence was confirmed by mass spectrometry conducted by United Biosystems. Lyophilized CTTC was dissolved in sterile H_2O at a concentration of 5 mg ml^{-1} and stored in 20 µl aliquots as described above. Circular dichroism studies were conducted on 50-100 µM samples of CXCL10 and CTTC resuspended in sterile H_2O to analyze secondary structure protein characteristics (AVIV 410 Circular Dichroism Spectropolarimeter, Lakewood, New Jersey). CD analysis of CTTC established that an α-helical structure was absent, as compared to the intact CXCL10 spectrum. Analyses were conducted using CDNN software (http://gerald-boehm.de/download/cdnn) and data were compared to the expected secondary structure prediction of CXCL10 and CTTC (https://www.predictprotein.org/) (PDB: 1080) (85, 128, 133). CD analysis of CTTC revealed an expected content of □-strands (39%), indicating that CTTC was properly folded.

Antimicrobial assays and light microscopy studies. Vegetative cells were diluted to approximately $2.5x10^5$ CFU ml^{-1} in fresh Dulbecco's modified Eagle's medium (Gibco-

Invitrogen, Carlsbad, CA) containing10% (v/v) fetal bovine serum (HyClone, Logan, UT) and the various concentrations of CXCL10 or CTTC to be tested. Aliquots of 100 µl were placed in triplicate wells in a 96-well plate and incubated at 37°C with 5% CO_2 for approximately 4 h, unless otherwise noted, at which point Alamar blue dye (AbD Serotech, Oxford, United Kingdom) was added at a 1:10 dilution and allowed to reach visual saturation in an untreated control under protection from light. Active metabolism of the vegetative cells was quantified via generation of a fluorescent signal from the reduction of the Alamar blue oxidation-reduction dye by measuring the fluorescence at 530-nm excitation and 590-nm emission wavelengths using a Perkin-Elmer Victor^3 multi-label plate reader (Perkin-Elmer, Waltham, MA). Percent control was calculated by comparison of the reading obtained for the chemokine-treated to that of the corresponding untreated samples. Light microscopy was used for bacterial cell visualization. Camera control and image capture were performed by using QCapture Pro-5.1 software, as described (105, 111).

Peptide competition assay. The FtsX peptide and the control scrambled FtsX peptide were commercially synthesized by United Biosystems (Herndon, VA). The FtsX peptide (KVEQDVEIRVHIDPAAKEADQKKLEDD) was derived from the CXCR3-similar region noted in Figure 2.1. The FtsX scrambled peptide (VEHRPQKADEDDALAKEKVKVIDQDIE) contained the same amino acids as the FtsX peptide but in random order. Each peptide was pre-incubated with 0.46 µM CXCL10 at a molar ratio of 10:1 or 20:1 (peptide:CXCL10) for 30 min at 37°C. The peptide:CXCL10 mixtures were then used in a standard antimicrobial assay, with equal volumes of buffer

containing 0.3% HSA as a vehicle control, as previously described (105). The antimicrobial assay incubation time was 2 h, followed by the addition of Alamar Blue dye. After visual saturation was reached, readings were obtained and the percent-of-control was calculated.

Membrane depolarization measurement. Membrane depolarization was measured after exposure of vegetative cells to various μM concentrations of CXCL10 or CTTC using a modification of a published protocol (141). Controls included LL-37 as a positive control (90) and CCL5 as a negative control (105). LL-37 (Alpha Diagnostic International, San Antonio, Texas) was reconstituted in 0.1% BSA with 0.01% acetic acid and used at a final concentration of 25 μM. CCL5 (Peprotech, Rocky Hill, New Jersey) was reconstituted in 0.3% HSA and used at a final concentration of 2.8 μM.

Briefly, *B. anthracis* cells were grown to mid-log phase, as described above. Aliquots (1.5 ml) were centrifuged at 15,000 rpm, and the supernatant was discarded. Vegetative cells were resuspended in respiration buffer (5 mM HEPES, 20 mM glucose, pH= 7.4) to an optical density of 0.100 at 600 nm. A 1 μl aliquot of 0.1 mM 3,3'-dipropylthiadicarbocyanine (diSC3-5) (AnaSpec, Fremont, CA) was added to 1.5 ml aliquots of the resuspended cells, gently mixed, and then incubated in the dark at room temperature for 1 h. After incubation, a 100 μl aliquot of dye-loaded bacteria was placed into a 96-well black bottom plate (VWR, Radnor, PA). An initial baseline fluorescence reading (F_0) of the sample well was measured every 5 seconds for a total of 120 seconds at 540-nm excitation and 680-nm emission using the Perkin-Elmer Victor^3 multi-label plate

reader. After collecting these baseline readings, the test antimicrobial molecule was added at various concentrations to the sample, and fluorescence (F) readings were collected every 5 seconds for 300 seconds. At this final time point, the bee venom peptide, melittin (Enzo Life Sciences, Farmingdale, NY), was added to a final concentration of 20 μM to complete depolarization and end point readings (maximum depolarization) (F_M) were collected every 5 seconds for 300 seconds. Using the initial (F_0), test (F), and final, maximum fluorescence readings (F_M), the values of each group were averaged together, and the following calculation was used to determine percent depolarization by the test molecule compared to complete depolarization by melittin: % Depolarization = $[(F-F_0)/(F_M-F_0)]X100$ (141).

In parallel with the above depolarization experiments, aliquots of samples prepared in the same way were collected (in the absence of melittin addition), and then diluted and inoculated onto BHI agar plates followed by for overnight incubation at 37°C to determine colony forming units ml^{-1} (CFU ml^{-1}). All treated bacteria were accompanied by an untreated control for comparison of CFU ml^{-1}.

Statistical Analyses

Statistical analyses and graphing were performed using GraphPad Prism 4.0 and 6.0 software. Experimental groups were analyzed using an unpaired, two-tailed student *t* test or two-way ANOVA as noted in the text. Significant differences were determined to have a P value of ≤ 0.05.

2.6 Acknowledgments

We thank Debra J. Fisher for her technical assistance, and Dr. Borna Mehrad, Dr. Barbara J. Mann, and Dr. Girija Ramakrishnan and members of their laboratories at the University of Virginia School of Medicine for their advice and helpful discussions. We thank Dr. Stephen A. Morse (Centers for Disease Control and Prevention, Atlanta, GA) for providing helpful comments on the manuscript. This work used the Aviv 410 Circular Dichroism Spectropolarimeter in the Shared Instrumentation Core, which is supported by the University of Virginia School of Medicine.

CHAPTER 3:

CXCL10 disrupts *Bacillus anthracis* peptidoglycan remodeling through FtsE/X

Margulieux KR, Liebov B, Kumar K, Singh A, Harman WD, Bushweller JH, Hughes MA

Adapted from: Manuscript in preparation

3.1 Abstract

The chemokine CXCL10 has been shown to exert bifunctional antimicrobial activity against *Bacillus anthracis* vegetative cells through bacterial FtsE/X-dependent and -independent mechanisms of action. The FtsE/X-dependent mechanism is likely mediated through interaction of the N-terminal region(s) of CXCL10 with a functional FtsE/X complex, while the FtsE/X-independent pathway is likely mediated through the C-terminal α-helix of CXCL10 and results in membrane depolarization. Both pathways result in cell lysis and death. In other bacterial species, FtsE/X is involved in cellular elongation, which occurs following the activation of peptidoglycan hydrolases associated with this complex. Therefore, we hypothesized that the FtsE/X-dependent pathway kills vegetative cells of *B. anthracis* through the disruption of peptidoglycan processing. Immunofluorescence microscopy studies using fluorescent peptidoglycan probes indicate that incubation of *B. anthracis* Sterne (parent) strain with either intact CXCL10 or a C-terminal truncated CXCL10 impacts peptidoglycan processing and/or incorporation into the cell wall when compared to untreated controls. *B. anthracis* Δ*ftsX* or *ftsE(K123A/D481N)* mutant strains, which lacked the FtsX or FtsE of the putative FtsE/X complex, showed no evidence of a disruption in peptidoglycan processing by either CXCL10 or CTTC. The level of peptidoglycan release was measured using a mammalian NFκ-B-based reporter cell line that overexpresses the NOD2 receptor, which detects bacterial peptidoglycan. The *B. anthracis* parent strain exhibited a statistically significant increase in peptidoglycan release in the presence of either CXCL10 or CTTC. *B. anthracis* Δ*ftsX* strain showed increased peptidoglycan release in the presence of CXCL10 but not CTTC. Our results support the

hypothesis that the mechanism of FtsE/X-dependent killing of *B. anthracis* vegetative cells results from a loss of cell wall integrity due to a disruption in peptidoglycan processing.

3.2 Introduction

As described in Chapter 2, CXCL10 acts as a bifunctional antimicrobial molecule against *B. anthracis* vegetative cells through FtsE/X-dependent and -independent mechanisms (145). The FtsE/X-dependent mechanism appears to require the N-terminal region of CXCL10 whereas the FtsE/X-independent pathway likely is mediated through the C-terminal α-helix and/or other structural regions of CXCL10. While FtsE/X has been identified as being important for N-terminal-mediated CXCL10 killing of *B. anthracis*, the exact mechanism of FtsE/X-dependent killing has remained unknown. An important structural component of *B. anthracis* vegetative cells is the thick cell wall that is comprised of the complex macromolecule peptidoglycan (39, 146–149). FtsE/X has been found to be widely conserved across Gram-positive, Gram-negative, and acid fast bacterial species and is thought to be part of a larger cell wall synthesis complex that is responsible for peptidoglycan remodeling (112, 113, 121–124, 126, 135, 136, 142, 150–153). Peptidoglycan remodeling is a tightly regulated process and a disruption may result in a loss of cell wall integrity and bacterial cell death, making FtsE/X an important complex to study further as potential bacterial targets for development of new antimicrobial strategies (146–149, 154–156).

In the Gram-positive bacterium *Bacillus subtilis*, FtsE/X has been shown to be involved in cellular elongation and sporulation through the localization and activation of peptidoglycan hydrolases that break old peptidoglycan bonds in order to make room for the insertion of

new peptidoglycan subunits (112, 113, 123, 124, 126, 136). FtsE provides energy through its activity as an ATP-hydrolase; FtsX is a membrane protein that has a hydrolase-associated domain located on the external side of the cell membrane (112, 113, 123, 124, 126, 135). Together, FtsE and FtsX form a dimerized FtsE/X complex that spans the bacterial cell membrane (112, 113, 123). FtsE hydrolysis of ATP is thought to result in a conformational change in FtsX, which then causes the activation and/or release of peptidoglycan hydrolases to process the covalent bonds within the peptidoglycan structure (112, 113, 124, 126, 157). This process is tightly controlled for maintaining bacterial cell wall integrity, and any disruption, either through inhibition or overactivation of the hydrolases can result in the inability of the bacteria to maintain the necessary internal pressure or withstand external environmental pressure (155). The FtsE/X-dependent mechanism of CXCL10 killing of *B. anthracis* appears to be mediated through interaction of the N-terminal/β-sheet portions of CXCL10 (and not the C-terminal amphipathic α-helix of CXCL10) with the membrane protein complex, FtsE/X (145). As stated in Chapter 2, the FtsE/X-dependent mechanism of CXCL10-mediated killing of *B. anthracis* requires an active FtsE/X complex and does not seem to utilize FtsX simply as a binding site for CXCL10 (145). CXCL10 appears to be targeting the active FtsE/X complex, which results in vegetative cell death. Recent advances in peptidoglycan imaging technology allow for a more detailed study into how peptidoglycan remodeling is impacted during killing by antimicrobial molecules and are utilized in this chapter (158–161).

Bacterial growth and replication are essential for surviving within a host (146, 147, 155, 156). Any disruption in peptidoglycan processing may have a detrimental effect on the

structural integrity of the cell and lead to cell death (154, 155, 162, 163). An active FtsE/X complex is important in mediating killing of *B. anthracis* by CXCL10*;* however, the mechanism by which this occurs is unknown. We hypothesized that the FtsE/X-dependent CXCL10 antimicrobial activity is a consequence of disruption or provocation of the FtsE/X complex and associated hydrolases, resulting in bacterial cell lysis. To establish baseline peptidoglycan incorporation patterns, we visually observed and quantified the cellular characteristics of the *B. anthracis* parent strain and Δ*ftsX* and *ftsE(K123A/D481N)* mutant strains using fluorescent labeling of the peptidoglycan during vegetative cell growth and elongation. Dual labeling of peptidoglycan incorporation before and after addition of CXCL10, CTTC, and/or control antimicrobials (penicillin, tetracycline) was used to determine the amount of peptidoglycan release and new incorporation upon exposure to CXCL10. Finally, we used a mammalian NFK-β-based reporter cell line that overexpresses NOD2 to measure the release of peptidoglycan subunits into the supernatant of samples treated with D-cycloserine penicillin, tetracycline, CXCL10, or CTTC compared to untreated cells. Our findings suggest that the FtsE/X-dependent pathway of killing results in an increase in peptidoglycan degradation and release that may contribute to cell lysis due to the loss of structural integrity.

3.3 Results

Fluorescent labeling of peptidoglycan.

Recent advances in the field of peptidoglycan labeling have resulted in the development of a variety of fluorescent peptidoglycan probes that can be incorporated into the peptidoglycan layer during cellular growth and division (Figure 3.1A and B) (158–161,

164, 165). Ethynyl-D-alanine (EDA) is a D- alanine molecule with an alkyne group modification that can be "clicked" together with various fluorophores containing a reactive azide group. The alkyne modification on EDA reacts (or "clicks", as described based on the technology used to establish the reaction) with the azide modification on the fluorophore through a copper-mediated reaction, resulting in a coupled, stable conjugate (166). We used the commercially available copper-mediated Click-iT Cell Reaction Buffer that "clicks" EDA with the fluorescent molecule Alexa Fluor 488 Azide and produces green fluorescence (158, 160, 161). EDA incorporation and visualization studies were performed with *B. anthracis* parent strain and the *B. anthracis* Δ*ftsX* and *ftsE(K123A/D481N)* mutant strains and imaged with laser scanning confocal microscopy at the University of Virginia School of Medicine Advanced Microscopy Center. The *B. anthracis* parent strain incorporated EDA along the septum, indicating active cellular division that appears highly regular, as evidenced by the even spacing of incorporated EDA in a chain of vegetative cells (Figure 3.2A). There was also diffuse, even EDA incorporation along the body of each vegetative bacterium, suggesting that the modified D-alanine was being incorporated into the cell wall during general peptidoglycan remodeling (Figure 3.2A). EDA labeling of the peptidoglycan of *B. anthracis* Δ*ftsX* and *ftsE(K123A/D481N)* demonstrated incorporation patterns that appeared to be different from the parent strain, but that were similar to each other as might be expected by mutations within the same (FtsE/X) complex. The mutant strains exhibited similar bacterial cell and chain morphologies under light microscopy as well (Figure 3.2B and C) (111, 145). As previously described, the *B. anthracis* Δ*ftsX* and *ftsE(K123A/D481N)* mutant strains exhibit a "kinked" morphology with irregular cellular elongation and chain

FIGURE 3.1

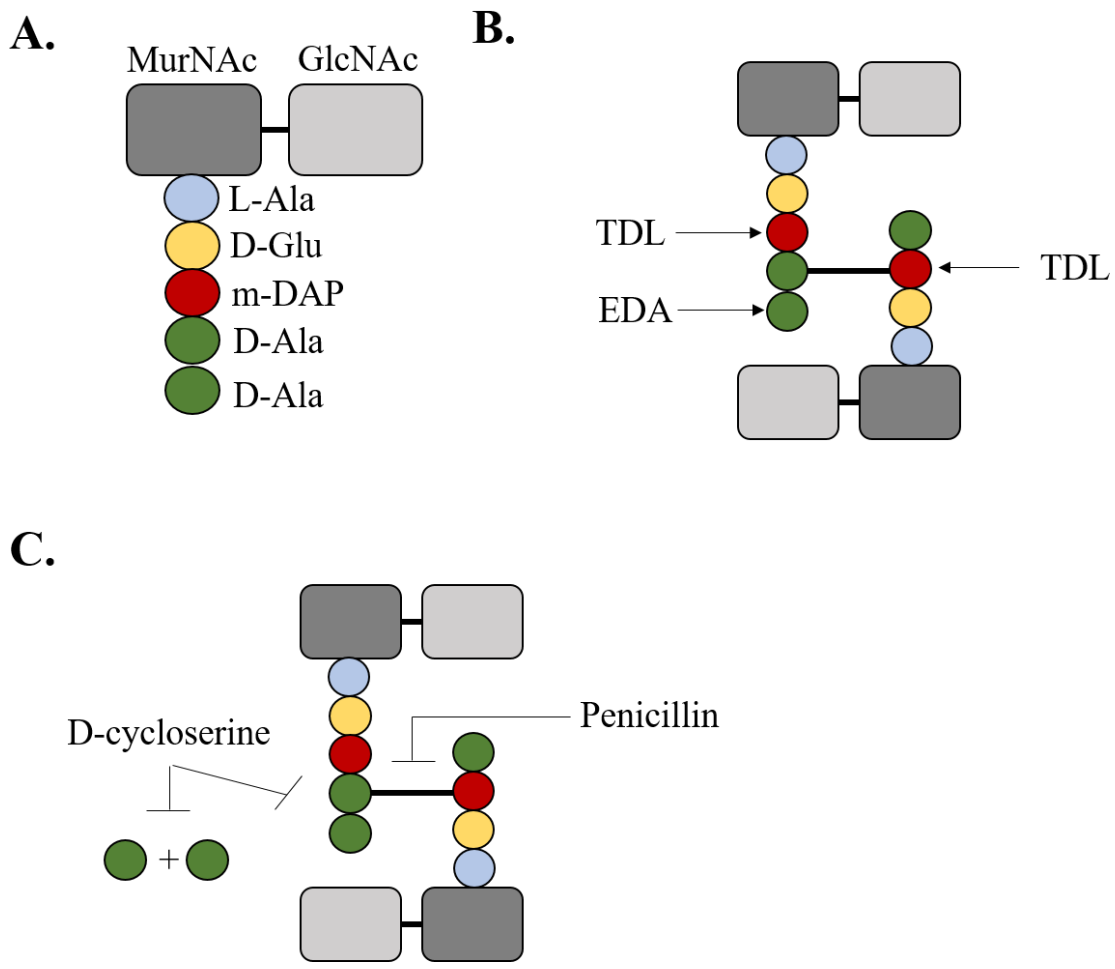

Figure 3.1: *B. anthracis* peptidoglycan. (A) Nascent peptidoglycan unit of *B. anthracis.* Included are the backbone molecules N-acetylmuramic acid (MurNAc) and N-acetylglucosamine (GlcNAc), as well as the pentapeptide stem comprised of L-alanine (L-Ala), D-glutamic acid (D-Glu), meso-diaminopimelic acid (m-DAP), and D-alanine (D-Ala). (B) Incorporation of EDA and TDL into peptidoglycan subunits. (C) Impact of the antibiotics penicillin and D-cycloserine on peptidoglycan subunit to cause a bactericidal effect. Based on modeling by Liechti *et al.*, 2014 (160)

FIGURE 3.2

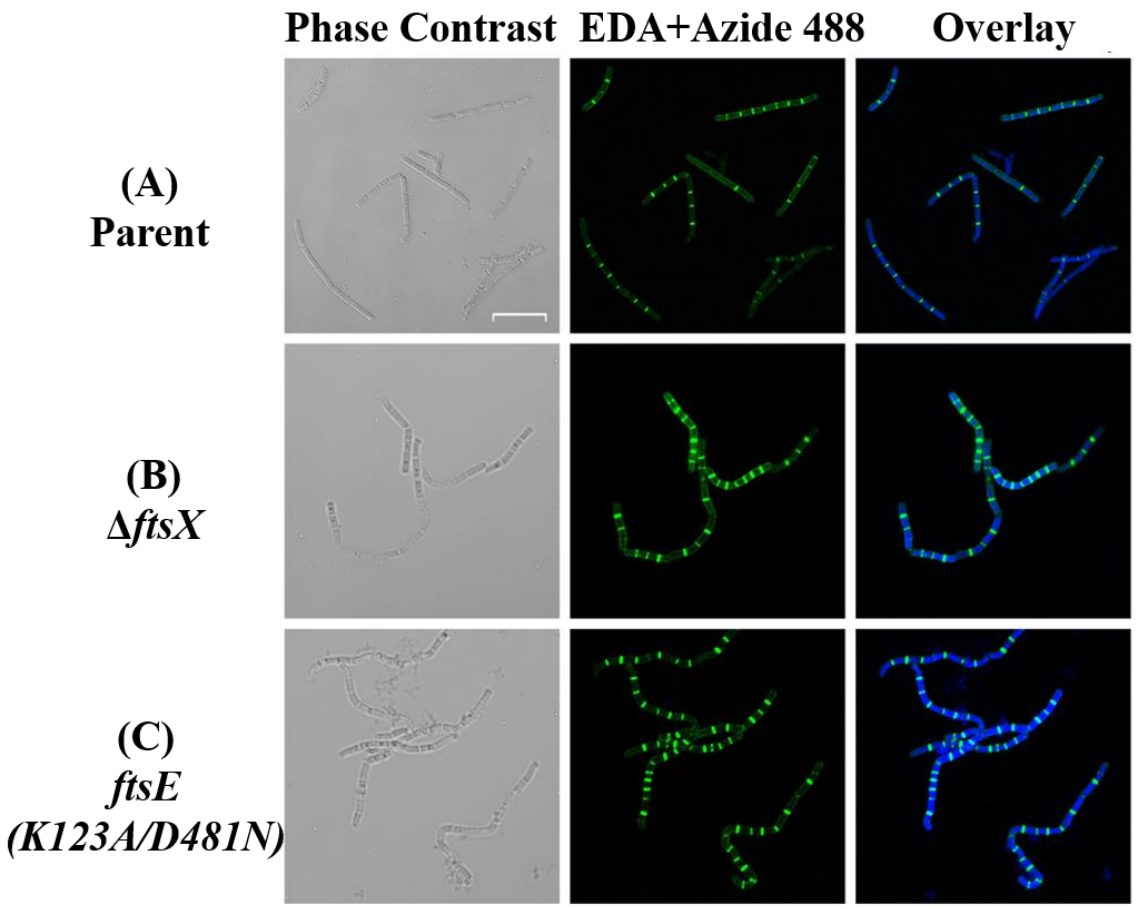
Phase Contrast
EDA+Azide 488
Overlay
(A)
Parent
(B)
ΔftsX
(C)
ftsE
(K123A/D481N)

Figure 3.2: Fluorescent peptidoglycan labeling of *B. anthracis* parent strain, Δ*ftsX* strain, and *ftsE(K123A/D481N)*. (A) *B. anthracis* parent strain, (B) *B. anthracis* Δ*ftsX* strain, and (C) *B. anthracis ftsE(K123A/D481N)* incorporation of EDA after "Click-iT" reaction using Alexa Fluor 488 azide. Microscopy images of the same field of bacteria for each treatment are shown as phase contrast images, EDA+488 Azide fluorescence images, and an overlay of the latter with nucleic acid staining by Hoechst 33342 dye. Scale bar is 10 μm. Images are representative of n=3 separate experiments with 10-20 images per experiment acquired per strain.

……

formation, as evidenced by uneven spacing of the septal division points with relatively sharp angles introduced into the bacterial chains that gave the chains a "kinked" appearance (Figure 3.2B and C).

B. anthracis Δ_ftsX_ and _ftsE(K123A/D481N)_ mutant strains exhibited significant morphological differences.

Significant morphological differences between the *B. anthracis* parent and mutant strains were observed (Figure 3.2). The *B. anthracis* Δ*ftsX* and *ftsE(K123A/D481N)* have individual cell measurements that were significantly shorter (measured as the septum-to-septum distance of bacterial cells in a chain) and wider (measured as the width across the midpoint of the bacterial rod shapes) compared to the parent strain (Figure 3.3 A and B). This observation was consistent with studies conducted with *Bacillus subtilis* mutants of the FtsE/X complex (112, 113, 123). In accordance with the morphological findings, *B. anthracis* Δ*ftsX* and *ftsE(K123A/D481N)* strains both showed an increased number of septal division points over an arbitrarily chosen distance of 10 μm highlighting the dysregulated nature of cellular division and/or elongation in these mutants as compared to the parent strain which consisted of regular, even, and smooth chains of vegetative cells (Figure 3.3 C). The *B. anthracis* Δ*ftsX* and *ftsE(K123A/D481N)* mutant strain "kinked" morphology, noted above, was quantified through measurement of vegetative cell chain angles from end-middle-end of the entire chain. These measurements indicated that, compared to the *B. anthracis* parent strain, the *B. anthracis* Δ*ftsX* and *ftsE(K123A/D481N)* mutant strains exhibited a wide array of sharper angles within chains of bacteria (Figure 3.3 D).

FIGURE 3.3

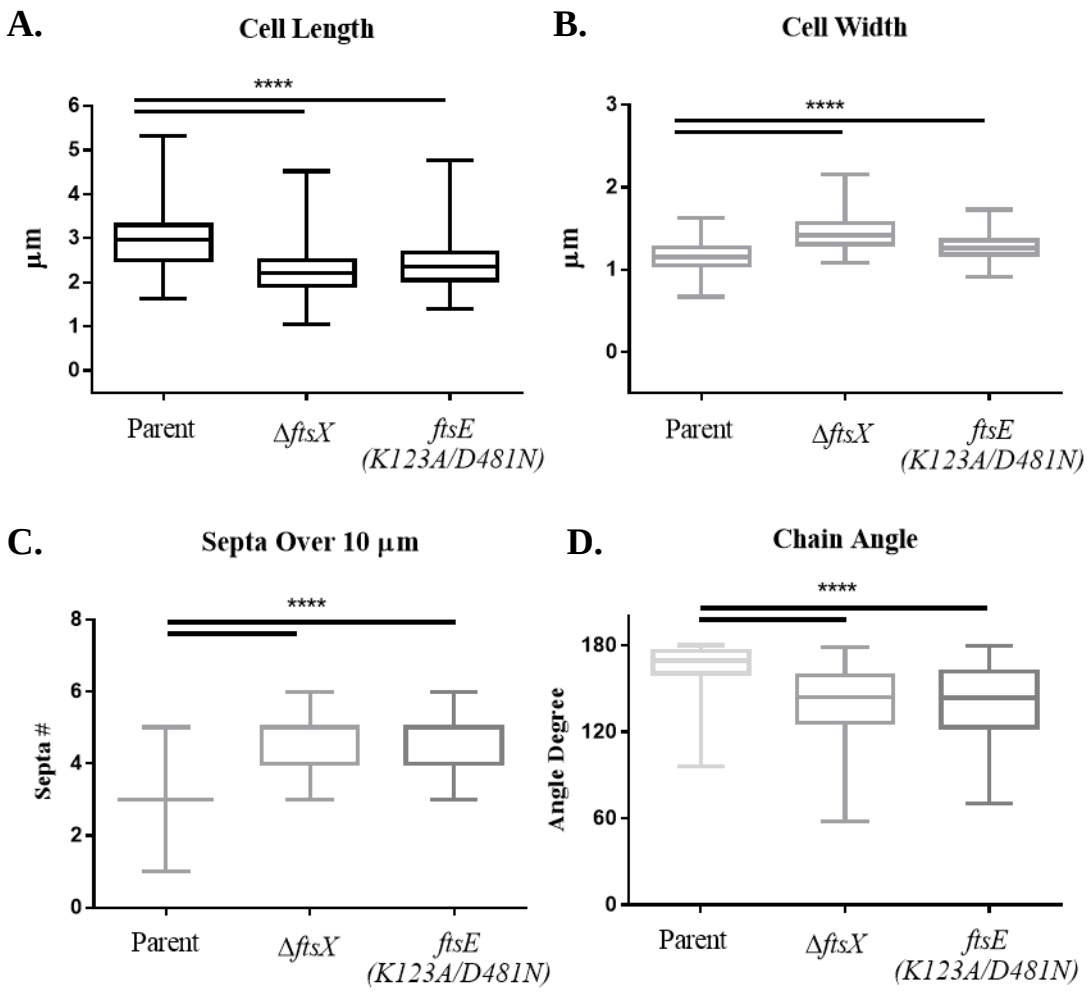
A.
Cell Length
****
µm
6
5
4
3
2
1
0
Parent
ΔftsX
ftsE (K123A/D481N)
B.
Cell Width
****
µm
3
2
1
0
Parent
ΔftsX
ftsE (K123A/D481N)
C.
Septa Over 10 µm
****
Septa #
8
6
4
2
0
Parent
ΔftsX
ftsE (K123A/D481N)
D.
Chain Angle
****
Angle Degree
180
120
60
0
Parent
ΔftsX
ftsE (K123A/D481N)

Figure 3.3: Quantification of parent and mutant strain vegetative cell morphology. Comparison of (A) individual cell length, measured as the distance from septum to septum in a bacterial chain, (B) individual cell width, measured at the midpoint of the bacterial rod, (C) total number of septa in a bacterial chain, measured over an arbitrarily chosen distance of 10 μm and (D) chain angle, as measured from end-middle-end of a chain of bacterial cells. Comparisons were made between *B. anthracis* parent strain, Δ*ftsX*, and *ftsE(K123A/D481N)*. Vegetative individual cell and chain measurements were made using Image J (167). A total of 100 measurements was collected for length and width for each strain and condition per experiment, and a total of 50 measurements was collected for septa count and chain angle determination for each strain and condition per experiment. Results are represented as a box-and-whisker plot with data points represented from minimum to maximum, n=3 separate experiments from which data was collected. Data were analyzed using a Mann-Whitney test, p****<0.0001.

……

Investigation of peptidoglycan amino acid incorporation using dual fluorescence labeling.

To study the impact of CXCL10 and CTTC treatment on *B. anthracis* parent strain and Δ*ftsX* and *ftsE(K123A/D481N)* mutant strains peptidoglycan, we dual labeled the peptidoglycan with EDA and a second fluorescent label, TAMRA-D-lysine (TDL) (Figure 3.1B) (158, 159). TDL was synthesized by coupling a D-lysine to the red fluorophore, TAMRA, which results in red fluorescent labeling of the peptidoglycan layer upon its incorporation and upon fluorescence imaging (158, 159). For dual labeling, mid log-phase bacteria were first incubated with 1 mM EDA for 1 h to label the bacterial peptidoglycan with the green fluorescent molecule. The medium containing EDA was removed by centrifugation, and medium containing the red fluorescent TDL was added followed by another 1 h incubation. The media containing TDL was removed and cells were ethanol fixed and processed for peptidoglycan labeling and nucleic acid staining. The resulting samples were placed on glass microscope slides with a coverslip for imaging. *B. anthracis* parent strain demonstrated sequential addition of EDA and TDL into the peptidoglycan layer of vegetative cells (Figure 3.4A). These results establish that we can utilize this method of peptidoglycan labeling to determine the impact of CXCL10 and CTTC on the processing of old (EDA labeled) and new (TDL labeled) peptidoglycan.

Incubation with CXCL10 and CTTC increases peptidoglycan release and decreases incorporation of new peptidoglycan in *B. anthracis* parent strain.

As noted earlier, we hypothesized that CXCL10 and CTTC were able to exert an antimicrobial effect against *B. anthracis* due to peptidoglycan processing. We performed

FIGURE 3.4

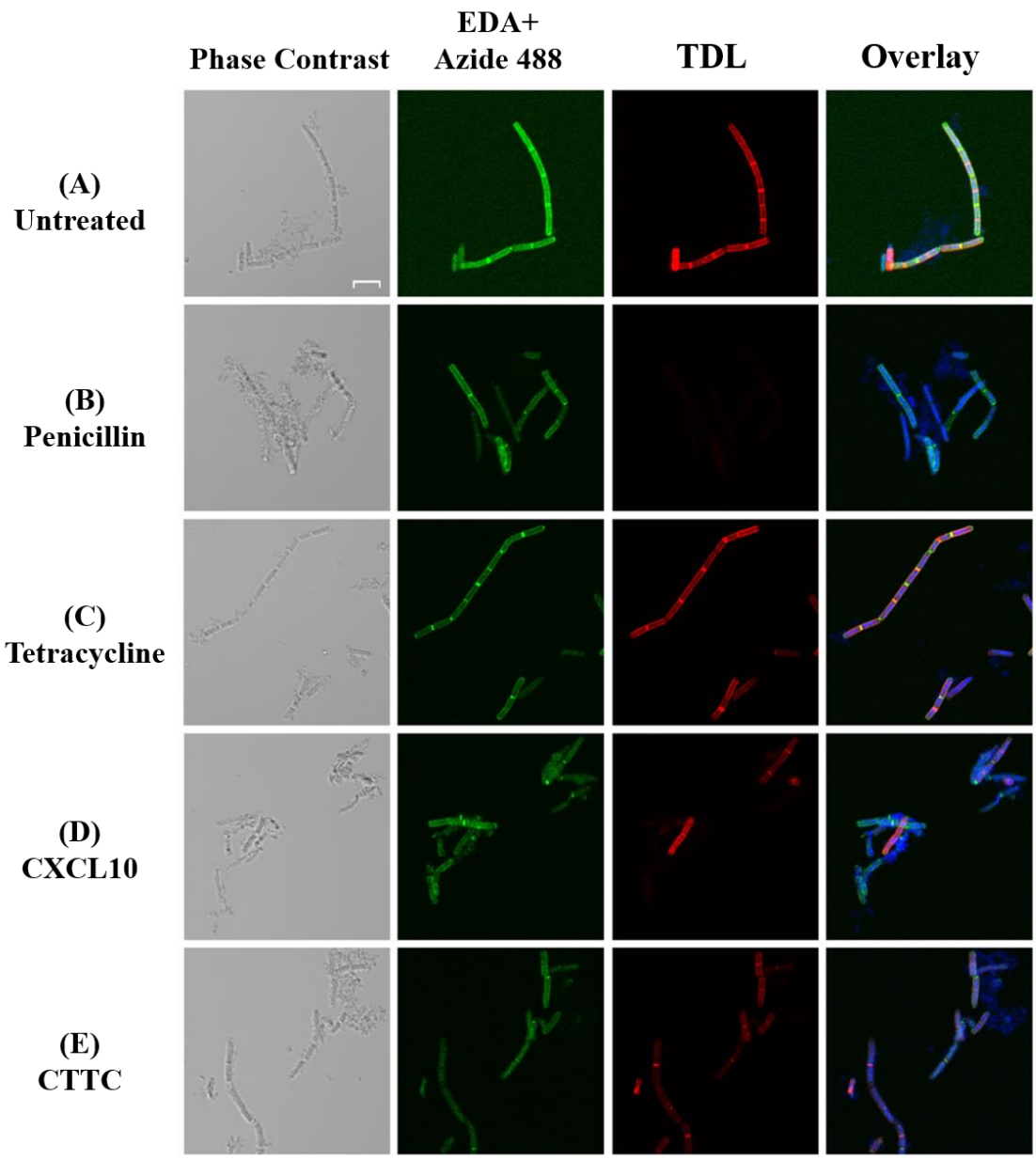
Phase Contrast
EDA+ Azide 488
TDL
Overlay
(A) Untreated
(B) Penicillin
(C) Tetracycline
(D) CXCL10
(E) CTTC

Figure 3.4: Comparison of antimicrobial treatment on *B. anthracis* parent strain peptidoglycan. *B. anthracis* parent strain (A) untreated control was compared to exposure with the antimicrobial molecules (B) penicillin (35 μg/ml), (C) tetracycline (40 μg/ml), (D) CXCL10 (2.8 μM), or (E) CTTC (2.8 μM) to determine the impact of exposure on peptidoglycan integrity and new subunit incorporation. Vegetative cells were incubated with EDA for 1 h before the addition of an antimicrobial agent (or buffer control) and with TDL for 1 h. Scale bar is 5 μm. n=2 separate experiments with 5-20 images being acquired for each treatment group.

……

dual labeling experiments, as described above, to determine if there was a difference in peptidoglycan remodeling (evidenced by EDA green fluorescence labeling initiated at the beginning of the experiment) or new peptidoglycan subunit addition (evidenced by later detection of the subsequent addition of the TDL for resultant red fluorescence labeling) in the absence or presence of CXCL10, CTTC, or other antimicrobial agents. Untreated *B. anthracis* parent strain showed clear evidence with green and red fluorescence from the EDA "pulse" and TDL "chase", respectively, such that an incorporation pattern could be appreciated for these peptidoglycan components, and cell morphology could be discerned (Figure 3.4A). In addition to CXCL10 and CTTC, we chose two commercially available antibiotics (penicillin and tetracycline) as controls in these experiments. Penicillin was chosen as a positive control for these experiments because it is a beta-lactam antibiotic that targets the bacterial cell wall and blocks the final cross-linking steps within peptidoglycan synthesis, resulting in a bactericidal effect through loss of peptidoglycan integrity and cell lysis (Figure 3.1C) (143, 168, 169). Tetracycline was chosen as a negative control for the cell wall experiments because it is a bacteriostatic agent that inhibits protein synthesis by targeting the bacterial aminoacyl-tRNAs and 30S ribosome complex rather than the bacterial cell wall (170). *B. anthracis* parent strain treated with penicillin (35 μg/ml) resulted in a loss of fluorescence signal from previously incorporated EDA peptidoglycan subunits with essentially a complete lack of new TDL peptidoglycan subunit integration as expected for a beta-lactam antibiotic treatment of the bacteria (Figure 3.4.B). In contrast, incubation of *B. anthracis* parent strain with tetracycline (40 μg/ml) did not impact the presence of EDA or incorporation of TDL into the bacterial peptidoglycan (Figure 3.4C). Incubation of the *B. anthracis* parent strain with CXCL10 (2.8 μM) resulted in a decreased

amount of both old EDA-labeled peptidoglycan and almost no new TDL-labeled peptidoglycan, similar to what was observed with the penicillin treatment of the organisms. This result suggests that peptidoglycan processing was disrupted by CXCL10. In previously published studies from our laboratory (145) and as described in Chapter 2, C-terminal truncated CXCL10, designated as CTTC, causes an antimicrobial effect only through an FtsE/X-dependent pathway. Incubation of *B. anthracis* parent strain with CTTC (2.8 μg/ml) resulted in a loss of fluorescence signal for both old EDA and new TDL incorporation into the cell wall. Since both CXCL10 and CTTC exhibit an antimicrobial effect against the *B. anthracis* parent strain through an FtsE/X-dependent pathway, these results supported the hypothesis that the deaths results from a disruption of peptidoglycan processing mediated through FtsE/X.

Incubation of *B. anthracis* Δ*ftsX* and *ftsE(K123A/D481N)* with CXCL10 or CTTC does not affect peptidoglycan detection.

Previous studies show that *B. anthracis* Δ*ftsX* is intermediately resistant to CXCL10 and completely resistant to CTTC (145). *B. anthracis* Δ*ftsX* killing by CXCL10 is thought to be mediated by the FtsE/X-independent pathway, resulting from general membrane depolarization from exposure to the CXC10 C-terminal α-helix (145). The untreated control sample of *B. anthracis* Δ*ftsX* shows incorporation of both EDA and TDL into the peptidoglycan (Figure 3.5A). Exposure of *B. anthracis* Δ*ftsX* to penicillin resulted in an absence of red fluorescence signal for TDL incorporation (Figure 3.5B). Notably, there was a substantial amount of green fluorescence signal from EDA still detectable after penicillin treatment compared to the penicillin treated parent strain (Figure 3.4B). It is

FIGURE 3.5

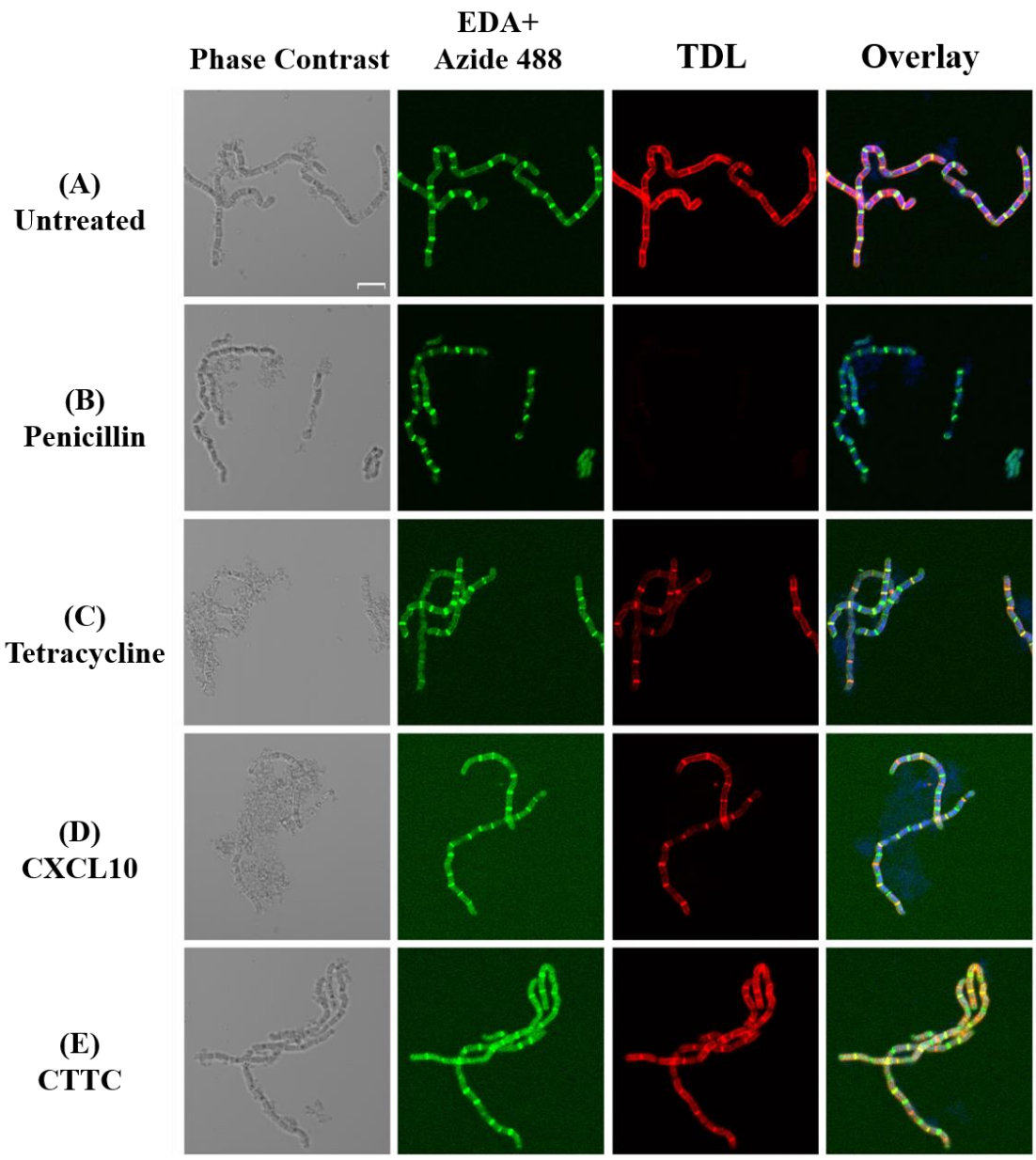
Phase Contrast
EDA+ Azide 488
TDL
Overlay
(A) Untreated
(B) Penicillin
(C) Tetracycline
(D) CXCL10
(E) CTTC

Figure 3.5: Comparison of antimicrobial treatment on *B. anthracis* Δ*ftsX* strain peptidoglycan. *B. anthracis* Δ*ftsX* strain (A) untreated control was compared to exposure with the antimicrobial molecules (B) penicillin (35 μg/ml), (C) tetracycline (40 μg/ml), (D) CXCL10 (2.8 μM), or (E) CTTC (2.8 μM) to determine the impact of the treatment on peptidoglycan integrity and new subunit incorporation. Vegetative cells were incubated with EDA for 1 h before the addition of an antimicrobial agent (or buffer control) and TDL for an additional 1 h incubation period. Scale bar is 5 μm. n=2 with 5-20 images being acquired for each treatment group.

……

possible there was a difference in peptidoglycan processing between the parent and mutant strains that resulted in different susceptibilities to penicillin. *B. anthracis* Δ*ftsX* incubation with tetracycline gave similar results to those observed with the parent strain (Figure 3.4C). Exposure of *B. anthracis* Δ*ftsX* to CXCL10 showed evidence of a significant fluorescent signal from EDA as well as evidence of incorporation of new TDL subunits, even though the vegetative cells appeared to be lysing and dying (Figure 3.5D). CTTC treatment had no impact on EDL and TDL incorporation/uptake in *B. anthracis* Δ*ftsX* when compared to the untreated control (Figure 3.5E). These data suggested that in the absence of FtsX, CXCL10 was not able to target the peptidoglycan remodeling complex to cause a bactericidal effect through peptidoglycan processing disruption.

B. anthracis ftsE(K123A/D481N) also has an intermediate level of resistance to CXCL10 but is completely resistant to CTTC, presumably through the same mechanisms as described above (145). Compared to the *B. anthracis ΔftsX* strain, the *ftsE(K123A/D481N)* mutant strain retains the intact FtsE/X complex while eliminating ATPase hydrolysis that provides the energy function for FtsE/X. Previous studies showed that the energy-providing activity of FtsE was important for mediating the antimicrobial activity of CXCL10 (145). Dual-labeling of untreated *B. anthracis ftsE(K123A/D481N)* mutant strain showed similar EDA and TDL incorporation as observed with *B. anthracis* Δ*ftsX* (Figure 3.6A). Incubation with penicillin resulted in a slight loss of EDA fluorescence signal detection compared to the untreated control, and no evidence of any TDL incorporation as was observed with the other bacterial strains above (Figure 3.6B). The results of tetracycline treatment on peptidoglycan yielded similar EDA and TDL incorporation

FIGURE 3.6

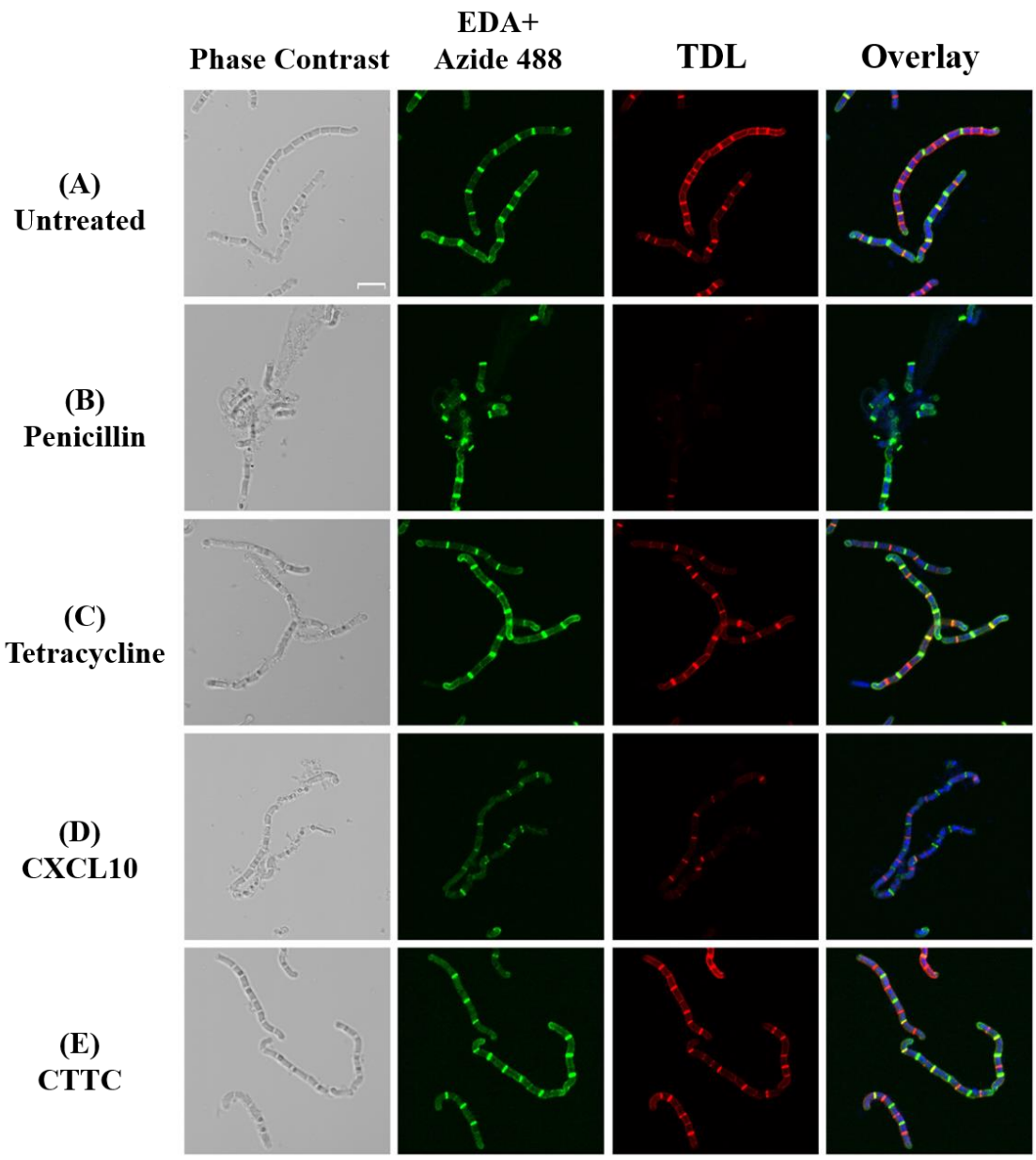
Phase Contrast
EDA+ Azide 488
TDL
Overlay
(A) Untreated
(B) Penicillin
(C) Tetracycline
(D) CXCL10
(E) CTTC

Figure 3.6: Comparison of antimicrobial treatment on *B. anthracis ftsE(K123A/D481N)* strain peptidoglycan incorporation. *B. anthracis ftsE(K123A/D481N)* strain (A) untreated control was compared to treatment with the antimicrobial molecules (B) penicillin (35 μg/ml), (C) tetracycline (40 μg/ml), (D) CXCL10 (2.8 μM), or (E) CTTC (2.8 μM) to determine the impact of the treatment on peptidoglycan integrity and new subunit incorporation. Vegetative cells were incubated with EDA for 1h before the addition of an antimicrobial agent (or vehicle control) and TDL for an additional 1h incubation period. Scale bar is 5 μm. n=2 with 5-20 images being acquired for each treatment group.

……

results as observed with the other strains (Figure 3.6C). Incubation of *B. anthracis ftsE(K123A/D481N)* with CXCL10 resulted in the detection of EDA and TDL even though bacterial lysis and death appeared to be occurring as evidenced with the phase contrast images (Figure 3.6D). Incubation with CTTC did not have any impact on the detection of EDA or TDL compared to the untreated control (Figure 3.6E). Overall, it appeared that CXCL10 resulted in the loss of peptidoglycan processing and incorporation in *B. anthracis* parent strain, but not in *B. anthracis* Δ*ftsX* or *ftsE(K123A/D481N)*.

Increased peptidoglycan release occurs as a result of exposure to CXCL10 or CTTC. In order to quantify the amount of peptidoglycan release during incubation of *B. anthracis* parent strain with CXCL10 or CTTC, a mammalian reporter cell line that overexpresses the immune cell receptor NOD2 was used (165, 171). This assay provides a sensitive detection method to quantitate the amount of peptidoglycan released into the media supernatant from bacteria (171–175). The NOD2 receptors on the reporter cell line are activated by the presence of muramyl dipeptide (MDP) fragments that are released from bacterial cell walls (173, 174). The NOD2 receptors subsequently activate an NF-κB construct in the mammalian cells that results in production of a secreted alkaline phosphatase (SEAP) reporter (165, 171). The SEAP molecule causes a colorimetric change upon addition in the appropriate detection medium, and the enzymatic activity of SEAP is proportional to the amount of MDP in the original sample. Antibiotics that target the cell wall (D-cycloserine and penicillin) were used as positive controls, while tetracycline was used as a negative control (Figure 3.1C). *B. anthracis* parent strain showed a significant increase in peptidoglycan release when compared to the untreated

FIGURE 3.7

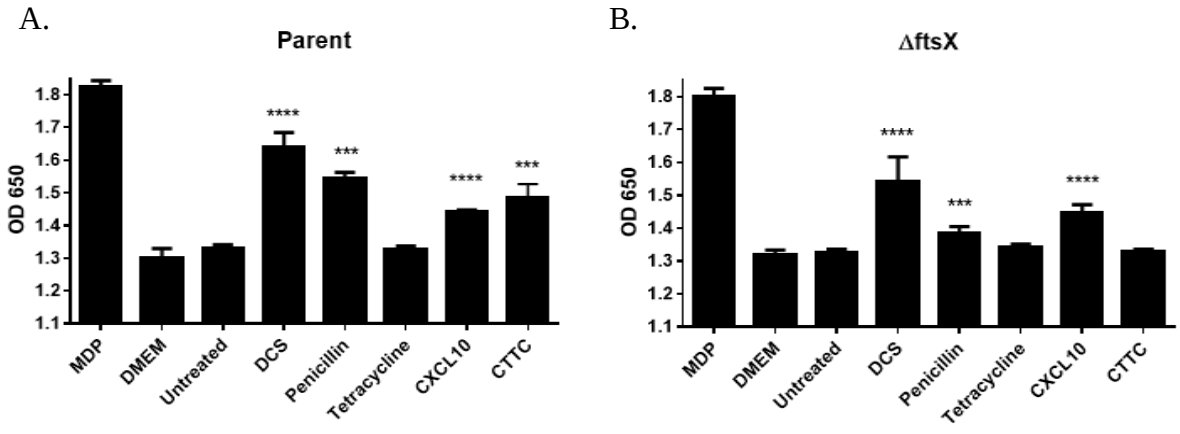

Figure 3.7: peptidoglycan release detection assay using HEK NOD2 expressing cells. The level of peptidoglycan subunit release into the supernatant of untreated or treated vegetative cells was measured by subsequent induction and analysis of NOD2 receptor reporter assay using HEK-Blue^{TM} hNOD2 mammalian cell line. (A) *B. anthracis* parent strain detection of peptidoglycan release in response to D-cycloserine (1.0 μg/ml), penicillin (0.5 μg/ml), tetracycline (10 μg/ml), CXCL10 (1.4 μM), or CTTC (2.8 μM), as compared to the untreated control group. (B) *B. anthracis* Δ*ftsX* strain detection of peptidoglycan release in response to D-cycloserine (1.0 μg/ml), penicillin (0.5 μg/ml), tetracycline (10 μg/ml), CXCL10 (1.4 μM), or CTTC (2.8 μM), as compared to the untreated control group. Results are represented +/- SEM, n=3 separate experiments with triplicate wells in each experiment. p***≤0.0001 p****<0.0001.

control in groups treated with D-cycloserine, penicillin, CXCL10 and CTTC (Figure 3.7A). In contrast, no increase was observed after incubation with tetracycline. With the *B. anthracis* Δ*ftsX* strain significant increases in peptidoglycan release upon treatment was detected with D-cycloserine, penicillin, or CXCL10 (Figure 3.7B). Importantly, there was no increase with CTTC, indicating CTTC was not causing peptidoglycan processing disruption. Colony forming units (CFUs) were also determined for all treatment groups under the same conditions (Figure 3.8). The data indicated that CXCL10 and CTTC were able to cause a statistically significant increase in peptidoglycan release in the *B. anthracis* parent strain. The *B. anthracis* Δ*ftsX* strain was increased by CXCL10 and not CTTC, an effect that may have been due (or partially due) to membrane disruption mediated by the C-terminal α-helix of CXCL10 through an FtsE/X-independent pathway (145).

3.4 Discussion

CXCL10 is a bifunctional antimicrobial molecule that kills *B. anthracis* via a combination of FtsE/X-dependent and FtsE/X-independent pathways, the latter of which is mediated by the amphipathic C-terminal α-helix and results in membrane depolarization. The FtsE/X-dependent pathway is mediated through the N-terminal region(s) of CXCL10, but the exact mechanism of action has remained unknown. Confocal microscopy with dual labeled peptidoglycan showed that *B. anthracis* parent strain exposure to CXCL10 and CTTC resulted in increased release and decreased incorporation of peptidoglycan subunits. The *B. anthracis* Δ*ftsX* and *ftsE(K123A/D481N)* did not show disruption of peptidoglycan in the presence of CXCL10, even though the treated cells appeared to be undergoing lysis (Figure 3.5D and 3.6D). *B. anthracis* Δ*ftsX*

FIGURE 3.8

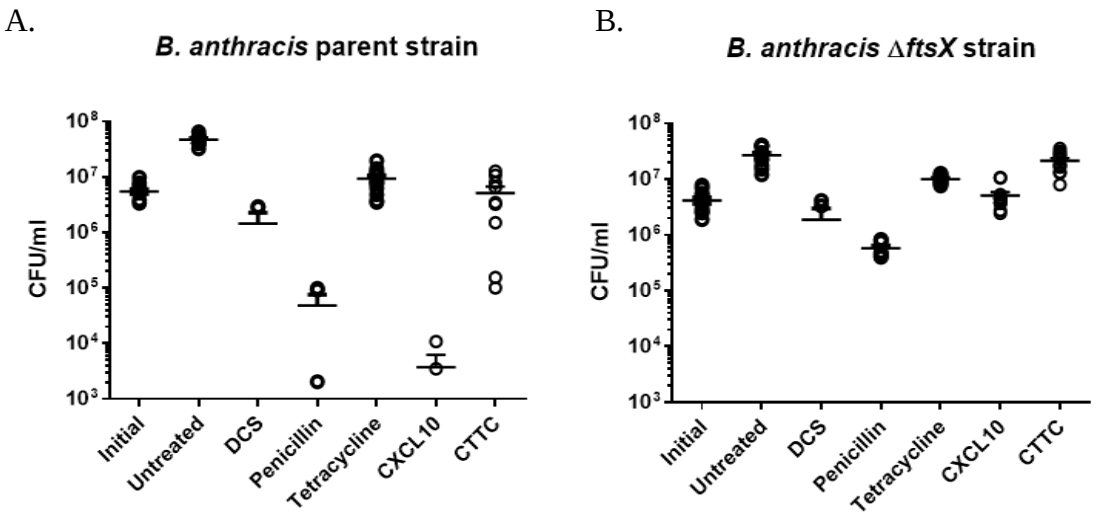

Figure 3.8: Corresponding CFU data for the peptidoglycan release detection assays. CFU enumeration was performed at the 2 h time point in parallel with supernatant collection and peptidoglycan release assay (Figure 3.6). (A) *B. anthracis* parent strain or (B) *B. anthracis* Δ*ftsX* strain exposed to D-cycloserine (1.0 μg/ml), penicillin (0.5 μg/ml), tetracycline (10 μg/ml), CXCL10 (1.4 μM), or CTTC (2.8 μM). n= 3 independent experiments.

and *ftsE(K123A/D481N)* were not visually affected by CTTC, a finding that corresponds to our previous work (145). Quantification of the amount of peptidoglycan released during antimicrobial treatment showed that the *B. anthracis* parent strain released increased amounts of peptidoglycan during incubation with either CXCL10 or CTTC. In contrast, *B. anthracis* Δ*ftsX* showed increased peptidoglycan release upon exposure to CXCL10 but not CTTC. These results support the hypothesis that FtsE/X-dependent killing by CXCL10 results from disruption of peptidoglycan processing.

Peptidoglycan is an essential component of the bacterial cell wall. It determines cell shape and promotes the structural integrity required to withstand internal and external pressures (146–148, 162, 176). Any disruption of peptidoglycan biosynthesis can be lethal, as evidenced by the many classes of antibiotics that target the cell wall biosynthetic pathway (127, 143, 155, 169, 177). In Gram-positive bacteria, FtsE/X has been shown to be part of a complex involved in cell wall biosynthesis and turnover, which requires the activation of various peptidoglycan hydrolases during cellular elongation (112, 113, 123, 124, 126, 142). FtsE/X is an intriguing antimicrobial target due to the role it has in hydrolase activation (146, 163, 178). Peptidoglycan hydrolase activity must be precisely regulated in order to maintain the balance between processing old bonds and making new peptidoglycan bonds, and dysregulation of hydrolase activity may result in bacterial lysis through the loss of cellular integrity (178). The requirement for an active FtsE/X in CXCL10 killing suggests that the mechanism of action involves the dysregulation of the FtsE/X complex-associated hydrolase (112, 113, 124, 135, 136, 151). It appears that CXCL10 disrupts the regulation

of peptidoglycan synthesis and turnover resulting in an increase in peptidoglycan release and cell wall breakdown that leads to cell death.

The findings presented in the current study suggest a novel mechanism for FtsE/X-dependent antimicrobial activity of CXCL10 by disrupting peptidoglycan remodeling. FtsE/X functions in Gram-positive bacteria at an intersection of bacterial growth and homeostatic peptidoglycan remodeling, making it an interesting target for antimicrobial molecules. FtsE/X is thought to exist within a larger cell wall synthesis complex, the continued identification and study of which will clarify further the impact CXCL10 has against *B. anthracis* vegetative cells through peptidoglycan disruption. Overall, these findings may lead to the development of novel small molecule therapeutics based on CXCL10 that target the FtsE/X complex to treat bacterial infections.

3.5 Materials and Methods

Bacterial strains and culture conditions. *B. anthracis* Sterne strain ATCC 7702 ($pXO1^+$, $pXO2^-$, American Type Culture Collection, Manassas, VA) was used in these experiments and designated as parent strain. *B. anthracis* Δ*ftsX* and *B. anthracis ftsE(K123A/D481N)* were derived from the Sterne strain (111, 145). Vegetative cells were prepared by inoculating *B. anthracis* parent strain spore stocks or *B. anthracis* mutant strain vegetative cell frozen stocks into 10 ml of brain heart infusion (BHI) broth (Difco, Franklin Lakes, New Jersey) and incubating overnight at 37°C with shaking (250 rpm). Mid-log phase cultures were prepared the next day by diluting the overnight culture 1:20 in fresh BHI broth followed by incubation at 37°C with shaking for ~2 h until an optical density at 600

nm (OD600) between 0.6 and 0.65 was achieved, at which time the cultures were used for experiments. All laboratory work involving *B. anthracis* Sterne or Sterne-derived strains was approved through the University of Virginia Institutional Biosafety Committee. Biosafety level 2 practices were used for all work involving *B. anthracis* Sterne or Sterne-derived strains.

Peptidoglycan Labeling Reagents. Ethynyl-D-alanine (EDA) ((S)-2-Amino-4-pentynoic acid) (Boaopharma, Inc., Natick, MA) was resuspended in H_2O and used for peptidoglycan labeling at a concentration of 100 mM. EDA was used in conjunction with the Click-iT® Cell Reaction Buffer Kit (Invitrogen, Carlsbad, CA) and 'clickable' Alexa Fluor 488 Azide (Invitrogen, Carlsbad, CA) according to manufacturer's instructions. TAMRA-D-lysine (TDL) was synthesized according to the protocol described previously (158, 159). Briefly, 5-carboxytetramethylrhodamine succinimidyl ester (Anaspec, Fremont, CA) and N-α-BocD-Lys-OH (Chem-Impex, Bensenville, IL) were mixed to form TDL. The product was purified using reverse phase HPLC on Waters ZQ 2000 LCMS system with a gradient of acetonitrile in water with 0.1% (vol/vol) formic acid 5-95% (vol/vol) acetonitrile for 20 min, eluting at 20 ml min^{-1}. The two isomers were eluted on a Waters Sunfire Prep C18 OBD column with a 5μm particle size, 19 mm internal diameter and length of 100 mm. The purified product solution was then lyophilized overnight to form a stable TDL powder.

Peptidoglycan Labeling Microscopy Studies. Overnight cultures of *B. anthracis* strains were diluted 1:20 in fresh BHI broth followed by a 1 h incubation at 37˚C with shaking at 250 rpm. After 1 h, 150 μl of a 100 mM EDA stock was added to the culture for a final

concentration of 1 mM and incubation continued until an OD_{600} of between 0.6-0.65 was reached. The entire culture was centrifuged for 5 min at 3600 rpm to collect a pellet of the log-phase bacteria. The supernatant was discarded, and a total of 5 µl of the resulting pellet was placed into 500 µl DMEM + 10% FBS + 1 mM EDA or 0.5 mM TDL, -/+ penicillin (35 µg/ml), tetracycline(40 µg/ml), CXCL10 (2.8 µM), or CTTC (µM) and incubated for 1 h at 37˚C in 5% CO_2. An aliquot was transferred to a 1.5 ml Eppendorf tubes and centrifuged for 8 min at 15,500 rpm after which the supernatant was discarded. A 1 ml volume of ice-cold 70% ethanol was added to the cell pellet and incubated for 1 h on ice. Bacterial cells were removed from the ethanol and incubated for 1 h at room temperature in 3% BSA/PBS. Cells were then incubated for 1 h at room temperature in 0.5 ml of Click-iT Cell Reaction Buffer according to the manufacturer's directions with Alexa Fluor 488 Azide (ThermoFisher Scientific, Waltham, MA) to fluorescently label the peptidoglycan cell wall. Nucleic acids were stained with Hoechst 33342 dye (Invitrogen, Carlsbad, CA) with a 20 min incubation, as per the manufacturer's directions. Cells were then washed 1x with PBS to remove excess dye. The bacterial cells were re-suspended in PBS and placed on glass slides with a coverslip and imaged using a Zeiss LSM 880 confocal microscope (Ziess, Oberkochem, Germany) at 63X magnification. Dual labeling confocal microscopy peptidoglycan labeling experiments were performed as described above, with the exception that 0.5 mM TDL was substituted for EDA during antimicrobial treatment. Images were acquired and analyzed using Zen 2.1 software (Zeiss, Oberkochem, Germany). Phase contrast and fluorescence images were collected with settings fixed on the untreated control group at the beginning of each session. Further analysis was completed using Image J (167).

Peptidoglycan Release Assay

Overnight cultures of *B. anthracis* parent and Δ*ftsX* strains were diluted 1:20 in fresh BHI broth followed by a 2 h incubation at 37˚C with shaking at 250 rpm. Vegetative cells were diluted to approximately 3.0x10^6 CFU ml^{-1} in fresh Dulbecco's modified Eagle's medium, high glucose, no glutamine, no phenol red (Gibco-Invitrogen, Carlsbad, CA) containing 4 mM GlutaMAX™ supplement, 10% (v/v) fetal bovine serum (HyClone, Logan, UT), and the penicillin, D-cycloserine, tetracycline, CXCL10, or CTTC to be tested. Aliquots of 400 µl were placed into 48 well plates and incubated at 37°C with 5% CO_2 for 0 or 2 h with various antimicrobial agents to be tested. Penicillin (0.5 µg ml^{-1}) and D-cycloserine (1.0 µg ml^{-1}) were used as positive controls; tetracycline (10 µg ml^{-1}) was used as a negative control. CXCL10 was tested at a concentration of 1.4 µM and CTTC was tested at 2.8 µM. After 0 or 2 h, the wells were collected in 1.5 ml Eppendorf tubes and centrifuged for 5 min at 15,000 rpm. The resulting supernatant was sterilized using a 13 mm 0.22 µM filter (ThermoFisher Scientific, Waltham, MA) and heat-inactivated for 5 min at 95˚C. Concurrent CFU ml^{-1} was determined for each sample. HEK-Blue™ hNOD2 mammalian cell line (Invivogen, San Diego, CA) at a concentration of 50,000 cell $well^{-1}$ in 180 µl was exposed to 20 µl of the filtered supernatant in triplicate and incubated for 20H at 37°C with 5% CO_2. Finally, 20 µl of the resulting HEK-Blue™ hNOD2 supernatant was added to 180 µl HEK-Blue™ Detection medium (Invivogen, San Diego, CA) and incubated for 24 h at 37°C with 5% CO_2. Muramyl dipeptide (Invivogen, San Diego, CA) was used as a positive control. The colormetric change of the detection media was measured at OD_{650} using the ELx800 Absorbance Reader (BioTek, Winooski, VT).

Statistical Analyses

Statistical analyses and graphing were performed using GraphPad Prism 6.0 software. Experimental groups were analyzed using an unpaired, two-tailed student *t* test or Mann-Whitney test as noted in the text or figure legends. Significant differences were determined to have a P value of ≤ 0.05.

3.6 Acknowledgements

We thank Barbara Mann and George Liechti for their advice and helpful discussions, and Stephen A. Morse (Centers for Disease Control and Prevention, Atlanta, GA) for providing helpful comments on the manuscript. This work used the Zeiss LSM 880 confocal microscope in the Advanced Microscopy Facility, which is supported by the University of Virginia School of Medicine.

CHAPTER 4:

CXCL10 impacts *B. anthracis* spore germination and viability through the putative DL-endopeptidase BAS0651

Barbier M*, Margulieux KR*, Sen E, Lowe DE, Crawford MA, Navarro AP, Damron FH, Hughes MA

Adapted from: Manuscript in Progress

*These authors contributed equally to this work.

4.1 Abstract

B. anthracis spores are the infectious agent of anthrax and can remain in a metabolically inert state that is unaffected by any currently available antibiotics. The interferon-γ inducible, ELR (-) CXC chemokine CXCL10 has been observed to have an antimicrobial effect against *B. anthracis* spores, but how CXCL10 targets the spore has remained unknown. In the present chapter, we sought to identify and characterize specific *B. anthracis* spore components that mediate CXCL10 antimicrobial activity against the spore. Bacterial spore proteins involved in the inhibition of spore germination by the chemokine CXCL10 were identified by screening a spore transposon mutant library for mutants resistant to CXCL10. The most prominent gene identified from the screen encoded a *B. anthracis* hypothetical protein identified as BAS0651, a putative peptidoglycan hydrolase likely involved in cell wall remodeling. Studies performed with a *B. anthracis* Δ*BAS0651* mutant strain supported the hypothesis that BAS0651 plays a key role in mediating antimicrobial activity of CXCL10 against *B. anthracis* spores. CXCL10 killing mediated by BAS0651 appears to involve an inhibition of spore germination and an increase in spore permeability, resulting in the loss of spore viability. *In vivo* murine studies using C57BL/6 mice revealed that, in the absence of BAS0651, *B. anthracis* Sterne strain spores appear to undergo a relatively higher percentage of bacterial germination and resultant vegetative cell proliferation during the acute infection stage as compared to the *B. anthracis* parent strain. The identification of BAS0651 as a novel antimicrobial target of CXCL10 in spores may lead to the development of novel therapeutic strategies for bacterial infections caused by *B. anthracis* and other spore-forming pathogens such as *Clostridium difficile*.

4.2 Introduction

The infectious form of *B. anthracis* is the spore, which is a hardy, metabolically dormant cell resistant to desiccation, chemical treatment, UV radiation, and high temperatures (20, 32–34). Deposition of *B. anthracis* spores into the airways results in inhalational anthrax, which has the highest associated mortality rate of anthrax infections, even with antibiotic treatment (2, 14, 19). Spores can reside in the lungs for an extended period of time and are not cleared by traditional antibiotics (24, 25, 179). As a result, patients who have been exposed to anthrax spores by the inhalational route of infection are advised to adhere to antibiotic treatment for at least 60 days to allow time for the spores to germinate to the vegetative form of the organism, which can be treated with an appropriately prescribed antibiotic (2). Once inhaled, spores are taken up by phagocytes, such as alveolar macrophages and dendritic cells, and are transported to the mediastinal lymph nodes (118). Spore germination leads to the production of toxins and proteases by the resulting vegetative cells that disrupt epithelial barriers, allowing dissemination throughout the host (180–183). Once germination occurs, the vegetative cells are also vulnerable to various clearance mechanisms of the innate immune system that can effectively eliminate many of the vegetative cells (172, 184, 185). However, host defense can be overcome, and vegetative cells can escape from the phagocytic vesicles and lymph nodes and enter the bloodstream, leading to bacterial dissemination, toxemia, and death (53, 118). Interestingly, while *B. anthracis* spores are resistant to a wide array of environmental stressors and immune effectors, the interferon-gamma inducible (IFN-γ), Glu-Leu-Arg negative [ELR(-)] CXC chemokines CXCL9, CXCL10, and CXCL11 have been shown to decrease spore and vegetative cell viability (105). While host phagocytic cells play a

crucial role in killing spores that they engulf, previous studies from our laboratory support that the IFN-γ inducible, ELR(-) CXC chemokines also directly kill *B. anthracis* Sterne strain *in vitro* as well as *in vivo* during pulmonary infection in a murine model of inhalational anthrax infection as addressed in Chapter 1.6 (110). The results support that there is direct antimicrobial killing of the organism by CXCL9, CXCL10, and/or CXCL11 during pulmonary infection (110).

While *B. anthracis* vegetative cells can be killed through appropriate antibiotic treatment, the spore form can remain in a metabolically inert state that is unaffected by any of the currently available antibiotics (2, 19). The IFN-γ inducible, ELR(-) CXC chemokines have been observed to mediate an antimicrobial effect against *B. anthracis* spores, however, the mechanism of action remains unknown (105, 110). In the present study, we sought to identify and characterize specific *B. anthracis* spore cellular components important for the anti-spore effects of CXCL10. We hypothesized that CXCL10 blocks spore germination by interaction with specific spore targets or bacterial effectors. Bacterial targets involved in the inhibition of spore germination by CXCL10 were identified by screening a transposon mutant library of *B. anthracis* Sterne strain spores for resistant isolates (i.e., mutant spores that were resistant to CXCL10 such that they survived and/or proceeded to undergo germination in the presence of CXCL10). Through this screen, we identified a gene or its gene product that appears to play a major role in mediating CXCL10 antimicrobial activity against the *B. anthracis* spore, and to a lesser extent against the vegetative cell. This gene is designated as *BAS0651*, which encodes a hypothetical *B. anthracis* Sterne strain protein that, according to amino acid sequence homology analysis,

appears to be a putative DL-endopeptidase that may be involved in cell wall remodeling. Moreover, we found that the absence of BAS0651 in *B. anthracis* Sterne strain spores was associated with a higher net result of bacterial germination and vegetative cell proliferation during early stages of pulmonary infection (within first 1-3 days) *in vivo* in mice compared to the *B. anthracis* parent strain. These observations support that CXCL10 plays a key role in innate immune defense against the *B. anthracis* spore by targeting a putative DL-endopeptidase, which may affect peptidoglycan remodeling during spore germination. The identification of BAS0651 as a novel antimicrobial target of CXCL10 provides a foundation for the development of therapeutic strategies for bacterial infections caused by *B. anthracis* or other spore-forming pathogens such as *Clostridium difficile*.

4.3 Results

Transposon library screen of *B. anthracis* Sterne strain mutant spores.

Previous studies from our laboratory characterized an antimicrobial effect of CXCL10 on *B. anthracis* vegetative cells, including identification of a putative vegetative cell membrane target, FtsX of the prokaryotic FtsE/X ATP-binding cassette (ABC) transporter complex (105, 110, 111, 145). Additionally, we also described an antimicrobial effect of CXCL10 against *B. anthracis* spores (105) that involves a spore target that is not FtsX (unpublished data), but the mechanism of action against the spore has not been further elucidated. To identify bacterial spore targets mediating CXCL10 antimicrobial activity, we screened spores derived from a *B. anthracis* transposon mutant library to enrich for isolates that are resistant to the sporicidal effects of CXCL10 (Figure 4.1A) (111, 186). Since CXCL10-resistant spores are expected to undergo germination in the presence of

FIGURE 4.1

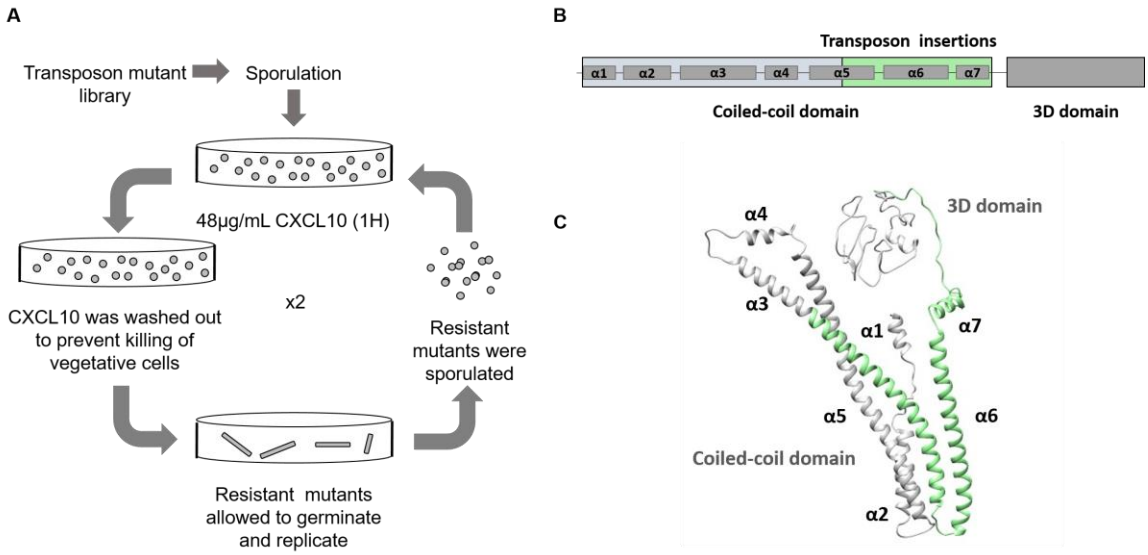

Figure 4.1: Transposon mutant library screen. (A) Schematic representation of the *B. anthracis* transposon mutant spore screen. Spores were submitted to two cycles of selection with CXCL10 in order to select for spores resistant to the antimicrobial effects of the chemokine. (B) 98% of resistant isolates were found to be disrupted in the gene *BAS0651*. All transposon insertions were found in the above indicated region (green) of the coiled-coil domain. **(C)** The three dimensional structure of BAS0651 was predicted using the I-TASSER server (187). BAS0651 is predicted to have an N-terminal coiled-coil domain similar to *Streptococcus pneumoniae* PcsB and *Bacillus subtilis* CwlO, and an enzymatic domain containing three conserved aspartic acids (3D domain) similar to *B. subtilis* CwlO (112, 113, 151)

CXCL10 and outgrowth into vegetative cells, a series of enrichment steps was undertaken in which the resultant vegetative cells from the first spore screen were sporulated. The resultant spores were exposed again to CXCL10. This process was repeated for combined sequential spore screens. A total of 188 colonies were recovered from the second screen of mutant spores, and the transposon insertion sites were determined through specific amplification of the DNA flanking *Himar1* insertion sites (186). Of the 188 isolates, 184 transposon mutant spores (98%) resistant to CXCL10 were found to have a transposon insertion in various locations of the *BAS0651* locus, which encodes a hypothetical protein. Based on National Center for Biotechnology Information (NCBI) protein blast searches, insertions in the gene *BAS0651* were found in at least four distinct sites between positions 500 and 1000 (NCBI Gene ID: 2851369) (Figure 4.1B) such that the isolates were not clones of each other. Of the remaining 4 isolates, three mutants were found to have a transposon insertion in the hypothetical *BAS1458* locus (NCBI Gene ID: 2852666) and one mutant had a transposon insertion in hypothetical *BAS5090* (NCBI Gene ID: 2848554). Based on NCBI BlastP searches, the gene products for each of these three transposon-disrupted genes indicates that they may be lytic enzymes, potentially associated with bacterial cell wall remodeling.

BAS0651 encodes a putative cell wall hydrolase, and analysis using the NCBI Conserved Domain Database (CDD) indicates that the protein is similar to the *Bacillus subtilis* DL-endopeptidase CwlO (47% positive) and *Streptococcus pneumoniae* muralytic enzyme PcsB (46% positive) (112, 113, 142, 151, 188). We modeled the three dimensional structure of BAS0651 using the program *I-TASSER* (187) (Figure 4.1C). The N-terminus

of BAS0651 is predicted to encode an N-terminal signal peptide and a coiled-coil domain formed by 7 α-helices (Figure 4.1C). The predicted coiled-coil domain is structurally similar to that observed in the crystal structure of PcsB from *Streptococcus pneumoniae* (TM-score 0.758) (151, 189) (Figure 4.2). The "3D" domain characterized by three conserved aspartate residues is located on the C-terminus of BAS0651 and is similar to the *B. subtilis* catalytic domain defined for CwlO (112, 113, 123, 151). These findings suggest that the *B. anthracis BAS0651* gene product contains a coiled-coil domain that interacts with membrane proteins and an enzymatic C-terminal domain that acts as DL-endopeptidase based on the active site, and overall may be involved in peptidoglycan remodeling (112, 113, 123, 124, 188). CDD analysis of the second identified gene, *BAS5090,* shows that it contains two putative SH3 domains, shown to be important for cell wall association, as well as a muralytic domain in the C-terminus. It has 61% positive similarity to the *B. subtilis* protein YocH that has been shown to function as a cell-wall binding protein and muralytic enzyme (190). CDD analysis of the third identified gene, *BAS1458,* suggests that it is a penicillin binding protein, which could be involved in peptidoglycan biosynthesis (188). Overall, the three genes identified appear to share a common feature of being potential lytic enzymes that could be involved in the maintenance and remodeling of the bacterial cell wall. Degradation of the thick, peptidoglycan-rich spore cortex is a critical aspect of spore germination. Disruption or dysregulation of the controlled processes that degrade or remodel the spore cortex during germination would be expected to be detrimental to successful germination of the spore (6, 8).

……

FIGURE 4.2

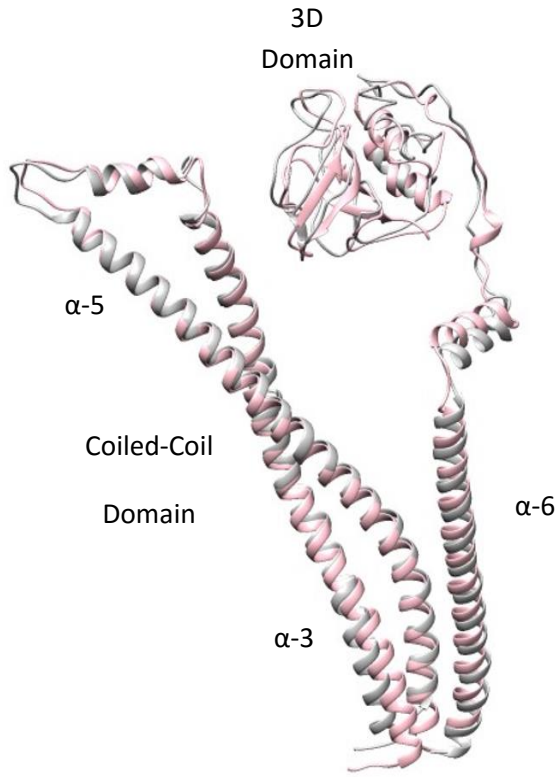

Figure 4.2: Superposition of modeled *B. anthracis* BAS0651 and *S. pneumoniae* PcsB. The structural model of BAS0651 predicted using I-TASSER server. The predicted model of BAS0651 suggests that there is a coiled-coil domain formed by 3 long α-helical strands designated as α3, α5, α6 at amino acid positions 61-124, 148-219 and 224-283. A predicted 3D domain is located in amino acid positions 361-419. Superposition of a modeled BAS0651 (pink) and *Streptococcus pneumoniae* PcsB protein (gray) (protein data base ID: 4cgkA) shows a significant overlap of the domains. Superposition modeling was performed using UCSF Chimera (191). Root Mean Square Deviation: 1.70 Å.

……

Deletion of the *B. anthracis* hypothetical gene, BAS0651, is associated with spore resistance to CXCL10.

To characterize the effect of *BAS0651* in spore susceptibility to CXCL10, we generated a *B. anthracis* Δ*BAS0651* strain. Phenotypically, Δ*BAS0651* mutant strain vegetative cells produced smaller colonies on agar plates even though the overall *in vitro* growth rate was similar to the parent strain (Figure 4.3A and 4.3B). Microscopy studies revealed that the Δ*BAS0651* mutant strain vegetative cells grew in slightly shorter chains compared to the parent strain (Figure 4.3C). Despite shorter chain lengths, the Δ*BAS0651* mutant strain had similar single cell dimensional traits as the parent strain (Figure 4.3D). To investigate whether *BAS0651* was a putative spore target of CXCL10 involved in the anti-spore effects of this chemokine, we performed spore germination and viability assays comparing *B. anthracis* parent and Δ*BAS0651* spores.

To test if germination differed between the *B. anthracis* parent strain and Δ*BAS0651* strain in the presence of CXCL10, parent strain and Δ*BAS0651* mutant strain spores were exposed to either 8 or 48 μg/ml of CXCL10 or a vehicle control in germination permissive medium for 4 h. The viability of the remaining (non-germinated) spores and newly germinated vegetative cells treated with or without CXCL10 was then determined by measuring colony forming units (CFUs) before and after heat treatment of the samples. Importantly, since heat treatment kills vegetative cells in the samples, the number of spores and vegetative cells can be quantified. The results indicated that each strain demonstrated germination by the loss of heat resistance quantified by CFU enumeration (Figure 4.4). However, the number of spores detected in the Δ*BAS0651* mutant strain after 4 h exposure to 8 or 48

FIGURE 4.3

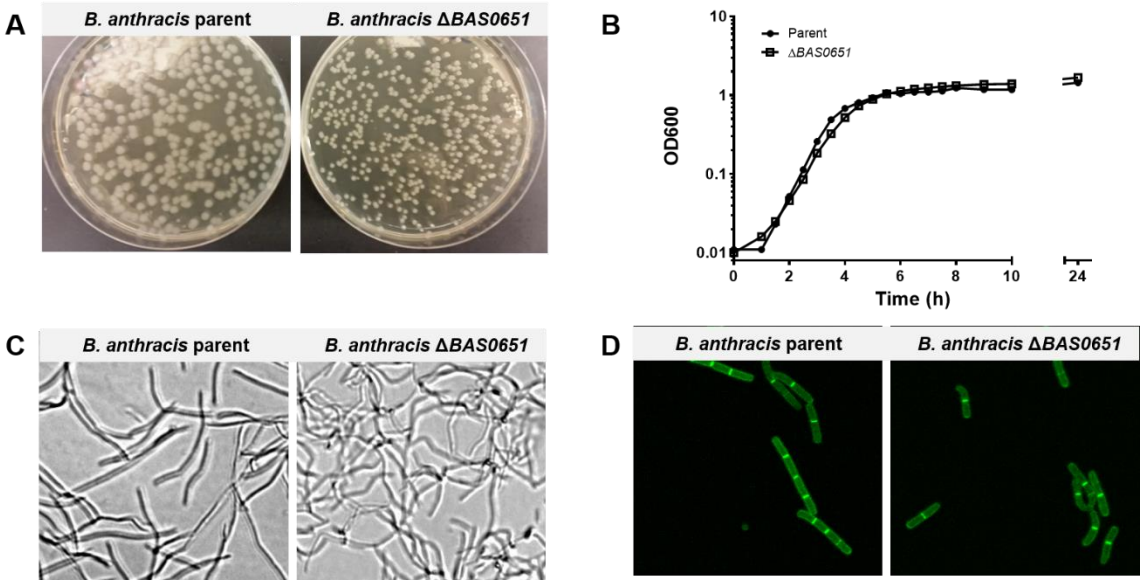
A
B. anthracis parent
B. anthracis ΔBAS0651
B
Parent
ΔBAS0651
OD600
10
1
0.1
0.01
0
2
4
6
8
10
24
Time (h)
C
B. anthracis parent
B. anthracis ΔBAS0651
D
B. anthracis parent
B. anthracis ΔBAS0651

Figure 4.3: Phenotypic characteristics of the vegetative cells of the *B. anthracis* Δ*BAS0651* mutant strain compared to the parent strain. (A) *B. anthracis* Δ*BAS0651* mutant strain produces smaller, more compact colonies on a BHI agar plate after overnight incubation at 37˚C. (B) Growth curves of *B. anthracis* parent and Δ*BAS0651* mutant vegetative strains. Although the Δ*BAS0651* mutant produces smaller colonies on agar, the appearance of the growth curve generated in BHI broth was almost identical to that of the parent strain. The doubling time for the parent strain was 0.99 hr^{-1} and for the Δ*BAS0651* strain was 1.08 hr^{-1}. (C) Light microscopy images of the parent and Δ*BAS0651* mutant strain (400X magnification) show slightly shorter bacterial chain lengths of the mutant strain. (D) Immunofluorescence confocal microscopy of the parent and Δ*BAS0651* mutant strain with modified D-alanine incorporated into the peptidoglycan using Click-iT technology and labeled with Alexa 488 green fluorescent probe (63X magnification) show chain length is shorter in the mutant strain, but single cell characteristics are similar.

……

FIGURE 4.4

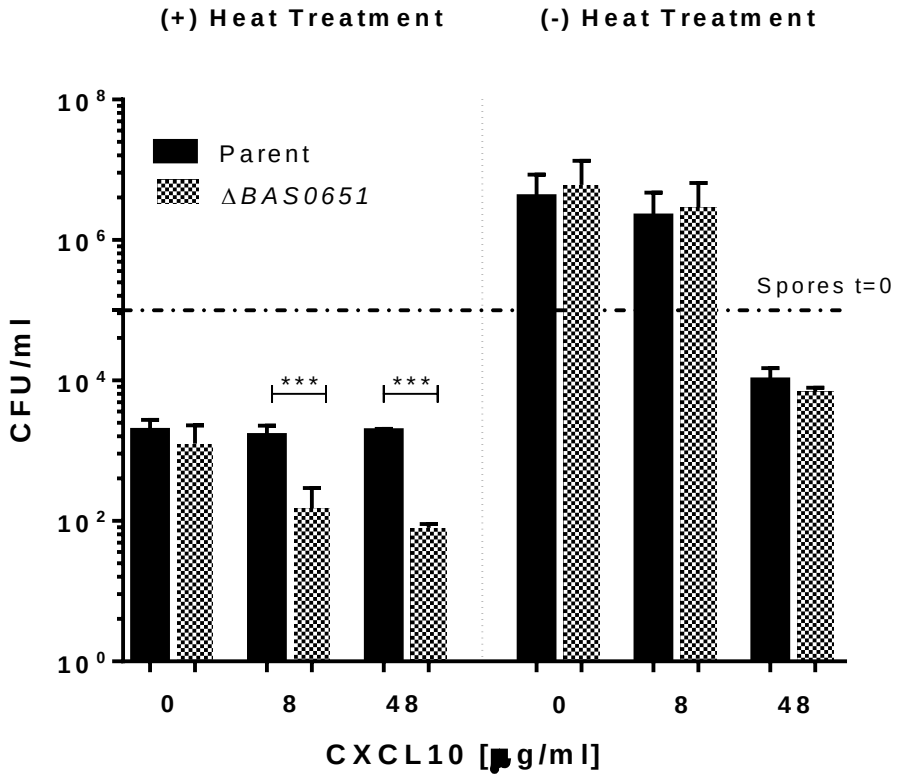

Figure 4.4: Effect of CXCL10 on spore viability. *B. anthracis* spores from the parent strain and the Δ*BAS0651* strain were incubated in the presence of 0, 8, or 48 μg/ml CXCL10. After 4 h of incubation, heat treatment was used to select for viable spores and CFUs were determined by plating. Vegetative cell number was calculated by subtracting the number of heat-resistant CFU from the total CFU obtained in the absence of heat treatment. Results represent total CFU/ml obtained from each sample and are represented +/- SEM, n=3. Data were analyzed using unpaired two-tail *t*-tests. * $p<0.05$, ** $p<0.01$ and *** $p<0.001$

μg/ml CXCL10 was significantly lower than the parent strain, suggesting that the germination of parent strain spores was inhibited in the presence of CXCL10 as compared to Δ*BAS0651* spores.

Studies were conducted to further assess the differences in germination and susceptibility to CXCL10 between *B. anthracis* parent strain and the Δ*BAS0651* strain. Spores from both strains were exposed to 48 μg/ml of CXCL10 and allowed to germinate for 6 h (Figure 4.5A). Alternatively, to prevent CXCL10-mediated killing of newly germinated vegetative cells, spores were incubated in the presence of 48 μg/ml of CXCL10 for 1 h, washed to remove CXCL10, and allowed to germinate for an additional 5 h (Figure 4.5B). Light microscopy images were obtained at regular intervals to assess the germination state of the spores versus germination with subsequent outgrowth of vegetative cells. The results obtained show that during continuous exposure to CXCL10, no vegetative bacilli were observed after 6 h of incubation for the parent strain and minimal germination was observed with the Δ*BAS0651* mutant strain (Figure 4.5A). When CXCL10 was removed after 1 h incubation and the spores were allowed to germinate in CXCL10-free medium, the parent strain still remained in spore form, but the Δ*BAS0651* mutant strain was able to undergo germination and vegetative outgrowth (Figure 4.5B). These data suggest that CXCL10-mediated spore anti-germination effects require BAS0651. Current work is being completed to fully characterize the inhibition of spore germination by CXCL10 and quantitate the difference in germination percent between the parent and mutant strains.

FIGURE 4.5

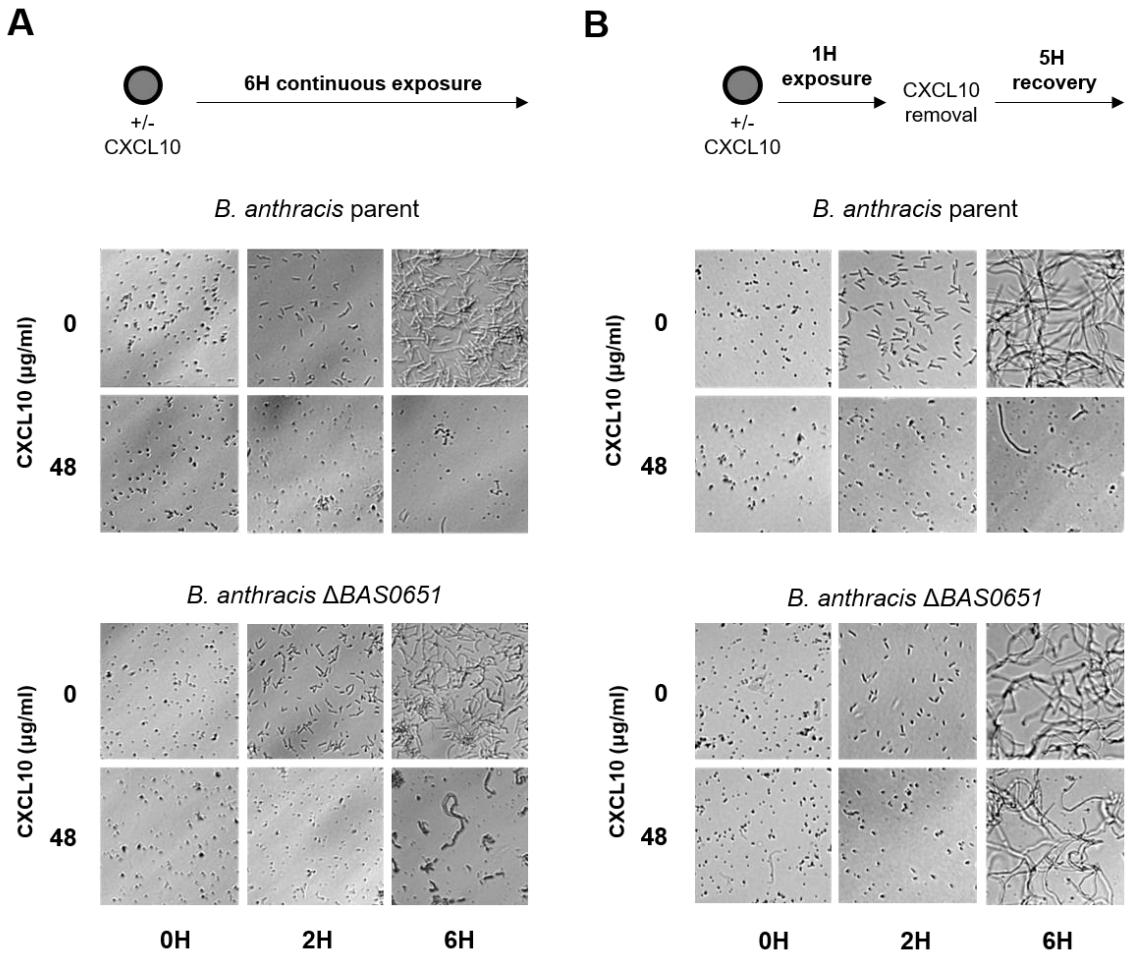
A
+/-
CXCL10
6H continuous exposure
B. anthracis parent
CXCL10 (µg/ml)
0
48
B. anthracis ΔBAS0651
0H
2H
6H
B
1H
exposure
CXCL10
removal
5H
recovery

Figure 4.5: CXCL10 inhibits spore germination. *B. anthracis* spores from the parent strain and Δ*BAS0651* mutant strain were incubated in the presence of 48 μg/ml of CXCL10 or vehicle control for 6 h. (A) Light microscopy images at 200X magnification were taken at regular intervals for 6 h after CXCL10 exposure to visualize spore germination and then vegetative cell outgrowth and cell division. (B) *B. anthracis* spores from the parent strain and the Δ*BAS0651* mutant strain were incubated in the presence of 48 μg/ml of CXCL10 or vehicle control for 1 h in germination-permissive medium. The cells were washed once, and the supernatant was replaced with fresh medium without CXCL10. Light microscopy images at 200X were taken at regular intervals to visualize spore germination and vegetative cell growth after 1 h of CXCL10 exposure, removal of CXCL10, and subsequent 5 h incubation. Light microscopy images shown are representative of a minimum of 5 separate images from three independent experiments.

……

Genetic complementation of *B. anthracis* Δ*BAS0651* vegetative cells results in restoration of CXCL10 susceptibility.

In a previously published *B. anthracis* vegetative cell transposon library screen, we found that transposon insertion in *BAS0651* conferred intermediate resistance to the antimicrobial effects of CXCL10 against *B. anthracis* vegetative cells (111). To confirm our previous findings, *B. anthracis* parent and *ΔBAS0651* strain vegetative cells were incubated with 0, 8, or 48 μg/ml of CXCL10 (105). Vegetative cell viability was detected using alamarBlue. Deletion of the locus *BAS0651* significantly increased the resistance level of vegetative cells to CXCL10 (Figure 4.6A). Susceptibility to CXCL10 was restored by complementation *in trans* of *BAS0651* gene expression by pUVA0651 after 10 μM isopropyl β-D-1-thiogalactopyranoside (IPTG) induction (Figure 4.6B). The presence of IPTG did not alter the susceptibility to CXCL10 or affect the baseline viability of the parent strain, Δ*BAS0651* strain, or Δ*BAS0651* strain carrying the pUTE973 empty control vector. These data extend our previous studies, and indicate that BAS0651 may be a bacterial target of *B. anthracis* vegetative cells involved with mediating the antimicrobial effects of CXCL10. However, it is important to note that *B. anthracis* Δ*BAS0651* vegetative cells are still susceptible to CXCL10 at higher concentrations.

BAS0651 mediates susceptibility to CXCL10 during early steps of spore germination.

Previous data from our laboratory have shown that CXCL10 interacts with the *B. anthracis* spore with localization to the exosporium and spore coat/cortex interface (105). In the present study, we initially sought to investigate if BAS0651 was involved in early phase I or phase II spore germination in untreated spores (no CXCL10 present). Early phase 1

FIGURE 4.6

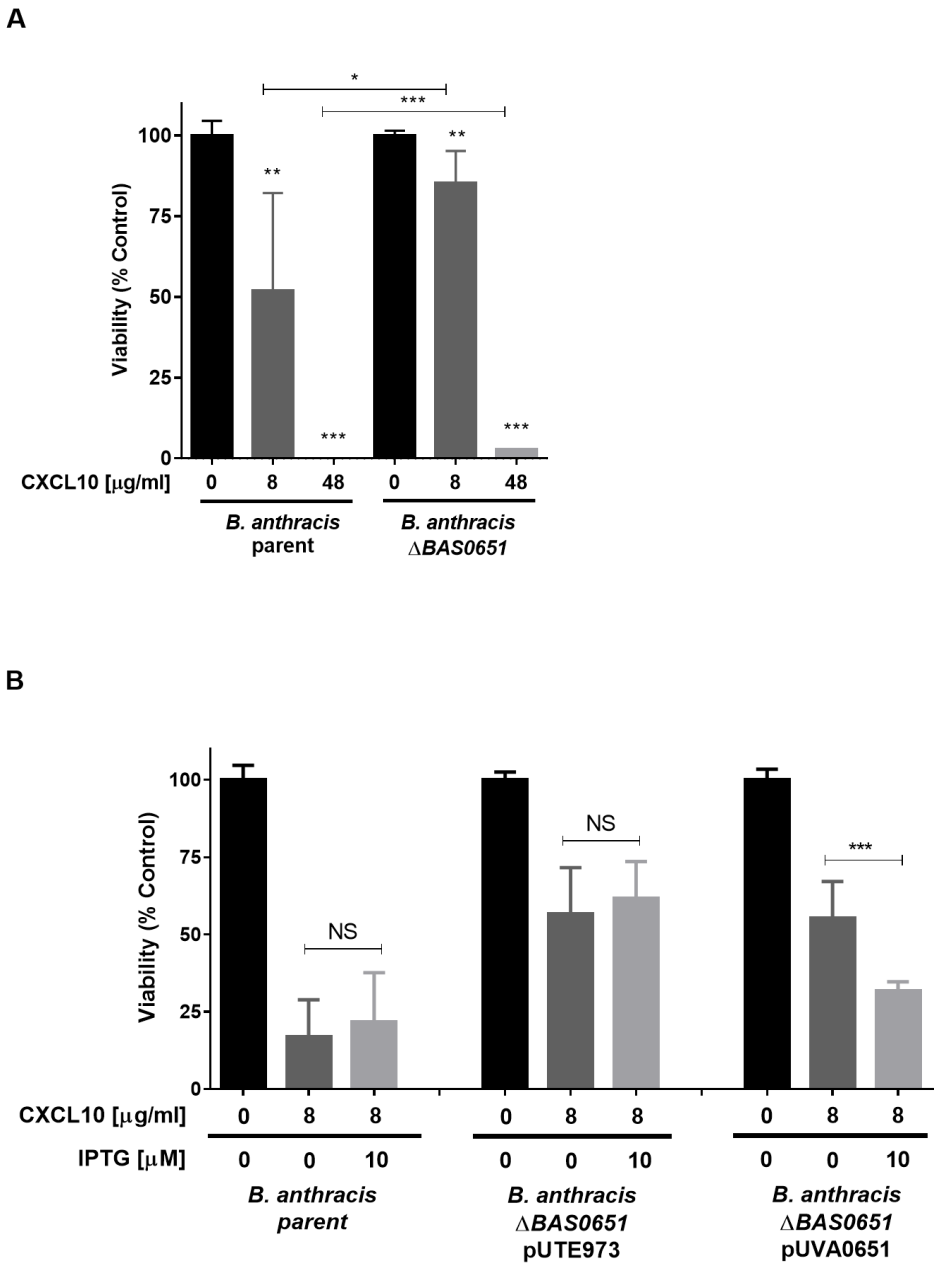
A
Viability (% Control)
100
75
50
25
0
*
***
**
**
***
***
CXCL10 [μg/ml]
0 8 48 0 8 48
B. anthracis parent
B. anthracis ΔBAS0651
B
Viability (% Control)
100
75
50
25
0
NS
NS
***
CXCL10 [μg/ml]
0 8 8 0 8 8 0 8 8
IPTG [μM]
0 0 10 0 0 10 0 0 10
B. anthracis parent
B. anthracis ΔBAS0651 pUTE973
B. anthracis ΔBAS0651 pUVA0651

Figure 4.6: *B. anthracis* vegetative cell susceptibility to CXCL10. (A) *B. anthracis* vegetative cells from the parent strain and Δ*BAS0651* strain were incubated in the presence of 0, 8, or 48 μg/ml of CXCL10. Viability was detected using alamarBlue dye after 4 h of incubation. (B) *B. anthracis* vegetative cells from the parent strain, Δ*BAS0651*, and Δ*BAS0651* complemented with the gene *BAS0651* were incubated in the presence of 8 μg/ml of CXCL10. Expression of the complementation gene was induced by addition of 10μM of IPTG. pUTE973 was used as empty vector control and pUVA0651 encoding *BAS0651* under IPTG expression control was used for *in trans* complementation of *BAS0651* expression. Viability was detected using alamarBlue dye after 4 h of incubation. Viability results are expressed as a percentage of the fluorescence detected for the samples compared to the untreated vehicle control group Data are represented as +/- SEM, n=3 separate experiments using triplicate wells in each experiment. Data were analyzed using unpaired two-tail *t*-tests. * $p<0.05$, ** $p<0.01$ and *** $p<0.001$

……

germination is characterized by breakdown of the exosporium and spore coat, and phase II of germination is characterized by spore cortex hydrolysis and uptake of water for cell rehydration (6, 8). Thus, we examined if BAS0651 plays a role in the shedding of the spore coat by measuring the amount of spore permeabilization during early phase I germination in native or de-coated spores (6). Native and de-coated spores were incubated in germination-permissive buffer in the presence of the fluorescent dye Syto-9 to determine if the absence of BAS0651 impacted early spore germination processes involving the coat (192). Spores are impermeable to this DNA-binding dye, but become permeable to Syto-9 during the germination process as the cell wall becomes more porous, allowing for spore rehydration and resulting in an increase in fluorescence that can be used as a readout (192, 193). Comparison between the germination efficiency of the parent strain or the Δ*BAS0651* showed that there were no significant differences between the germination of these two strains when the spore coat is still present (Figure 4.7A) or when the spore coat is removed prior to germination initiation (Figure 4.7B). These data support that BAS0651 was not involved in the loss of the coat during normal germination phases. However, further investigation of the germination differences, such as electron microscopy studies to visually assess the spore coat structure, can be conducted to determine the exact role of BAS0651 in spore germination. As indicated previously, sequence alignments and bioinformatics analyses predicted that BAS0651 is a DL-endopeptidase or muralytic enzyme, a finding that suggests a possible role in peptidoglycan remodeling, which would be expected to occur at the more internal spore cortex during phase two of germination (112, 123).

FIGURE 4.7

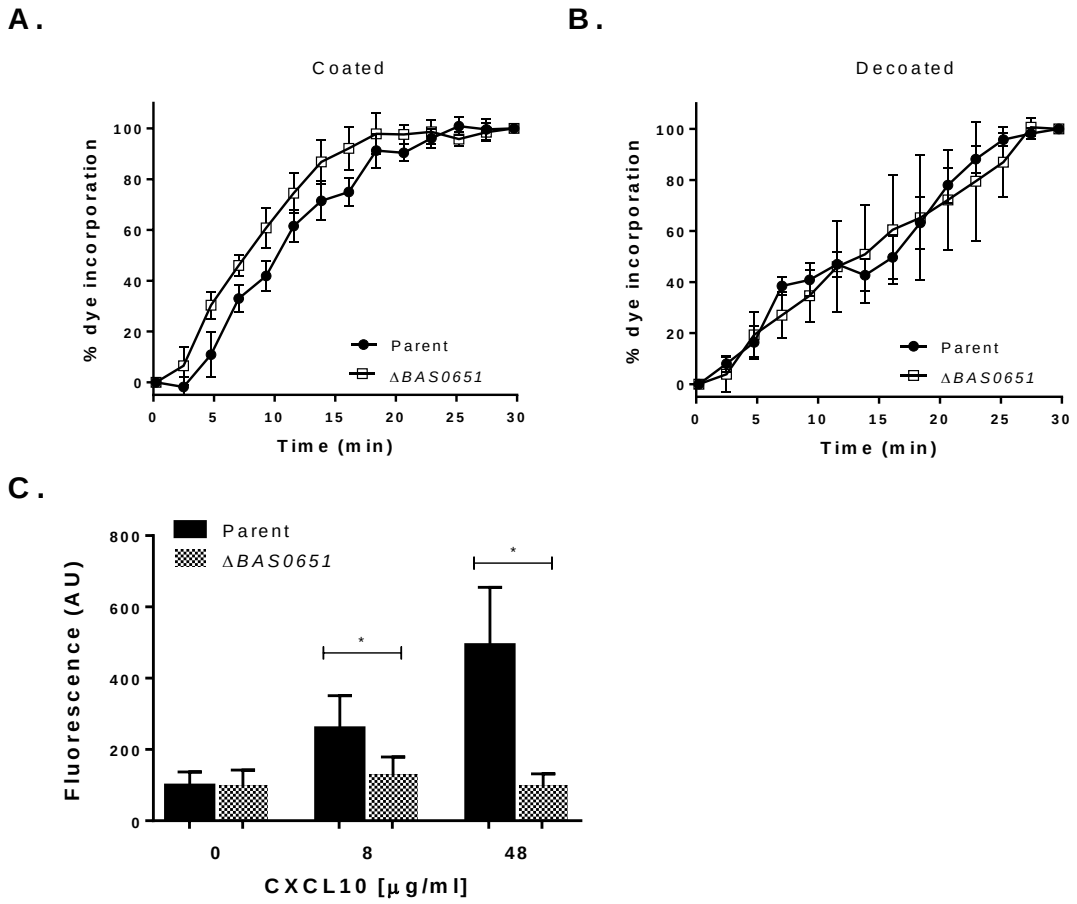
A.
Coated
% dye incorporation
Time (min)
Parent
ΔBAS0651
B.
Decoated
% dye incorporation
Time (min)
Parent
ΔBAS0651
C.
Parent
ΔBAS0651
Fluorescence (AU)
CXCL10 [µg/ml]
0
8
48
*
*

Figure 4.7: Effect of CXCL10 on the early stages of *B. anthracis* spore germination. (A) Coated or (B) decoated spores from *B. anthracis* parent strain and Δ*BAS0651* strain were incubated in the presence of Syto9 dye. Dye incorporation was used as measurement of spore permeabilization during germination and was detected using a fluorescence microplate reader (C) Coated spores from the parent strain and Δ*BAS0651* strain were incubated in the presence of 0, 8, or 48μg/ml of CXCL10 (or same volume of 0.3% HSA vehicle control) in the presence of the fluorescent dye Syto9. Data are represented as the total fluorescence of the signal. Results are represented +/- SEM, n=3 separate experiments using triplicate wells for each experiment. Data were analyzed using unpaired two-tail *t*-tests. * $p<0.05$

Since there is no basal difference in shedding of the spore coat during germination of the *B. anthracis* parent or Δ*BAS0651* strains, BAS0651 may be active during spore cortex removal, and disruption of this process by CXCL10 may lead to a loss of spore viability. To understand the mechanism by which BAS0651 mediates the antimicrobial activity of CXCL10, we studied the effect of the chemokine on early spore germination. To test our hypothesis, spores were incubated in presence of CXCL10 (8 or 48μg/ml) and Syto-9 in a germination-permissive medium. Permeabilization of the spore was assessed by measuring the level of resulting fluorescence from Syto-9/DNA interaction after 30 min of incubation. In the presence of CXCL10, the total fluorescence measured in the *B. anthracis* parent strain spores was significantly higher than the fluorescence measured in the Δ*BAS0651* mutant strain (Figure 4.7C). CXCL10 treatment results in an increase in permeabilization of *B. anthracis* parent strain spores, and this effect requires the presence of BAS0651. These data suggested that CXCL10 exposure may trigger a loss of spore integrity, and thus viability, through the disruption of cell wall remodeling during active germination. The loss of spore integrity appears to be mediated through interaction of CXCL10 and BAS0651.

BAS0651 is involved in *B. anthracis* pathogenesis during infection in a murine model of inhalational anthrax.

Our results support that BAS0651 plays an important role in *B. anthracis* spore susceptibility to CXCL10. Therefore, we hypothesized that deletion of *BAS0651* would promote bacterial infection during murine pulmonary infection. C57BL/6 mice were infected intranasally with ~$5x10^7$ *B. anthracis* parent or Δ*BAS0651* spores. Total CFUs

were determined 24, 48, and 72 h post-infection in the lung by plating samples of tissue homogenates, both before and after heat treatment, to quantify the number of vegetative cells and spores present in each tissue. The number of spores detected in the lungs after 24 h was similar in mice infected with the parent strain or the Δ*BAS0651* strain. Indeed, over 99% of the parent strain or Δ*BAS0651* spores administered intranasally germinated in the lungs by 24 h (Figure 4.8A). However, the number of vegetative cells detected in the lungs of mice infected with Δ*BAS0651* was approximately 10^3 higher after 24 h compared to the parent strain. This may indicate that the parent strain is cleared more effectively than the mutant strain, perhaps due to the intermediate level resistance that the mutant strain exhibits towards CXCL10 (Figure 4.6). After 48 and 72 h of infection, spore levels in the lungs inoculated with the Δ*BAS0651* strain were significantly lower than the parent strain. No statistically significant differences were observed in the number of vegetative cells in the lungs at these later time points. These data suggested that, while the spores from both strains underwent germination in the lungs, the parent strain appeared to be more efficiently cleared than the Δ*BAS0651* mutant strain during initial infection and germination. The lower number of spores detected in the lungs of mice infected with the Δ*BAS0651* mutant strain compared to the parent strain also suggested that either the host blocked germination of the parent strain or that the germination of the mutant strain might be more efficient during infection because it is not being blocked. Overall, a deletion of *BAS0651* appeared to provide an initial advantage in infection of the lung by Δ*BAS0651* compared to the parental strain, and lower spore CFUs were detected between the bacterial strains in the lungs at later time points. While these are interesting findings, more work needs to be conducted to definitively conclude the role of BAS0651 during *in vivo* pulmonary anthrax

FIGURE 4.8

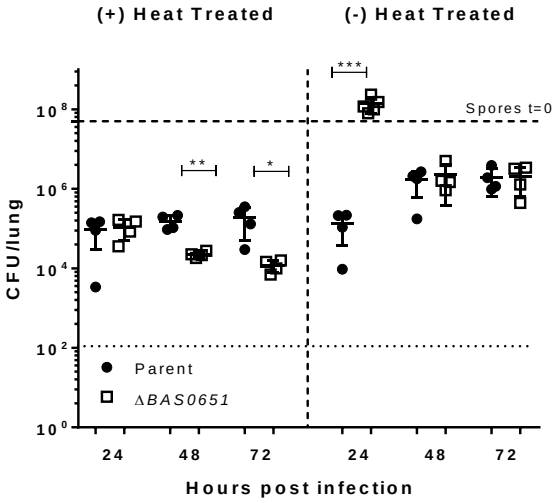

Figure 4.8: Effect of BAS0651 on *B. anthracis* infection in an *in vivo* mouse model of anthrax. C57BL/6 mice were challenged intranasally with ~5x10^7 *B. anthracis* parent or Δ*BAS0651* mutant spores. Tissue homogenates were prepared from the lungs, spleen, and liver of animals euthanized at 24, 48, and 72 h post-infection. Dilutions of the tissue homogenates were either heat treated or not heat treated and then spread onto BHI agar plates to determine CFUs. Heat-treated samples represent CFUs from spores only; non-heat treated samples represent total CFUs from spores and vegetative cells. There was a statistically significant difference in the non-heat treated (total) CFUs from spores and vegetative cells of Δ*BAS0651* in the lungs at 24 h, compared to the parent strain. At 48 and 72 h post infection, there were fewer Δ*BAS0651* heat-treated CFUs (spores) detected in the mouse lungs compared to the parent strain. Results are represented +/- SEM, n=4-5 mice per group per time point. Data were analyzed using unpaired two-tail *t*-tests. * $p<0.05$, ** $p<0.01$ and *** $p<0.001$

infection with spores. Further studies should be performed to measure the level of CXCL9, CXCL10, and CXCL11 induced upon exposure to *B. anthracis* parent and Δ*BAS0651* mutant strains in the lungs. Antibody neutralization of CXCL9, CXCL10, and/or CXCL11, along with control neutralization of the receptor CXCR3, will further show the role of the chemokines in direct antimicrobial activity against the *B. anthracis* parent and mutant spores during pulmonary infection.

4.4 Discussion

Introduction of *B. anthracis* spores into the lungs results in pulmonary anthrax, the most lethal form of anthrax infection (2, 14, 19). An immediate response of the immune system is necessary to stop disease progression (185, 194, 195). In the current study, we sought to determine important bacterial components mediating IFN-γ inducible, ELR(-) CXC chemokine CXCL10 killing of *B. anthracis* spores. A screen was conducted using a *B. anthracis* spore transposon library to identify isolates resistant to CXCL10. Of the 188 resistant isolates collected, 184 (98%) were found to have a disruption in the *B. anthracis* gene *BAS0651*. The remaining CXCL10-resistant spore isolates had a disruption in *B. anthracis* genes *BAS1458* and *BAS5090.* All three genes are hypothetical but predicted to be endopeptidase or muralytic enzymes based on conserved domains. BAS0651 was identified in both the *B. anthracis* spore transposon mutant library screen conducted in the present study, and a vegetative cell transposon mutant library screen conducted previously (111) to identify vegetative cell bacterial targets of CXCL10. In the present study, we found that *B. anthracis* Δ*BAS0651* spores exhibited resistance to CXCL10, yielding a higher amount of germination and viability than parent strain upon exposure to CXCL10.

In addition, CXCL10 was shown to increase spore permeability of the parent strain after chemokine exposure; no increase in spore permeability as a result of CXCL10 exposure was observed in the Δ*BAS0651* strain, indicating BAS0651 is mediating the increase of spore permeability. Using a murine model of inhalational anthrax, an increase in vegetative cell proliferation of *B. anthracis* Δ*BAS0651* was seen at 24 h compared to the parent strain. A decrease of mutant strain spores were detected at later time points, suggesting that the mutant strain continued to germinate more effectively in the lungs compared to the parent strain, which may have been blocked from undergoing germination by CXCL10 (110). The *in vivo* data suggest that BAS0651 may be important as a CXCL10 antimicrobial target during initial infection, but additional innate and adaptive immune system mechanisms are likely involved in the overall clearance of *B. anthracis* infection from the host. These observations suggest that CXCL10 mediated killing *in vivo* is a defense against the initial acute infection of *B. anthracis* spores. Cumulatively, these data indicate that BAS0651 acts as a target of CXCL10-mediated antimicrobial activity against *B. anthracis* spores and participates in both the inhibition of spore germination and an increase of spore permeability leading to a loss of viability and bacterial death (Figure 4.9). Additional experiments are underway to further elucidate the role of CXCL10 and related chemokines in *B. anthracis* spore killing.

The genes *ftsX* and *lytE* were also identified from the previous vegetative cell transposon library screen. Notably, all the identified genes from both the spore and vegetative cell screens are predicted to be involved in cell wall processing by regulating or performing peptidoglycan hydrolysis. The gene products also appear to associate in the same cell wall

FIGURE 4.9

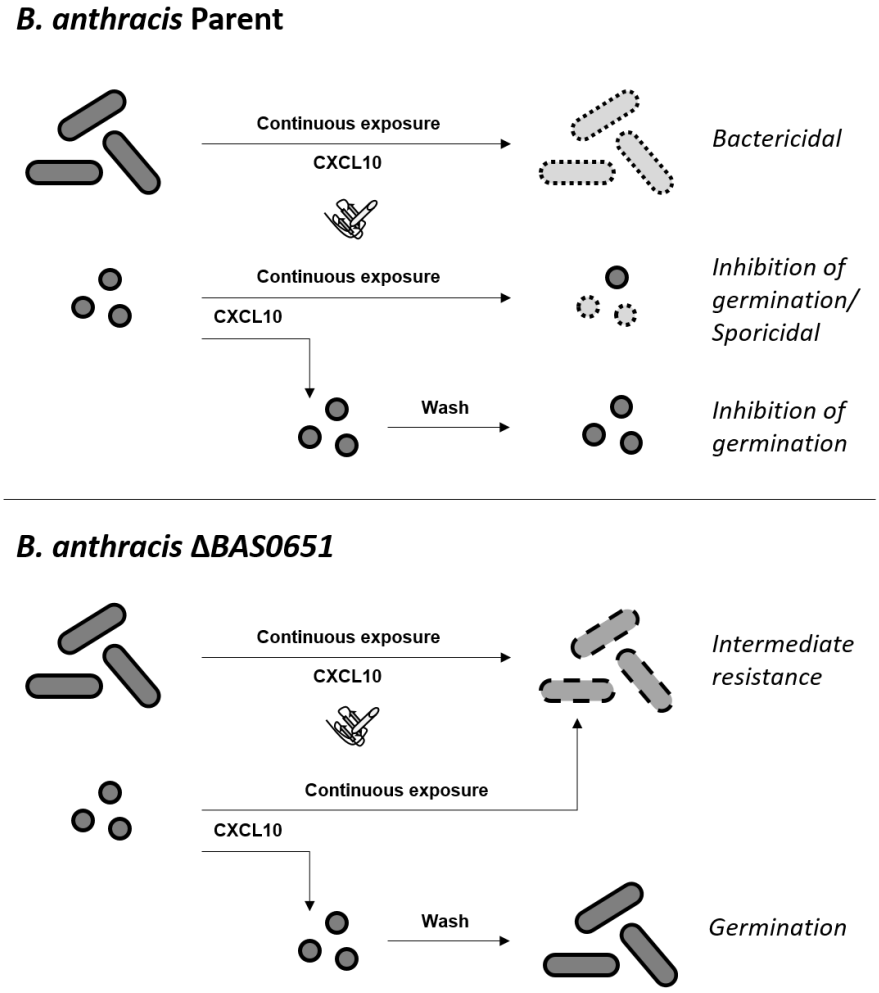

Figure 4.9: Overview of the role of BAS0651 in CXCL10 antimicrobial activity on *B. anthracis* in spore and vegetative forms. Visual representation of CXCL10 antimicrobial effect on *B. anthracis* in presence (A) or absence (B) of BAS0651. Dashed lines represent spore or cell permeabilization and subsequent loss of integrity and viability.

synthesis complex in Gram-positive bacteria. The gene *ftsX* is the membrane component of the ABC transporter-like complex FtsE/X that is involved with peptidoglycan processing during cellular elongation and spore formation in Gram-positive bacteria (112, 113, 123). Characterization of the FtsE/X complex in *B. subtilis* has shown that FtsE/X associates with the DL-endopeptidase CwlO, of which BAS0651 has been shown to share similarity (112, 113). Additionally, BAS0651 shows similarity to *S. pneumoniae* PcsB, which also associates with FtsE/X in that bacterial system (142, 150, 151). The gene product of *lytE* is an uncharacterized *B. anthracis* protein that contains conserved hydrolytic domains thought to process peptidoglycan bonds within the bacterial cell wall (111). Disruption of peptidoglycan processing is detrimental to bacterial cells in all stages of germination, growth, and sporulation, making any protein involved in the process a potential antimicrobial target (144, 196). Additional studies from our laboratory have shown that an active FtsE/X complex is important for the antimicrobial activity of CXCL10 against vegetative cells (145). FtsE hydrolyses ATP which is thought to result in a conformational change in FtsX, resulting in the activation of peptidoglycan hydrolases to process the cell wall during bacterial elongation and spore formation (112, 113, 123, 124, 126, 142, 151). Combined with the previous work, our findings suggest that CXCL10 actively targets components of the cell wall synthesis complex to disrupt peptidoglycan remodeling in order to kill *B. anthracis* spores and vegetative cells. Ongoing studies in our laboratory are focused on investigating whether FtsE/X and BAS0651 interact and how these bacterial components facilitate CXCL10-mediated antimicrobial activity against *B. anthracis* spores and vegetative cells.

Pulmonary anthrax infection can progress rapidly, and the initial immune response of the host is vital in helping to control tissue invasion of the bacteria and dissemination of infection. There are many unanswered questions about how *B. anthracis* spore particles are neutralized and cleared by the host. The chemokine family is well characterized as playing a key role in the innate and adaptive immune system through immunomodulation, and a number of chemokines also have been shown to exhibit direct killing against a wide variety of pathogens (55, 56, 197). We show that CXCL10 has a direct biological effect against *B. anthracis* spores mediated by the putative DL-endopeptidase BAS0651. BAS0651 represents a novel spore target that supports an overall mechanism of CXCL10 antimicrobial activity killing of *B. anthracis* during early spore germination stages. The present work suggests a novel mechanism for immune system deactivation of spores by the chemokine CXCL10, opening up exciting possibilities to further study the role of immune system components as direct antimicrobial molecules. Further study of BAS0651 and the FtsE/X complex as an antimicrobial target may lead to innovative therapeutics that target both the spore form and vegetative cell form of *B. anthracis* for effective and rapid bacterial clearance during infection.

4.5 Materials and Methods

Bacterial strains and spores. *B. anthracis* Sterne strain 7702 (pXO1+ pXO2−) (BEI Resources, Manassas, VA) was used throughout and is designated in the text as the parent strain for our studies. Vegetative bacilli were cultured from spore or frozen stocks at 37°C with constant shaking in 10 ml brain heart infusion (BHI) medium. *B. anthracis* spores were prepared in Difco sporulation medium and purified using a Percoll (MP Biomedicals,

Santa Ana, CA) gradient as described previously and below (110). The *E. coli* strain α-select was grown in Luria-Bertani (LB) medium for use in plasmid construction and propagation. *E. coli* strain GM119 was similarly cultured and used to produce unmethylated DNA for *B. anthracis* transformation. The following antibiotics were included in growth medium as appropriate: erythromycin, 5 μg/mL; tetracycline, 5 μg/mL; and kanamycin, 20 μg/mL (*E. coli*) or 100 μg/mL (*B. anthracis*). Growth rate was calculated from a semilogarithmic plot of the OD600 growth curve vs time using the equation growth rate = lnOD2-(lnOD1/(t2-t1)) where t denotes time (108).

***B. anthracis* spore generation and purification.** *B. anthracis* was grown from a freezer stock by overnight culture in BHI broth at 37ºC. The overnight culture was then inoculated at a ratio of 1:60 (v/v) into warm Difco Sporulation Medium (DSM) (8g nutrient broth, 0.1% KCl, 0.012% $MgSO_4$, 1% NaOH in 1L of distilled water, pH 7.6 supplemented with 10mM $Ca(NO_3)_2$, 100μM $MnCl_2$ and 10μM $FeSO_4 \cdot 7H_2O$; antibiotics were added after autoclaving). The bacterial broth cultures were incubated at 37ºC until mid-log phase of growth was reached, and then the cultures were diluted at a ratio of 1:5 (v/v) in warm DSM, and incubated for 5 days at 37ºC with constant shaking at 150 rpm. Cells (spores and/or vegetative cells) were harvested by centrifugation for 15min at 3,600g at 4ºC and washed in cold distilled water. Cells were then heat treated at 65ºC for 30 min (to kill any remaining vegetative cells) and washed again in 10ml of cold water. The resuspended cells were applied to 15ml percoll to create a gradient, centrifuged for 25min at 3,600g to separate spores from vegetative cells and their cellular debris, and the spore pellet was immediately recovered after centrifugation. Spores were then washed 5 times in cold distilled water by

centrifugation for 25 min at 3,600 and enumerated by preparing serial dilutions and plating the samples onto BHI agar followed by overnight incubation at 37ºC and then counting the CFUs generated by the spores.

Transposon mutant library spore screen. Spores were generated from the previously described mariner-based transposon library of *B. anthracis* parent strain vegetative mutant isolates used in our laboratory (111, 186). The resultant transposon mutant library of *B. anthracis* spores was then treated with 48 μg/ml of CXCL10 for 1 h in triplicate in 96 well plates with $1x10^5$ spores/well. Any CXCL10 remaining in the supernatant was then removed by centrifuging the spores 2x at 1,000 rpm for 5 min with removal of the medium after each centrifugation. The remaining spores were then placed into Dulbecco's modified Eagle's medium (DMEM) (Gibco-Invitrogen, Carlsbad, CA) + 10% fetal bovine serum (HyClone, Logan, UT) (FBS) and incubated 5 h at 37˚C with shaking at 250 rpm. Mutant spores that were resistant to treatment with CXCL10 were identified as those that germinated in the presence of CXCL10 and replicated as vegetative cells in the medium. Because the resultant vegetative cells were potentially susceptible to CXCL10-mediated killing (for example, due to a different vegetative bacterial target distinct from a spore target), the medium was promptly exchanged after the initial 1 h incubation for fresh medium without CXCL10. The resultant vegetative cells were then sporulated and purified as described above. The resultant spores were exposed to a second round of treatment with CXCL10 as described above. Mutant spores that were resistant to CXCL10 were subsequently plated onto BHI agar for growth as vegetative cells, and individual colonies were isolated and used to prepare freezer stocks (BHI + 20% glycerol) that were stored at

-80°C until further use. The transposon insertion sites in each CXCL10-resistant mutant strain were identified as described previously (111). Briefly, chromosomal DNA from each spore mutant identified from the mutant library screen as having resistance to CXCL10 was isolated from an overnight vegetative cell cultures by using the GenElute bacterial genomic DNA kit (Sigma-Aldrich, St. Louis, MO). DNA was digested with HinP1I and ligated with a partially double stranded Y-linker. DNA off the transposon was then amplified by PCR using GoTaq Green Master Mix (Promega, Madison, WI) with either the primer FIG6 (AACATGACGAATCCCTCCTTCT), FDLBAS0651 (GCCTAGGATCCTTTTGTGCTTTCCGCTGT), or FIG7 (GCCTACGGGGAATTTGTATCG) in order to enrich for single-stranded DNA fragments flaking the transposon insertion site. Subsequently, primer JZ99 (ACTACGCACCGGACGAGACGT) was added for double-stranded PCR amplification. Amplicons were sequenced using Sanger sequencing at the University of Virginia Biomolecular Research Facility.

BAS0651 deletion and complementation. Markerless gene deletion of *BAS0651* was performed as described previously (134, 198). The locus *BAS0651* was amplified using the primers FDLBAS0651 (GCCTAGGATCCTTTTGTGCTTTCCGCTGT) and RDLBAS0651 (ACCATGTCGACAAAAACCAACCGCACAAG). This product was digested with BamHI and Sal-HF, designed into the primers, and cloned into plasmid pRP1028. This construct was then introduced into *B. anthracis* parent strain vegetative cells by conjugation with Dam$^-$ *E. coli* at room temperature followed by maintenance in the presence of spectinomycin. *B. anthracis* recombinant cells harboring the allelic-

exchange construct were isolated by culture in the presence of spectinomycin, and incubated at 37ºC to induce pRP1028 integration into the chromosome. The plasmid pBKJ223 was then introduced by electroporation. This plasmid expresses SceI involved in the cleavage of the integrated pBKJ236 which facilitates recombination and excision of *BAS0651*. Colonies that displayed a loss of spectinomycin resistance were screened by PCR to confirm gene deletion. The plasmid pBKJ223 was then lost spontaneously through multiple passages of *B. anthracis* in BHI medium lacking tetracycline. The resultant *BAS0651* deletion mutant was verified by PCR and Sanger sequencing and designated as *B. anthracis* Δ*BAS0651*.

Complementation of *BAS0651* gene expression in *B. anthracis* Δ*BAS0651* was performed according to previously published complementation protocols from our laboratory (111, 145). Briefly, the *B. anthracis* parent strain *BAS0651* gene was amplified using a forward primer carrying a ribosome binding site and SphI restriction site (CCGGATACTCGAGTGAGGAGGAACTGTATAAGAAGGGAGTC) and a reverse primer carrying a PspXI restriction site (GCCTAGGCATGCACAATATGTAAAGTTGGATT). The empty plasmid vector, pUTE973, kindly provided by Theresa Koehler (137) was double digested with SphI-HF and Sal-HF (111, 145). The *BAS0651* PCR product was double digested with SphI-HF and PspXI. The digested PCR product was purified and ligated into the digested empty vector with compatible DNA nucleotide overhangs. The resulting vector was transformed into TOP10 *E. coli* (Invitrogen, Carlsbad, CA). The plasmid was then isolated, verified by sequencing, and electroporated into GM119 *E. coli* to remove all methylation. The

BAS0651 complementation plasmid (pUVA0651), or the empty control vector (pUTE973), was electroporated into the *B. anthracis* parent strain or Δ*BAS0651* strain. All plasmids generated were sequence verified.

Peptidoglycan labeling using fluorescence microscopy. Overnight cultures of *B. anthracis* parent and Δ*BAS0651* vegetative cells were diluted 1:20 in fresh BHI broth followed by a 1 h incubation at 37˚C with shaking at 250rpm. After 1 h, a final concentration of 1 mM of modified D-alanine ((S)-2-Amino-4-pentynoic acid) (Boaopharma, Inc., Natick, MA) was added to the culture and incubated an additional 1 h until reaching an OD_{600} of 0.6 to 0.65. The culture was centrifuged for 5 min at 3,600 rpm to produce a pellet of log-phase bacteria. The supernatant was discarded, and a total of 5 µl of the resulting pellet was placed into 500 µl DMEM with 10% FBS and 1 mM modified D-alanine and incubated for 1 h at 37˚C in 5% CO_2 (158, 159). The bacterial cultures were then centrifuged for 8 minutes at 15,500 rpm, and the supernatant was discarded. A 1 ml aliquot of ice-cold 70% ethanol was added to the remaining bacterial pellet and incubated for 1 h on ice. Bacterial cells were removed from the ethanol and incubated for 1 h at room temperature in PBS with 3% BSA. Vegetative cells were then incubated for 1 h at room temperature using 0.5 ml of Click-iT Cell Reaction Buffer, according to the manufacturer's directions. Briefly, using the Click-iT technology and reagents, Alexa Fluor 488 Azide (ThermoFisher Scientific, Waltham, MA) was added to the samples and incubated for 1 h, in the dark, at room temp in Click-iT Cell Reaction Buffer (ThermoFisher Scientific, Waltham, MA) to attach a green fluorescent label to the modified D-alanine residues incorporated into the bacterial peptidoglycan cell wall (158–160). Nucleic acids were

stained by incubating the bacteria with Hoechst 33342 dye for 20 min and then washing the bacteria 1x with PBS to remove excess dye. Finally, the bacterial cells were re-suspended in PBS and placed on glass slides with a coverslip and imaged with a Zeiss LSM 880 confocal microscope under oil immersion at 63X magnification.

Recombinant human CXCL10 and antimicrobial assays. Recombinant human CXCL10 (PeproTech, Rocky Hill, NJ) was reconstituted in sterile water at a stock concentration of 1 mg/mL and stabilized by addition of 0.3% (final v/v) human serum albumin (HSA) (Grifols, Los Angeles, CA). Aliquots of CXCL10 were stored at -80°C until used and each aliquot was exposed to only one freeze/thaw cycle. Spores or vegetative cells from the *B. anthracis* parent strain, *ΔBAS0651*, *ΔBAS0651* transformed with the empty control vector (pUTE973), and *ΔBAS0651* transformed with the plasmid containing the IPTG-inducible *BAS0651* gene (pUVA0651) were tested for susceptibility to CXCL10 utilizing methods described previously (105, 137). Spores (~$2x10^5$ spores/sample) or vegetative cells (~$2.5x10^5$ cells/sample) of each strain were placed in triplicate wells of a 96-well plate and treated with 8 μg/ml or 48 μg/ml of CXCL10, or an equal volume of 0.3% HSA alone (as vehicle, untreated control) in DMEM containing 10% (v/v) FBS for 4 h. To induce expression of *BAS0651* by pUVA0651, 10μM IPTG or an equal volume of water (as vehicle, untreated control) was added to each well. Colony forming units (CFUs) were quantified at the time 0 and 4 h incubation times by plating appropriate dilutions onto BHI agar and then counting the CFUs after overnight incubation at 37ºC. Spore viability was quantified by treating the samples at 65ºC for 30 min, plating dilutions of the samples onto BHI agar, and subsequently counting CFUs produced by the surviving spores after

overnight incubation at 37ºC. Viability of vegetative cells (produced by germinating spores or by directly adding vegetative cells to assay wells) was also determined by adding alamarBlue dye (AbD Serotech, Oxford, United Kingdom) at a final concentration of 10% to each well. Fluorescence was measured at 560nm excitation and 585nm emission after 1.5 h incubation using a Perkin-Elmer Victor^3 multi-label plate reader (Perkin-Elmer, Waltham, MA). Viability was calculated as a percentage of the fluorescence readings as compared to untreated controls. Each experiment was performed three separate times using triplicate wells in each experiment.

Light microscopy observation of CXCL10 effect on spore germination. Spores (~2x10^5 spores/sample) of the *B. anthracis* parent strain and *ΔBAS0651* strain were placed in triplicate wells of a 96-well plate and treated with 48 μg/ml of CXCL10 or an equal volume of 0.3% HSA alone (as vehicle, untreated control) in a final volume of 100μl of DMEM containing 10% (v/v) FBS. Plates were centrifuged at 3,500 rpm for 10 min and incubated at 37ºC for 6 h. Wells were imaged every 30 min using an Olympus IX51 inverted microscope (Olympus America, Melville, NY). Camera control and image capture were performed by using QCapture Pro-5.1 software, as previously described (110, 111). In some cases, CXCL10-treated media was removed by washing after 1 h. Washes were accomplished by centrifugation of the plates, and removal of 75 μl of the supernatant and replacing it with 175μl of fresh DMEM containing 10% (v/v) FBS without CXCL10. Plates were mixed manually by gently swirling and centrifuged at 3,500 rpm for 10 min. A total of 175μl volume of supernatant was then removed from each well and replaced by 175μl of fresh medium as described above. This step was repeated three times and spores were

re-suspended in a volume of 100µl and centrifuged again at 3,500 rpm for 10 min. Plates were finally incubated at 37ºC for an additional 5 h and imaged by light microscopy at 400x magnification every 30 min. Images shown are representative of three of experiments with over 5 images analyzed in each sample.

CXCL10 spore permeabilization assays. Spores were treated using a decoating solution (50mM Tris-HCl, 8M urea, 1% sodium dodecyl sulfate, 50mM dithiothreitol) for 1 h at 37ºC and washed three times with distilled water, as described previously (199). Permeabilization and germination assays were performed using a microtiter fluorometric assay (192). Briefly, Syto-9 green fluorescent nucleic acid stain (Life Technologies, Carlsbad, CA) was used according to the manufacturer's instructions. The dye was diluted in a two-component germination medium (10mM potassium phosphate, 0.1M NaCl, 0.25mM L-alanine, 1mM inosine pH 7.2) (200) and incubated in the presence of $2.5x10^7$ spores in triplicate wells of a 96-well plate and treated with CXCL10 at 0, 8, or 48 µg/ml or an equal volume of 0.3% HSA alone (vehicle, untreated control). Fluorescence was measured every two minutes (Excitation: 485nm, Emission: 530nm) for a total of 30 min. Each experiment was performed three separate times using triplicate wells in each experiment.

Murine infection experiments. The effect of *B. anthracis* Sterne strain *BAS0651* gene deletion on initial lung infection and subsequent dissemination to distal organs was determined by infecting 5-week old female C57B/6 mice (6 mice per group) intranasally with either *B. anthracis* parent strain or the *ΔBAS0651* strain at ~$5x10^7$ spores total

administered in 20 µl of water. At 24, 48, or 72 h post-infection, mice were euthanized by Euthasol intraperitoneal injection at a concentration of 100 mg/kg and CFU were determined by plating serial dilutions of lung, liver, and spleen tissue homogenates on BHI agar. Samples were heat treated for 30 min at 65ºC and plated on BHI to quantify the number of viable, ungerminated spores in each sample. Animal experiments were performed according to protocols approved by the Institutional Animal Care and Use Committee (IACUC) (University of Virginia animal protocol number: 3677 and West Virginia University animal protocol number: 15-1113). The animal studies were carried out in accordance with the US Public Health Service Policy on the Humane Care and Use of Laboratory Animals (PHS Assurance #A3245-01 and the US Department of Agriculture Animal Welfare Act (USDA Registration #52-R-0011).

Protein structure prediction and modeling. The amino acid sequence of the *B. anthracis* hypothetical protein BAS0651 was searched against the NCBI database using the NCBI BLAST online tool (201, 202). Protein domains were predicted using the NCBI Conserved Domain Database (188). The three dimensional (3-D) structure of BAS0651 was predicted using the I-TASSER server (187). Default search parameters were used for protein data base (PDB) templates. The highest C-scored model was selected as the best structural model. The protein-protein interaction predictions were made using ClusPro FFT-based protein docking tool by using electrostatically favored scoring function (203). ClusPro docking server generated clusters for 1000 ligand positions with the lowest energy score according to their 9 angstrom C-alpha RMSD radius and ranked as the best models by the

cluster size (203). All figures were generated using University of California San Francisco (UCSF) Chimera (191).

Statistical Analyses

Statistical analyses and graphing were performed using GraphPad Prism 6.0 software. Experimental groups were analyzed using an unpaired, two-tailed student t-test. Significant differences were determined to have a P value of ≤ 0.05.

CHAPTER 5:

Summary and Future Directions

5.1 Summary

The IFN-γ inducible, ELR(-) CXC chemokine CXCL10 has been shown to exhibit direct antimicrobial activity against *B. anthracis* spores and vegetative cells (105, 110, 111, 145). However, the mechanism(s) of action underlying the CXCL10 antimicrobial effect had remained previously unknown, although a bacterial target (FtsX) had been identified as being important in the killing effect of the chemokine (111). In the current body of work, we have characterized multiple, unique mechanisms of action that CXCL10 utilizes to exert an antimicrobial effect against *B. anthracis* spores and vegetative cells. We have found that CXCL10 is able to target and kill *B. anthracis* vegetative cells through two separate, yet complementary mechanisms. One mechanism is dependent upon the presence of an active bacterial FtsE/X ATP-binding cassette (ABC) complex, and a second mechanism is independent of the bacterial FtsE/X complex (Chapter 2) (145). Further investigation into the FtsE/X-dependent mechanism suggested that exposure of *B. anthracis* vegetative cells to CXCL10 may lead to the dysregulation of peptidoglycan remodeling and incorporation (Chapter 3). The FtsE/X-independent mechanism appeared to be the result of non-specific membrane depolarization mediated primarily by the CXCL10 C-terminal α-helix, which has a similar positive charge and overall amphipathic α-helical structure as the antimicrobial defensins or cationic antimicrobial peptides (CAMPs) (Chapter 2) (67, 69, 106, 145). The most potent killing effect of CXCL10 against vegetative cells was observed when an active FtsE/X complex is present and when an intact CXCL10 protein used for the antimicrobial effect (Chapter 2) (145). Notably, both FtsE/X-dependent and FtsE/X-independent mechanisms of CXCL10-mediated antimicrobial activity have the same end result of eliciting bacterial cell lysis. Additional studies on the mechanism(s) of action of

CXCL10 against *B. anthracis* spores resulted in the finding that a putative DL-endopeptidase BAS0651 played a role in the observed anti-spore effects of CXCL10 (Chapter 4). It appears that BAS0651 acts as a spore target for CXCL10 in order to inhibit spore germination and increase permeability, resulting in the loss of spore viability (Chapter 4). Interestingly, while CXCL10 appears to elicit an antimicrobial effect against *B. anthracis* via different primary targets in the two distinct forms of the organism (BAS0651 in spores and FtsE/X in vegetative cells), these primary targets may be related in function (i.e., affecting cell wall integrity), as discussed in Chapters 2-4 and below.

Both the *B. anthracis* transposon library screen conducted with vegetative cells (111) and with spores (Chapter 4) identified genes that were each predicted to be involved in affecting cell wall synthesis and integrity. Such findings suggest that there may be a common overall mechanism of action for CXCL10 antimicrobial activity against both *B. anthracis* vegetative cells and spores that involves the targeting of the bacterial cell wall synthesis machinery. Based on studies performed in *B. subtilis*, FtsE/X is thought to direct cellular elongation and sporulation of vegetative cells by activating various peptidoglycan hydrolases during cell wall remodeling (112, 113, 123). Interestingly, a number of putative hydrolases (*lytE, BAS0651,* and *BAS1458)* were identified from our transposon mutant library screen of *B. anthracis* Sterne strain vegetative cells and/or spores as being potentially involved in the CXCL10-mediated antimicrobial effect (Chapter 4) (111). The *B. anthracis* hypothetical gene *BAS0651,* which is a predicted DL-endopeptidase, was identified as a result of a separate transposon mutant library screens of *B. anthracis* vegetative cells and spores, and appears to play a role in the CXCL10-mediated

antimicrobial activity against both forms (Chapter 4). Structural protein studies indicate that BAS0651 contains an N-terminal coiled-coil domain, found in proteins that associate with membrane complexes, and a "3D" domain, named for three conserved aspartic acid residues that define the domain (112, 113, 123, 124, 150, 151). These features of BAS0651 would predict it to be a putative DL-endopeptidase that may have peptidoglycan hydrolase activity (111–113, 123, 124, 136, 151). Studies in *B. subtilis* have shown that a homologous peptidoglycan hydrolase, CwlO, appears to associate directly with FtsE/X and is activated by FtsE/X binding and hydrolysis of ATP during cellular elongation and spore formation (112, 113, 123). The possibility that FtsE/X and BAS0651 interact in *B. anthracis* opens up interesting questions about how this entire complex may be functioning and why it is such an effective target for CXCL10-mediated antimicrobial killing of vegetative cells and/or spores. Overall, it appears that CXCL10 targets the bacterial cell wall elongation complex in order to disrupt peptidoglycan remodeling against both the *B. anthracis* spores and vegetative cells (Figure 5.1).

5.2 Future Work

The bacterial cell wall needs to maintain its integrity in order to sustain internal pressure and to protect the cell from external environmental pressures (147–149). Any disruption to the cell wall or its synthetic capacity can be detrimental to the survival of the bacterial cell, making the cell wall and cell wall synthesis complex an excellent target of antimicrobial molecules (146, 155). The cell wall synthesis complex involved in cellular elongation is important, but is not fully characterized in *B. anthracis* (112, 113, 124, 151). Studies conducted in *B. subtilis* show that FtsE/X and associated cell wall hydrolases are

FIGURE 5.1

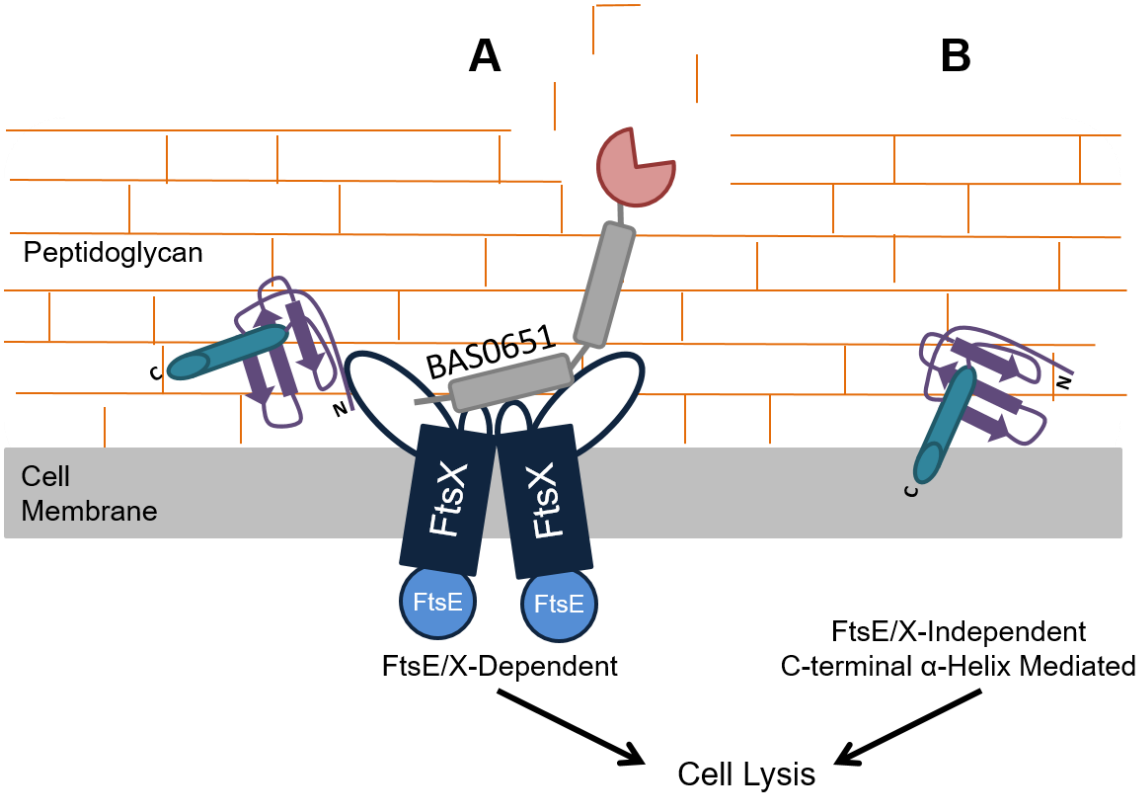

Figure 5.1: Model of CXCL10 antimicrobial activity with (A) FtsE/X-dependent mechanisms involving FtsE/X and an active putative BAS0651 hydrolase and (B) FtsE/X-independent. Modified from Margulieux *et al.*, 2016 (145).

an integral part of the cell wall synthesis complex during cellular elongation and spore formation (112, 113, 123, 124, 126). It is anticipated that *B. anthracis* FtsE/X and BAS0651 have similar functions as the homologous complex components in *B. subtilis*, and studying the expression and activation profiles of the *B. anthracis* genes and resulting proteins will allow us to gain a better understanding of what role(s) they play in vegetative growth, sporulation, and germination and how their presence and function may play a role in the mechanism underlying CXCL10 antimicrobial activity. Further characterization of the cell wall synthesis complex in *B. anthracis* will set the foundation for the future development of chemokine or small molecule-based inhibitors that target these vital components of the bacterial structure.

The finding of a bifunctional activity for CXCL10 has led to the identification of multiple antimicrobial regions of CXCL10. The N-terminal region(s) of CXCL10 are able to exert antimicrobial activity against *B. anthracis* vegetative cells, independent of the CXCL10 C-terminal α-helix. However, the amphipathic C-terminal α-helix also plays a role in bacterial killing through membrane depolarization and disruption, even in the absence of any of the abovementioned bacterial components, which act as CXCL10 targets. CXCL10 has many characteristic secondary and tertiary structures typical of chemokines; future studies will be focused on investigating these structural elements in detail by testing how disruption of these secondary and tertiary structures impacts the CXCL10 antimicrobial activity. Modification of the CXCL10 C-terminal α-helix through disruption of the amphipathic properties would provide valuable insight into further defining its role in eliciting membrane depolarization and subsequent death of the vegetative cells. The

overall tertiary structure of CXCL10 can be studied to determine the role that the two conserved disulfide bonds and overall compact nature of the chemokine play in causing bacterial killing. Expression and purification of recombinant CXCL10 mutated proteins will further increase the understanding of how CXCL10 results in an antimicrobial effect against *B. anthracis* and other bacterial pathogens.

The data generated and presented in this dissertation focused on studying the chemokine CXCL10 and its antimicrobial mechanism(s) of action. However, the IFN-γ inducible ELR(-) CXC chemokines, CXCL9 and CXCL11, also have been observed to have an antimicrobial effect against *B. anthracis* vegetative cells and spores. Some nuanced structural differences have been described between CXCL9, CXCL10, and CXCL11, which may account for the differences in potency between these three chemokines with recombinant human CXCL10 > CXCL9 > CXCL11, with CXCL10 being the most potent (67, 86, 105). Future work will focus on investigating important structural characteristics of the three chemokines that contribute to antimicrobial activity, with a focus on secondary and tertiary structures. For example, experiments are planned to generate chimeric CXCL9, CXCL10, and CXCL11 proteins to assess the features that contribute to CXCL10 being the most potent of the three chemokines and/or why CXCL11 is the least potent of the three chemokines against B. anthracis. Investigation into the unique properties of each of the IFN-γ inducible ELR(-) CXC chemokines, CXCL9, CXCL10, and CXCL11, should help elucidate how these chemokines function as important antimicrobial peptides within the innate immune system.

5.3 Impact

Chemokines are an integral part of the innate and adaptive immune system (55, 59, 77, 115). They have well-defined roles in a variety of biological processes such as immunomodulation, angiogenesis, and wound repair (59, 62, 65, 66). Observations have been made regarding antimicrobial characteristics of a variety of chemokines, but the mechanisms by which chemokines exert an antimicrobial response have remained largely uncharacterized (55, 67–69, 88, 89, 91, 101, 104–108). Understanding how chemokines target pathogenic microbes will lead to a greater understanding of the role of chemokines within the innate immune system and allow for a more detailed study of host-pathogen interactions. This current body of work demonstrates that chemokine targeting of microbes goes beyond non-specific charge-charge interactions between the chemokine and the microbial surface, and establishes a range of nuanced interactions that chemokines may have with individual pathogens. Additionally, given the recent emergence and global spread of multi-drug resistant bacteria, the development of novel therapeutics is a high priority (204–206). By understanding the mechanisms responsible for CXCL10 targeting of *B. anthracis*, novel therapies can be developed in order to treat both spore and vegetative cell infections.

In conclusion, chemokines are an important family of proteins in both innate and adaptive immune defense in the host through immune cell activation, chemoattractant roles, and antimicrobial activity (55, 85, 86, 105, 108, 207). We have determined that CXCL10 is able to exert an antimicrobial effect against *B. anthracis* vegetative cells via two separate but complementary mechanisms. The identification of specific bacterial targets that

mediate CXCL10 antimicrobial activity for both *B. anthracis* spores and vegetative cells opens the door for a more in depth analysis of chemokine activity beyond immunomodulation. There is much more to learn about chemokine influence on the innate immune system and new therapeutic approaches to microbial infections based on those findings.

6 Cited Literature

1. **Mock M**, **Fouet A**. 2001. Anthrax. Annu Rev Microbiol **55**:647–671.
2. **Spencer RC**. 2003. *Bacillus anthracis*. J Clin Pathol **56**:182–187.
3. **Blevins SM**, **Bronze MS**. 2010. Robert Koch and the "golden age" of bacteriology. Int J Infect Dis **14**:e744–751.
4. **WHO**. 2008. Anthrax in humans and animals. World Health Organization, Geneva, Switzerland.
5. **Goel AK**. 2015. Anthrax: A disease of biowarfare and public health importance. World J Clin cases **3**:20–33.
6. **Setlow P**. 2003. Spore germination. Curr Opin Microbiol **6**:550–556.
7. **Moir A**. 2006. How do spores germinate? J Appl Microbiol **101**:526–530.
8. **Driks A**. 2009. The *Bacillus anthracis* spore. Mol Aspects Med **30**:368–373.
9. **Heffron JD**, **Orsburn B**, **Popham DL**. 2009. Roles of germination-specific lytic enzymes CwlJ and SleB in *Bacillus anthracis*. J Bacteriol **191**:2237–2247.
10. **Henriques AO**, **Moran CP**. 2007. Structure, assembly, and function of the spore surface layers. Annu Rev Microbiol **61**:555–588.
11. **Stewart GC**. 2015. The exosporium layer of bacterial spores: a connection to the environment and the infected host. Microbiol Mol Biol Rev **79**:437–457.
12. **Hugh-Jones M**, **Blackburn J**. 2009. The ecology of *Bacillus anthracis.* Mol Aspects Med **30**:356–367.
13. **Dey R**, **Hoffman PS**, **Glomski IJ**. 2012. Germination and amplification of anthrax spores by soil-dwelling amoebas. Appl Environ Microbiol **78**:8075–8081.
14. **Sweeney DE**, **Hicks CW**, **Cui X**, **Li Y**, **Eichacker PQ**. 2011. Anthrax infection.

Am J Respir Crit Care Med **184**:1333–1341.

15. **Fasanella A**, **Scasciamacchia S**, **Garofolo G**, **Giangaspero A**, **Tarsitano E**, **Adone R**. 2010. Evaluation of the house fly *Musca domestica* as a mechanical vector for an anthrax. PLoS One **5**:e12219.

16. **Turell MJ**, **Knudson GB**. 1987. Mechanical transmission of Bacillus anthracis by stable flies (*Stomoxys calcitrans*) and mosquitoes (*Aedes aegypti* and *Aedes taeniorhynchus*). Infect Immun **55**:1859–1861.

17. **Beatty ME**, **Ashford DA**, **Griffin PM**, **Tauxe R V**, **Sobel J**. 2003. Gastrointestinal anthrax. Arch Intern Med **163**:2527–2531.

18. **Berger T**, **Kassirer M**, **Aran AA**. 2014. Injectional anthrax - new presentation of an old disease. Euro Surveill **19**:pii=20877.

19. **Hicks CW**, **Sweeney DA**, **Cui X**, **Li Y**, **Eichacker PQ**. 2012. An overview of anthrax infection including the recently identified form of disease in injection drug users. Intensive Care Med **38**:1092–1104.

20. **Cote CK**, **Welkos SL**, **Bozue J**. 2011. Key aspects of the molecular and cellular basis of inhalational anthrax. Microbes Infect **13**:1146–1155.

21. **Cote CK**, **DiMezzo TL**, **Banks DJ**, **France B**, **Bradley KA**, **Welkos SL**. 2008. Early interactions between fully virulent *Bacillus anthracis* and macrophages that influence the balance between spore clearance and development of a lethal infection. Microbes Infect **10**:613–619.

22. **Welkos S**, **Friedlander A**, **Weeks S**, **Little S**, **Mendelson I**. 2002. *In-vitro* characterisation of the phagocytosis and fate of anthrax spores in macrophages and the effects of anti-PA antibody. J Med Microbiol **51**:821–831.

23. **Jernigan JA**, **Stephens DS**, **Ashford DA**, **Omenaca C**, **Topiel MS**, **Galbraith M**, **Tapper M**, **Fisk TL**, **Zaki S**, **Popovic T**, **Meyer RF**, **Quinn CP**, **Harper SA**, **Fridkin SK**, **Sejvar JJ**, **Shepard CW**, **McConnell M**, **Guarner J**, **Shieh WJ**, **Malecki JM**, **Gerberding JL**, **Hughes JM**, **Perkins BA**. 2001. Bioterrorism-related inhalational anthrax: the first 10 cases reported in the United States. Emerg Infect Dis **7**:933–944.

24. **Henderson DW**, **Peacock S**, **Belton FC**. 1956. Observations on the prophylaxis of experimental pulmonary anthrax in the monkey. J Hyg (Lond) **54**:28–36.

25. **Meselson M**, **Guillemin J**, **Hugh-Jones M**, **Langmuir A**, **Popova I**, **Shelokov A**, **Yampolskaya O**. 1994. The Sverdlovsk anthrax outbreak of 1979. Science **266**:1202–1208.

26. **Joellenbeck LM**, **Zwanziger LL**, **Durch JS**, **Strom BL**. 2002. Anthrax vaccine: is it safe? does it work? National Academies Press, Washington, D.C.

27. **Quinn CP**, **Sabourin CL**, **Schiffer JM**, **Niemuth NA**, **Semenova VA**, **Li H**, **Rudge TL**, **Brys AM**, **Mittler RS**, **Ibegbu CC**, **Wrammert J**, **Ahmed R**, **Parker SD**, **Babcock J**, **Keitel W**, **Poland GA**, **Keyserling HL**, **El Sahly H**, **Jacobson RM**, **Marano N**, **Plikaytis BD**, **Wright JG**. 2016. Humoral and cell-mediated immune responses to alternate booster schedules of anthrax vaccine adsorbed in humans. Clin vaccine Immunol **23**:326–338.

28. **Hopkins RJ**, **Daczkowski NF**, **Kaptur PE**, **Muse D**, **Sheldon E**, **LaForce C**, **Sari S**, **Rudge TL**, **Bernton E**. 2013. Randomized, double-blind, placebo-controlled, safety and immunogenicity study of 4 formulations of Anthrax Vaccine Adsorbed plus CPG 7909 (AV7909) in healthy adult volunteers. Vaccine **31**:3051–

3058.

29. **CDC**. 2013. Considerations for Anthrax Vaccine Adsorbed (AVA) post-exposure prioritization. Atlanta, Georgia.

30. **Kolsto A-B**, **Tourasse NJ**, **Okstad OA**. 2009. What sets *Bacillus anthracis* apart from other *Bacillus* species? Annu Rev Microbiol **63**:451–476.

31. **Barras V**, **Greub G**. 2014. History of biological warfare and bioterrorism. Clin Microbiol Infect **20**:497–502.

32. **Setlow P**. 2014. Spore resistance properties. Microbiol Spectr **2**:TBS–003–2012.

33. **Setlow P**. 2006. Spores of *Bacillus subtilis*: their resistance to and killing by radiation, heat and chemicals. J Appl Microbiol **101**:514–525.

34. **Toth DJA**, **Gundlapalli A V**, **Schell WA**, **Bulmahn K**, **Walton TE**, **Woods CW**, **Coghill C**, **Gallegos F**, **Samore MH**, **Adler FR**. 2013. Quantitative models of the dose-response and time course of inhalational anthrax in humans. PLoS Pathog **9**:e1003555.

35. **Henderson DA**, **Bartlett JG**, **Ascher MS**, **Eitzen E**, **Friedlander AM**, **Hauer J**, **Mcdade J**, **Osterholm MT**, **Toole TO**, **Parker G**, **Perl TM**, **Russell PK**. 1999. Anthrax as a biological weapon. J Am Med Assoc **281**:1735–1963.

36. **Errington J**. 2003. Regulation of endospore formation in *Bacillus subtilis*. Nat Rev Microbiol **1**:117–126.

37. **Ireland JAW**, **Hanna PC**. 2002. Amino acid and purine ribonucleoside-induced germination of *Bacillus anthracis* DSterne endospores: gerS mediates responses to aromatic ring structures. J Bacteriol **184**:1296–1303.

38. **Koehler TM**. 2009. *Bacillus anthracis* physiology and genetics. Mol Aspects Med

30:386–396.

39. **Fouet A**. 2009. The surface of *Bacillus anthracis*. Mol Aspects Med **30**:374–385.

40. **Okinaka R**, **Cloud K**, **Hampton O**, **Hoffmaster A**, **Hill K**, **Keim P**, **Koehler T**, **Lamke G**, **Kumano S**, **Manter D**, **Martinez Y**, **Ricke D**, **Svensson R**, **Jackson P**. 1999. Sequence, assembly and analysis of pX01 and pX02. J Appl Microbiol **87**:261–262.

41. **Kintzer AF**, **Thoren KL**, **Sterling HJ**, **Dong KC**, **Feld GK**, **Tang II**, **Zhang TT**, **Williams ER**, **Berger JM**, **Krantz BA**. 2009. The protective antigen component of anthrax toxin forms functional octameric complexes. J Mol Biol **392**:614–629.

42. **Abrami L**, **Reig N**, **van der Goot FG**. 2005. Anthrax toxin: the long and winding road that leads to the kill. Trends Microbiol **13**:72–78.

43. **Scobie HM**, **Rainey GJA**, **Bradley KA**, **Young JAT**. 2003. Human capillary morphogenesis protein 2 functions as an anthrax toxin receptor. Proc Natl Acad Sci U S A **100**:5170–5174.

44. **Friebe S**, **van der Goot FG**, **Bürgi J**. 2016. The ins and outs of anthrax toxin. Toxins (Basel) **8**:pii: E69.

45. **Abrami L**, **Liu S**, **Cosson P**, **Leppla SH**, **van der Goot FG**. 2003. Anthrax toxin triggers endocytosis of its receptor via a lipid raft-mediated clathrin-dependent process. J Cell Biol **160**:321–328.

46. **Abrami L**, **Lindsay M**, **Parton RG**, **Leppla SH**, **van der Goot FG**. 2004. Membrane insertion of anthrax protective antigen and cytoplasmic delivery of lethal factor occur at different stages of the endocytic pathway. J Cell Biol **166**:645–651.

47. **Banks DJ**, **Ward SC**, **Bradley KA**. 2006. New insights into the functions of anthrax toxin. Expert Rev Mol Med **8**:1–18.

48. **Baldari CT**, **Tonello F**, **Paccani SR**, **Montecucco C**. 2006. Anthrax toxins: A paradigm of bacterial immune suppression. Trends Immunol **27**:434–440.

49. **Turk BE**. 2007. Manipulation of host signalling pathways by anthrax toxins. Biochem J **402**:405–417.

50. **Makino S**, **Uchida I**, **Terakado N**, **Sasakawa C**, **Yoshikawa M**. 1989. Molecular characterization and protein analysis of the cap region, which is essential for encapsulation in *Bacillus anthracis*. J Bacteriol **171**:722–730.

51. **Welkos SL**. 1991. Plasmid-associated virulence factors of non-toxigenic (pX01-) *Bacillus anthracis*. Microb Pathog **10**:183–198.

52. **Dixon TC**, **Fadl AA**, **Koehler TM**, **Swanson JA**, **Hanna PC**. 2000. Early *Bacillus anthracis*-macrophage interactions: intracellular survival survival and escape. Cell Microbiol **2**:453–463.

53. **Barua S**, **Iyer JK**, **Larabee JL**, **Raisley B**, **Hughes MA**, **Coggeshall KM**, **Ballard JD**. 2013. Toxin inhibition of antimicrobial factors induced by *Bacillus anthracis* peptidoglycan in human blood. Infect Immun **81**:3693–3702.

54. **Zlotnik A**, **Yoshie O**. 2000. Chemokines: a new classification system and their role in immunity. Immunity **12**:121–127.

55. **Zlotnik A**, **Yoshie O**. 2012. The chemokine superfamily revisited. Immunity **36**:705–716.

56. **Griffith JW**, **Sokol CL**, **Luster AD**. 2014. Chemokines and chemokine receptors: positioning cells for host defense and immunity. Annu Rev Immunol **32**:659–702.

57. **Luster AD**. 1998. Chemokines-chemotactic cytokines that mediate inflammation. N Engl J Med **338**:436–445.

58. **Allen SJ**, **Crown SE**, **Handel TM**. 2007. Chemokine: receptor structure, interactions, and antagonism. Annu Rev Immunol **25**:787–820.

59. **Campbell DJ**, **Kim CH**, **Butcher EC**. 2003. Chemokines in the systemic organization of immunity. Immunol Rev **195**:58–71.

60. **Kufareva I**, **Salanga CL**, **Handel TM**. 2015. Chemokine and chemokine receptor structure and interactions: implications for therapeutic strategies. Immunol Cell Biol **93**:372–383.

61. **Ransohoff RM**. 2009. Chemokines and chemokine receptors: standing at the crossroads of immunobiology and neurobiology. Immunity **31**:711–721.

62. **Mehrad B**, **Keane MP**, **Strieter RM**. 2007. Chemokines as mediators of angiogenesis. Thromb Haemost **98**:262–273.

63. **Bosisio D**, **Salvi V**, **Gagliostro V**, **Sozzani S**. 2014. Angiogenic and antiangiogenic chemokines. Chem Immunol Allergy **99**:89–104.

64. **Devalaraja RM**, **Nanney LB**, **Du J**, **Qian Q**, **Yu Y**, **Devalaraja MN**, **Richmond A**. 2000. Delayed wound healing in CXCR2 knockout mice. J Invest Dermatol **115**:234–244.

65. **Ding J**, **Tredget EE**. 2015. The role of chemokines in fibrotic wound healing. Adv wound care **4**:673–686.

66. **Gillitzer R**, **Goebeler M**. 2001. Chemokines in cutaneous wound healing. J Leukoc Biol **69**:513–521.

67. **Cole AM**, **Ganz T**, **Liese AM**, **Burdick MD**, **Liu L**, **Strieter RM**. 2001. Cutting

edge: IFN-inducible ELR- CXC chemokines display defensin-like antimicrobial activity. J Immunol **167**:623–627.

68. **Yang D**, **Chen Q**, **Hoover DM**, **Staley P**, **Tucker KD**, **Lubkowski J**, **Oppenheim JJ**. 2003. Many chemokines including CCL20/MIP-3alpha display antimicrobial activity. J Leukoc Biol **74**:448–455.

69. **Yung SC**, **Murphy PM**. 2012. Antimicrobial chemokines. Front Immunol **3**:1–11.

70. **Elias J. Fernandez**, **Lolis E**. 2002. Structure, function, and inhibition of chemokines. Annu Rev Pharmacol Toxicol **42**:469–499.

71. **Frederick MJ**, **Clayman GL**. 2001. Chemokines in cancer. Expert Rev Mol Med **3**:1–18.

72. **Kuloğlu ES**, **McCaslin DR**, **Markley JL**, **Volkman BF**. 2002. Structural rearrangement of human lymphotactin, a C chemokine, under physiological solution conditions. J Biol Chem **277**:17863–17870.

73. **Guzzo C**, **Fox JC**, **Miao H**, **Volkman BF**, **Lusso P**. 2015. Structural determinants for the selective anti-HIV-1 activity of the all-β alternative conformer of XCL1. J Virol **89**:9061–9067.

74. **Wojdasiewicz P**, **Poniatowski LA**, **Kotela A**, **Deszczyński J**, **Kotela I**, **Szukiewicz D**. 2014. The chemokine CX3CL1 (fractalkine) and its receptor CX3CR1: occurrence and potential role in osteoarthritis. Arch Immunol Ther Exp (Warsz) **62**:395–403.

75. **Hamel DJ**, **Sielaff I**, **Proudfoot AEI**, **Handel TM**. 2009. Interactions of chemokines with glycosaminoglycans. Methods Enzymol **461**:71–102.

76. **Liu L**, **Callahan MK**, **Huang D**, **Ransohoff RM**. 2005. Chemokine receptor

CXCR3: an unexpected enigma. Curr Top Dev Biol **68**:149–181.

77. **Rossi D**, **Zlotnik A**. 2000. The biology of chemokines and their receptors. Annu Rev Immunol **18**:217–242.

78. **Vaidehi N**, **Bhattacharya S**, **Larsen AB**. 2014. Structure and dynamics of G-protein coupled receptors. Adv Exp Med Biol **796**:37–54.

79. **Amarandi R-M**, **Hjorto GM**, **Rosenkilde MM**, **Karlshoj S**. 2015. Probing biased signaling in chemokine receptors. Methods Enzymol **570**:155–186.

80. **Van Raemdonck K**, **Van den Steen PE**, **Liekens S**, **Van Damme J**, **Struyf S**. 2014. CXCR3 ligands in disease and therapy. Cytokine Growth Factor Rev **26**:311–327.

81. **Zeng X**, **Moore TA**, **Newstead MW**, **Deng JC**, **Kunkel SL**, **Luster AD**, **Standiford TJ**. 2005. Interferon-inducible protein 10, but not monokine induced by gamma interferon, promotes protective type 1 immunity in murine *Klebsiella pneumoniae* pneumonia. Infect Immun **73**:8226–8236.

82. **Trotta T**, **Costantini S**, **Colonna G**. 2009. Modelling of the membrane receptor CXCR3 and its complexes with CXCL9, CXCL10 and CXCL11 chemokines: Putative target for new drug design. Mol Immunol **47**:332–339.

83. **Groom JR**, **Luster AD**. 2011. CXCR3 ligands: redundant, collaborative and antagonistic functions. Immunol Cell Biol **89**:207–215.

84. **Booth V**, **Clark-lewis I**, **Sykes BD**. 2004. NMR structure of CXCR3 binding chemokine CXCL11 (ITAC). Protein Sci **11**:2022–2028.

85. **Booth V**, **Keizer DW**, **Kamphuis MB**, **Clark-Lewis I**, **Sykes BD**. 2002. The CXCR3 binding chemokine IP-10/CXCL10: structure and receptor interactions.

Biochemistry **41**:10418–10425.

86. **Colvin RA**, **Campanella GS V**, **Manice LA**, **Luster AD**. 2006. CXCR3 requires tyrosine sulfation for ligand binding and a second extracellular loop arginine residue for ligand-induced chemotaxis. Mol Cell Biol **26**:5838–5849.

87. **Xanthou G**, **Williams TJ**, **Pease JE**. 2003. Molecular characterization of the chemokine receptor CXCR3: evidence for the involvement of distinct extracellular domains in a multi-step model of ligand binding and receptor activation. Eur J Immunol **33**:2927–2936.

88. **Yeaman MR**, **Yount NY**. 2007. Unifying themes in host defence effector polypeptides. Nat Rev Microbiol **5**:727–740.

89. **Durr M**, **Peschel A**. 2002. Chemokines meet defensins : the merging concepts of chemoattractants and antimicrobial peptides in host defense. Infect Immun **70**:6515–6517.

90. **Oppenheim JJ**, **Biragyn A**, **Kwak LW**, **Yang D**. 2003. Roles of antimicrobial peptides such as defensins in innate and adaptive immunity. Ann Rheum Dis **62**:ii17–ii21.

91. **Nguyen LT**, **Vogel HJ**. 2012. Structural perspectives on antimicrobial chemokines. Front Immunol **3**:1–11.

92. **Krijgsveld J**, **Zaat SA**, **Meeldijk J**, **van Veelen PA**, **Fang G**, **Poolman B**, **Brandt E**, **Ehlert JE**, **Kuijpers AJ**, **Engbers GH**, **Feijen J**, **Dankert J**. 2000. Thrombocidins, microbicidal proteins from human blood platelets, are C-terminal deletion products of CXC chemokines. J Biol Chem **275**:20374–40381.

93. **Chensue SW**. 2001. Molecular machinations : chemokine signals in host-pathogen

interactions. Clin Microbiol Rev **14**:821–835.

94. **Söbirk SK**, **Mörgelin M**, **Egesten A**, **Bates P**, **Shannon O**, **Collin M**. 2013. Human chemokines as antimicrobial peptides with direct parasiticidal effect on Leishmania mexicana in vitro. PLoS One **8**:e58129.

95. **Nakayama T**, **Shirane J**, **Hieshima K**, **Shibano M**, **Watanabe M**, **Jin Z**, **Nagakubo D**, **Saito T**, **Shimomura Y**, **Yoshie O**. 2006. Novel antiviral activity of chemokines. Virology **350**:484–492.

96. **Brogden KA**. 2005. Antimicrobial peptides: pore formers or metabolic inhibitors in bacteria? Nat Rev Microbiol **3**:238–250.

97. **Hancock REW**, **Sahl H-G**. 2006. Antimicrobial and host-defense peptides as new anti-infective therapeutic strategies. Nat Biotechnol **24**:1551–1557.

98. **Hieshima K**, **Ohtani H**, **Shibano M**, **Izawa D**, **Nakayama T**, **Kawasaki Y**, **Shiba F**, **Shiota M**, **Katou F**, **Saito T**, **Yoshie O**. 2003. CCL28 has dual roles in mucosal immunity as a chemokine with broad-spectrum antimicrobial activity. J Immunol **170**:1452–1461.

99. **Bjorstad A**, **Fu H**, **Karlsson A**, **Dahlgren C**, **Bylund J**. 2005. Interleukin-8-derived peptide has antibacterial activity. Antimicrob Agents Chemother **49**:3889–3895.

100. **Nguyen LT**, **Chan DI**, **Boszhard L**, **Zaat S a J**, **Vogel HJ**. 2010. Structure-function studies of chemokine-derived carboxy-terminal antimicrobial peptides. Biochim Biophys Acta **1798**:1062–1072.

101. **Linge HM**, **Collin M**, **Giwercman A**, **Malm J**, **Bjartell A**, **Egesten A**. 2008. The antibacterial chemokine MIG/CXCL9 is constitutively expressed in epithelial cells

of the male urogenital tract and is present in seminal plasma. J Interf cytokine Res **28**:191–196.

102. **Valdivia-Silva J**, **Medina-Tamayo J**, **Garcia-Zepeda EA**. 2015. Chemokine-derived peptides: novel antimicrobial and antineoplasic agents. Int J Mol Sci **16**:12958–12985.

103. **Zasloff M**. 2002. Antimicrobial peptides of multicellular organisms. Nature **415**:389–395.

104. **Egesten A**, **Eliasson M**, **Johansson HM**, **Olin AI**, **Morgelin M**, **Mueller A**, **Pease JE**, **Frick I-M**, **Bjorck L**. 2007. The CXC chemokine MIG/CXCL9 is important in innate immunity against *Streptococcus pyogenes.* J Infect Dis **195**:684–693.

105. **Crawford MA**, **Zhu Y**, **Green CS**, **Burdick MD**, **Sanz P**, **Alem F**, **O'Brien AD**, **Mehrad B**, **Strieter RM**, **Hughes MA**. 2009. Antimicrobial effects of interferon-inducible CXC chemokines against *Bacillus anthracis* spores and bacilli. Infect Immun **77**:1664–1678.

106. **Holdren GO**, **Rosenthal DJ**, **Yang J**, **Bates AM**, **Fischer CL**, **Zhang Y**, **Brogden NK**, **Brogden KA**. 2014. Antimicrobial activity of chemokine CXCL10 for dermal and oral microorganisms. Antibiotics **3**:527–539.

107. **Reid-Yu SA**, **Tuinema BR**, **Small CN**, **Xing L**, **Coombes BK**. 2015. CXCL9 contributes to antimicrobial protection of the gut during *Citrobacter rodentium* infection independent of chemokine-receptor signaling. PLoS Pathog **11**:e1004648.

108. **Schutte KM**, **Fisher DJ**, **Burdick MD**, **Mehrad B**, **Mathers AJ**, **Mann BJ**,

Nakamoto RK, **Hughes MA**. 2016. *Escherichia coli* pyruvate dehydrogenase complex is an important component of CXCL10-mediated antimicrobial activity. Infect Immun **84**:320–328.

109. **Balogh EP**, **Faludi I**, **Virók DP**, **Endrész V**, **Burián K**. 2011. Chlamydophila pneumoniae induces production of the defensin-like MIG/CXCL9, which has in vitro antichlamydial activity. Int J Med Microbiol **301**:252–259.

110. **Crawford MA**, **Burdick MD**, **Glomski IJ**, **Boyer AE**, **Barr JR**, **Mehrad B**, **Strieter RM**, **Hughes MA**. 2010. Interferon-inducible CXC chemokines directly contribute to host defense against inhalational anthrax in a murine model of infection. PLoS Pathog **6**:e1001199.

111. **Crawford MA**, **Lowe DE**, **Fisher DJ**, **Stibitz S**, **Plaut RD**, **Beaber JW**, **Zemansky J**, **Mehrad B**, **Glomski IJ**, **Strieter RM**, **Hughes MA**. 2011. Identification of the bacterial protein FtsX as a unique target of chemokine-mediated antimicrobial activity against *Bacillus anthracis*. Proc Natl Acad Sci U S A **108**:17159–17164.

112. **Meisner J**, **Montero Llopis P**, **Sham L-T**, **Garner E**, **Bernhardt TG**, **Rudner DZ**. 2013. FtsEX is required for CwlO peptidoglycan hydrolase activity during cell wall elongation in *Bacillus subtilis.* Mol Microbiol **89**:1069–1083.

113. **Domínguez-Cuevas P**, **Porcelli I**, **Daniel RA**, **Errington J**. 2013. Differentiated roles for MreB-actin isologues and autolytic enzymes in *Bacillus subtilis* morphogenesis. Mol Microbiol **89**:1084–1098.

114. **Murray CJL**, **Lopez AD**. 2014. Global, regional, and national age–sex specific all-cause and cause-specific mortality for 240 causes of death, 1990–2013: a

systematic analysis for the Global Burden of Disease Study 2013. Lancet **385**:117–171.

115. **Bonecchi R**, **Galliera E**, **Borroni EM**, **Corsi MM**, **Locati M**, **Mantovani A**. 2009. Chemokines and chemokine receptors: an overview. Front Biosci **14**:540–551.

116. **Lacotte S**, **Brun S**, **Muller S**, **Dumortier H**. 2009. CXCR3, inflammation, and autoimmune diseases. Ann N Y Acad Sci **1173**:310–317.

117. **Loetscher M**, **Loetscher P**, **Brass N**, **Meese E**, **Moser B**. 1998. Lymphocyte-specific chemokine receptor CXCR3: regulation, chemokine binding and gene localization. Eur J Immunol **28**:3696–3705.

118. **Weiner ZP**, **Glomski IJ**. 2012. Updating perspectives on the initiation of *Bacillus anthracis* growth and dissemination through its host. Infect Immun **80**:1626–1633.

119. **De Smet K**, **Contreras R**. 2005. Human antimicrobial peptides: defensins, cathelicidins and histatins. Biotechnol Lett **27**:1337–1347.

120. **Chang WK**, **Wimley WC**, **Searson PC**, **Hristova K**. 2008. Characterization of antimicrobial peptide activity by electrochemical impedance spectroscopy **1778**:2430–2436.

121. **de Leeuw E**, **Graham B**, **Phillips GJ**, **ten Hagen-Jongman CM**, **Oudega B**, **Luirink J**. 1999. Molecular characterization of *Escherichia coli* FtsE and FtsX. Mol Microbiol **31**:983–993.

122. **Schmidt KL**, **Peterson ND**, **Kustusch RJ**, **Wissel MC**, **Graham B**, **Phillips GJ**, **Weiss DS**. 2004. A predicted ABC transporter, FtsEX, is needed for cell division in *Escherichia coli.* J Bacteriol **186**:785–793.

123. **Garti-Levi S**, **Hazan R**, **Kain J**, **Fujita M**, **Ben-Yehuda S**. 2008. The FtsEX ABC transporter directs cellular differentiation in *Bacillus subtilis*. Mol Microbiol **69**:1018–1028.

124. **Mavrici D**, **Marakalala MJ**, **Holton JM**, **Prigozhin DM**, **Gee CL**, **Zhang YJ**, **Rubin EJ**, **Alber T**. 2014. *Mycobacterium tuberculosis* FtsX extracellular domain activates the peptidoglycan hydrolase, RipC. Proc Natl Acad Sci U S A **111**:8037–8042.

125. **Arends SJR**, **Kustusch RJ**, **Weiss DS**. 2009. ATP-binding site lesions in FtsE impair cell division. J Bacteriol **191**:3772–3784.

126. **Mir MA**, **Arumugam M**, **Mondal S**, **Rajeswari HS**, **Ramakumar S**, **Ajitkumar P**. 2015. *Mycobacterium tuberculosis* cell division protein, FtsE, is an ATPase in dimeric form. Protein J **34**:35–47.

127. **Kohanski MA**, **Dwyer DJ**, **Collins JJ**. 2010. How antibiotics kill bacteria: from targets to networks. Nat Rev Microbiol **8**:423–435.

128. **Swaminathan GJ**, **Holloway DE**, **Colvin R a.**, **Campanella GK**, **Papageorgiou AC**, **Luster AD**, **Acharya KR**. 2003. Crystal structures of oligomeric forms of the IP-10/CXCL10 chemokine. Structure **11**:521–532.

129. **Notredame C**, **Higgins DG**, **Heringa J**. 2000. T-Coffee: A novel method for fast and accurate multiple sequence alignment. J Mol Biol **302**:205–217.

130. **Di Tommaso P**, **Moretti S**, **Xenarios I**, **Orobitg M**, **Montanyola A**, **Chang J-M**, **Taly J-F**, **Notredame C**. 2011. T-Coffee: a web server for the multiple sequence alignment of protein and RNA sequences using structural information and homology extension. Nucleic Acids Res **39**:W13–7.

131. **Yang DC**, **Peters NT**, **Parzych KR**, **Uehara T**, **Markovski M**, **Bernhardt TG**. 2011. An ATP-binding cassette transporter-like complex governs cell-wall hydrolysis at the bacterial cytokinetic ring. PNAS **108**:e1052–60.

132. **Shahabuddin S**, **Rong J**, **Wang P**, **Brailoiu E**, **Dun N**, **Yang Y**, **Aksoy O**, **Kelsen SG**, **Aksoy MO**, **Dun N**. 2011. CXCR3 chemokine receptor-induced chemotaxis in human airway epithelial cells: role of p38 MAPK and PI3K signaling pathways. Am J Cell Physiol **291**:34–39.

133. **Greenfield NJ**. 2006. Using circular dichroism spectra to estimate protein secondary structure. Nat Protoc **1**:2876–2890.

134. **Janes BK**, **Stibitz S**. 2006. Routine markerless gene replacement in *Bacillus anthracis*. Infect Immun **74**:1949–1953.

135. **Sham L**, **Jensen KR**, **Bruce KE**, **Winkler ME**. 2013. Involvement of FtsE ATPase and FtsX extracellular loops 1 and 2 in FtsEX-PcsB complex function in cell division of *Streptococcus pneumoniae* D39. MBio **4**:e00431–413.

136. **Mir MA**, **Rajeswari HS**, **Veeraraghavan U**, **Ajitkumar P**. 2006. Molecular characterisation of ABC transporter type FtsE and FtsX proteins of *Mycobacterium tuberculosis*. Arch Microbiol **185**:147–158.

137. **Pflughoeft KJ**, **Sumby P**, **Koehler TM**. 2011. *Bacillus anthracis* sin locus and regulation of secreted proteases. J Bacteriol **193**:631–639.

138. **Rueff A-S**, **Chastanet A**, **Domínguez-Escobar J**, **Yao Z**, **Yates J**, **Prejean M-V**, **Delumeau O**, **Noirot P**, **Wedlich-Söldner R**, **Filipe SR**, **Carballido-López R**. 2014. An early cytoplasmic step of peptidoglycan synthesis is associated to MreB in *Bacillus subtilis*. Mol Microbiol **91**:348–362.

139. **Formstone A**, **Errington J**. 2005. A magnesium-dependent mreB null mutant: implications for the role of mreB in *Bacillus subtilis.* Mol Microbiol **55**:1646–1657.

140. **Su M**, **He C**, **West C a**, **Mentzer SJ**. 2001. Cytolytic peptides induce biphasic permeability changes in mammalian cell membranes. J Immunol Methods **252**:63–71.

141. **Chongsiriwatana NP**, **Barron AE**. 2010. Comparing bacterial membrane interactions of antimicrobial peptides and their mimics. Methods Mol Biol **618**:171–182.

142. **Sham L**, **Barendt SM**, **Kopecky KE**, **Winkler ME**. 2011. Essential PcsB putative peptidoglycan hydrolase interacts with the essential FtsXSpn cell division protein in *Streptococcus pneumoniae* D39. Proc Natl Acad Sci U S A **108**:E1061–9.

143. **Novak R**, **Charpentier E**, **Braun JS**, **Tuomanen E**. 2000. Signal transduction by a death signal peptide: uncovering the mechanism of bacterial killing by penicillin. Mol Cell **5**:49–57.

144. **Yount NY**, **Yeaman MR**. 2013. Peptide antimicrobials: cell wall as a bacterial target. Ann N Y Acad Sci **1277**:127–138.

145. **Margulieux KR**, **Fox JW**, **Nakamoto RK**, **Hughes MA**. 2016. CXCL10 acts as a bifunctional antimicrobial molecule against *Bacillus anthracis*. mBio **7**:pii: e00334–16.

146. **Reith J**, **Mayer C**. 2011. Peptidoglycan turnover and recycling in Gram-positive bacteria. Appl Microbiol Biotechnol **92**:1–11.

147. **Vollmer W**, **Seligman SJ**. 2010. Architecture of peptidoglycan: more data and more models. Trends Microbiol **18**:59–66.

148. **Turner RD**, **Vollmer W**, **Foster SJ**. 2014. Different walls for rods and balls: the diversity of peptidoglycan. Mol Microbiol **91**:862–874.

149. **Vollmer W**, **Blanot D**, **de Pedro MA**. 2008. Peptidoglycan structure and architecture. FEMS Microbiol Rev **32**:149–167.

150. **Bajaj R**, **Bruce KE**, **Davidson AL**, **Rued BE**, **Stauffacher C V**, **Winkler ME**. 2016. Biochemical characterization of essential cell division proteins FtsX and FtsE that mediate peptidoglycan hydrolysis by PcsB in *Streptococcus pneumoniae*. Microbiologyopen **3**:1–15.

151. **Bartual SG**, **Straume D**, **Stamsås GA**, **Muñoz IG**, **Alfonso C**, **Martínez-Ripoll M**, **Håvarstein LS**, **Hermoso JA**. 2014. Structural basis of PcsB-mediated cell separation in *Streptococcus pneumoniae*. Nat Commun **5**:3842.

152. **Reddy M**. 2007. Role of FtsEX in cell division of *Escherichia coli:* viability of ftsEX mutants is dependent on functional SufI or high osmotic strength. J Bacteriol **189**:98–108.

153. **Bernatchez S**, **Francis FM**, **Salimnia H**, **Beveridge TJ**, **Li H**, **Dillon J a**. 2000. Genomic, transcriptional and phenotypic analysis of ftsE and ftsX of *Neisseria gonorrhoeae*. DNA Res **7**:75–81.

154. **Lovering AL**, **Safadi SS**, **Strynadka NCJ**. 2012. Structural Perspective of Peptidoglycan Biosynthesis and Assembly. Annu Rev Biochem **81**:451–478.

155. **Bugg TDH**, **Braddick D**, **Dowson CG**, **Roper DI**. 2011. Bacterial cell wall assembly: still an attractive antibacterial target. Trends Biotechnol **29**:167–173.

156. **Typas A**, **Banzhaf M**, **Gross CA**, **Vollmer W**. 2011. From the regulation of peptidoglycan synthesis to bacterial growth and morphology. Nat Rev Microbiol **10**:123.

157. **Vollmer W**, **Joris B**, **Charlier P**, **Foster S**. 2008. Bacterial peptidoglycan (murein) hydrolases. FEMS Microbiol Rev **32**:259–286.

158. **Kuru E**, **Hughes HV**, **Brown PJ**, **Hall E**, **Tekkam S**, **Cava F**, **de Pedro MA**, **Brun Y V**, **VanNieuwenhze MS**. 2012. In Situ probing of newly synthesized peptidoglycan in live bacteria with fluorescent D-amino acids. Angew Chemie **51**:12519–12523.

159. **Kuru E**, **Tekkam S**, **Hall E**, **Brun Y V**, **Van Nieuwenhze MS**. 2015. Synthesis of fluorescent D-amino acids and their use for probing peptidoglycan synthesis and bacterial growth in situ. Nat Protoc **10**:33–52.

160. **Liechti GW**, **Kuru E**, **Hall E**, **Kalinda A**, **Brun Y V**, **VanNieuwenhze M**, **Maurelli AT**. 2014. A new metabolic cell-wall labelling method reveals peptidoglycan in *Chlamydia trachomatis*. Nature **506**:507–510.

161. **Boersma MJ**, **Kuru E**, **Rittichier JT**, **VanNieuwenhze MS**, **Brun Y V**, **Winkler ME**. 2015. Minimal peptidoglycan turnover in wild-type and PG hydrolase and cell division mutants of *Streptococcus pneumoniae* D39 growing planktonically and in host-relevant biofilms. J Bacteriol **197**:3472–3485.

162. **Sobhanifar S**, **King DT**, **Strynadka NC**. 2013. Fortifying the wall: synthesis, regulation and degradation of bacterial peptidoglycan. Curr Opin Struct Biol **23**:695–703.

163. **Vollmer W**. 2012. Bacterial growth does require peptidoglycan hydrolases. Mol

Microbiol **86**:1031–1035.

164. **Popham DL**. 2013. Visualizing the production and arrangement of peptidoglycan in Gram-positive cells. Mol Microbiol **88**:645–649.

165. **Liechti G**, **Kuru E**, **Packiam M**, **Hsu Y-P**, **Tekkam S**, **Hall E**, **Rittichier JT**, **VanNieuwenhze M**, **Brun Y V**, **Maurelli AT**. 2016. Pathogenic chlamydia lack a classical sacculus but synthesize a narrow, mid-cell peptidoglycan ring, regulated by MreB, for cell division. PLoS Pathog **12**:e1005590.

166. **Kolb HC**, **Finn MG**, **Sharpless KB**. 2001. Click chemistry: diverse chemical function from a few good reactions. Angew Chemie Int Ed **40**:2004–2021.

167. **Schneider CA**, **Rasband WS**, **Eliceiri KW**. 2012. NIH Image to ImageJ: 25 years of image analysis. Nat Methods **9**:671–675.

168. **Tipper DJ**, **Strominger JL**. 1965. Mechanism of action of penicillins: a proposal based on their structural similarity to acyl-D-alanyl-D-alanine. Proc Natl Acad Sci U S A **54**:1133–1141.

169. **Wise EM**, **Park JT**. 1965. Penicillin: its basic site of action as an inhibitor of a peptide cross-linking reaction in cell wall mucopeptide synthesis. Proc Natl Acad Sci U S A **54**:75–81.

170. **Chopra I**, **Roberts M**. 2001. Tetracycline antibiotics: mode of action, applications, molecular biology, and epidemiology of bacterial resistance. Microbiol Mol Biol Rev **65**:232–60.

171. **Packiam M**, **Weinrick B**, **Jacobs WR**, **Maurelli AT**. 2015. Structural characterization of muropeptides from *Chlamydia trachomatis* peptidoglycan by mass spectrometry resolves “chlamydial anomaly”. Proc Natl Acad Sci U S A

112:11660–11665.

172. **Loving CL**, **Osorio M**, **Kim Y-G**, **Nuñez G**, **Hughes MA**, **Merkel TJ**. 2009. Nod1/Nod2-mediated recognition plays a critical role in induction of adaptive immunity to anthrax after aerosol exposure. Infect Immun **77**:4529–4537.

173. **Girardin SE**, **Travassos LH**, **Hervé M**, **Blanot D**, **Boneca IG**, **Philpott DJ**, **Sansonetti PJ**, **Mengin-Lecreulx D**. 2003. Peptidoglycan molecular requirements allowing detection by Nod1 and Nod2. J Biol Chem **278**:41702–41708.

174. **Girardin SE**, **Boneca IG**, **Viala J**, **Chamaillard M**, **Labigne A**, **Thomas G**, **Philpott DJ**, **Sansonetti PJ**. 2003. Nod2 is a general sensor of peptidoglycan through muramyl dipeptide (MDP) detection. J Biol Chem **278**:8869–8872.

175. **Philpott DJ**, **Sorbara MT**, **Robertson SJ**, **Croitoru K**, **Girardin SE**. 2014. NOD proteins: regulators of inflammation in health and disease. Nat Rev Immunol **14**:9–23.

176. **Vollmer W**, **Blanot D**, **de Pedro MA**. 2008. Peptidoglycan structure and architecture. FEMS Microbiol Rev **32**:149–167.

177. **Omotade TO**, **Heffron JD**, **Klimko CP**, **Marchand CL**, **Miller LL**, **Halasahoris SA**, **Bozue JA**, **Welkos SL**, **Cote CK**. 2013. D-cycloserine or similar physiochemical compounds may be uniquely suited for use in *Bacillus anthracis* spore decontamination strategies. J Appl Microbiol **115**:1343–1356.

178. **Uehara T**, **Bernhardt TG**. 2011. More than just lysins: peptidoglycan hydrolases tailor the cell wall. Curr Opin Microbiol **14**:698–703.

179. **Jenkins SA**, **Xu Y**. 2013. Characterization of *Bacillus anthracis* persistence in vivo. PLoS One **8**:e66177.

180. **Cote CK**, **Welkos SL**. 2015. Anthrax toxins in context of *Bacillus anthracis* spores and spore germination. Toxins (Basel) **7**:3167–3178.

181. **Goossens PL**. 2009. Animal models of human anthrax: the quest for the holy grail. Mol Aspects Med **30**:467–480.

182. **Guidi-rontani C**, **Levy M**, **Ohayon H**, **Mock M**. 2001. Fate of germinated Bacillus anthracis spores in primary murine macrophages. Mol Microbiol **42**:931–938.

183. **Guidi-Rontani C**, **Weber-Levy M**, **Labruyère E**, **Mock M**. 1999. Germination of *Bacillus anthracis* spores within alveolar macrophages. Mol Microbiol **31**:9–17.

184. **Cote CK**, **DiMezzo TL**, **Banks DJ**, **France B**, **Bradley KA**, **Welkos SL**. 2008. Early interactions between fully virulent *Bacillus anthracis* and macrophages that influence the balance between spore clearance and development of a lethal infection. Microbes Infect **10**:613–619.

185. **Moayeri M**, **Leppla SH**, **Vrentas C**, **Pomerantsev AP**, **Liu S**. 2015. Anthrax pathogenesis. Annu Rev Microbiol **69**:185–208.

186. **Zemansky J**, **Kline BC**, **Woodward JJ**, **Leber JH**, **Marquis H**, **Portnoy DA**. 2009. Development of a mariner-based transposon and identification of Listeria monocytogenes determinants, including the peptidyl-prolyl isomerase PrsA2, that contribute to its hemolytic phenotype. J Bacteriol **191**:3950–3964.

187. **Yang J**, **Yan R**, **Roy A**, **Xu D**, **Poisson J**, **Zhang Y**. 2014. The I-TASSER Suite: protein structure and function prediction. Nat Methods **12**:7–8.

188. **Marchler-Bauer A**, **Derbyshire MK**, **Gonzales NR**, **Lu S**, **Chitsaz F**, **Geer LY**, **Geer RC**, **He J**, **Gwadz M**, **Hurwitz DI**, **Lanczycki CJ**, **Lu F**, **Marchler GH**,

Song JS, **Thanki N**, **Wang Z**, **Yamashita RA**, **Zhang D**, **Zheng C**, **Bryant SH**. 2014. CDD: NCBI's conserved domain database. Nucleic Acids Res **43**:D222–6.

189. **Zhang Y**, **Skolnick J**. 2004. Scoring function for automated assessment of protein structure template quality. Proteins **57**:702–10.

190. **Shah IM**, **Dworkin J**. 2010. Induction and regulation of a secreted peptidoglycan hydrolase by a membrane Ser/Thr kinase that detects muropeptides. Mol Microbiol **10**:1365–2958.

191. **Huang CC**, **Couch GS**, **Pettersen EF**, **Ferrin TE**. 1996. Chimera: an extensible molecular modeling application constructed using standard components. Pacific Symp Biocomput **1**:724.

192. **Welkos SL**, **Cote CK**, **Rea KM**, **Gibbs PH**. 2004. A microtiter fluorometric assay to detect the germination of *Bacillus anthracis* spores and the germination inhibitory effects of antibodies. J Microbiol Methods **56**:253–265.

193. **Cronin UP**, **Wilkinson MG**. 2007. The use of flow cytometry to study the germination of *Bacillus cereus* endospores. Cytometry A **71**:143–153.

194. **Evans SE**, **Xu Y**, **Tuvim MJ**, **Dickey BF**. 2010. Inducible innate resistance of lung epithelium to infection. Annu Rev Physiol **72**:413–435.

195. **Lowe DE**, **Ernst SMC**, **Zito C**, **Ya J**, **Glomski IJ**. 2013. *Bacillus anthracis* has two independent bottlenecks that are dependent on the portal of entry in an intranasal model of inhalational infection. Infect Immun **81**:4408–4420.

196. **Beeby M**, **Gumbart JC**, **Roux B**, **Jensen GJ**. 2013. Architecture and assembly of the Gram-positive cell wall. Mol Microbiol **88**:664–672.

197. **Wolf M**, **Moser B**. 2012. Antimicrobial activities of chemokines: not just a side-

effect? Front Immunol **3**:1–12.

198. **Plaut RD**, **Stibitz S**. 2015. Improvements to a markerless allelic exchange system for *Bacillus anthracis*. PLoS One **10**:e0142758.

199. **Bernhards CB**, **Popham DL**. 2014. Role of YpeB in cortex hydrolysis during germination of *Bacillus anthracis* spores. J Bacteriol **196**:3399–3409.

200. **Stewart GS**, **Johnstone K**, **Hagelberg E**, **Ellar DJ**. 1981. Commitment of bacterial spores to germinate. A measure of the trigger reaction. Biochem J **198**:101–106.

201. **States DJ**, **Gish W**. 1994. Combined use of sequence similarity and codon bias for coding region identification. J Comput Biol **1**:39–50.

202. **Altschul SF**, **Gish W**, **Miller W**, **Myers EW**, **Lipman DJ**. 1990. Basic local alignment search tool. J Mol Biol **215**:403–410.

203. **Comeau SR**, **Gatchell DW**, **Vajda S**, **Camacho CJ**. 2004. ClusPro: an automated docking and discrimination method for the prediction of protein complexes. Bioinformatics **20**:45–50.

204. **Alanis AJ**. 2005. Resistance to antibiotics : are we in the post-antibiotic era ? Arch Med Res **36**:697–705.

205. **Prestinaci F**, **Pezzotti P**, **Pantosti A**. 2015. Antimicrobial resistance: a global multifaceted phenomenon. Pathog Glob Health 309–318.

206. **Boucher HW**, **Talbot GH**, **Bradley JS**, **Edwards JE**, **Gilbert D**, **Rice LB**, **Scheld M**, **Spellberg B**, **Bartlett J**. 2009. Bad bugs, no drugs: no ESKAPE! An update from the Infectious Diseases Society of America. Clin Infect Dis **48**:1–12.

207. **Neville LF**, **Mathiak G**, **Bagasra O**. 1997. The immunobiology of interferon-

gamma inducible protein 10 kD (IP-10): A novel, pleiotropic member of the C-X-C chemokine superfamily. Cytokine Growth Factor Rev **8**:207–219.